The deconfinement phase transition and the chiral condensate in an effective theory for QCD using analytical and Complex Langevin methods

Abschlussarbeit

zur Erlangung des akademischen Grades
Master of Science

vorgelegt von

Alena Zmarsly

Oktober 2021

Institut für theorethische Physik
J.W. Goethe Universität Frankfurt a.M.

Erstgutachter:	Prof. Dr. Owe Philipsen
Zweitgutachter:	Prof. Dr. Marc Wagner
Betreuer:	Dr. Jangho Kim

Contents

Chapter 1

Introduction

Visible matter underlies four fundamental forces. The standard model of particle physics is capable of describing three of them, namely electromagnetic, weak and strong force. However, by now it is not possible to include gravity into the model. The theory of strong interaction is called Quantum Chromodynamics, QCD. Gell-Mann and Zweig proposed a model of the three light quarks, up, down and strange, which groups hadronic matter into octets and decuplets. Later three more quarks were found, charm, bottom and top. It was found that the $\Delta++$ baryon, which consists of three up quarks with parallel spin, does not obey the *Pauli principle*. Thus a new quantum number, *color* had to be introduced. It was confirmed by studying the crosssection of the electron-positron annihilation, that there exist three different colors, $N_c = 3$. Color-neutral bound states can be formed by either combing three quarks of all three colors or combining two quarks of the same flavor, one with color and another one with anti-color. This means bound states can be formed from three quarks of three different colors (baryons) or quark-anti-quark pairs (mesons). Mesonic states can be grouped into a singlet and an octet for $SU(3)$ and baryonic states can be grouped into a singlet, two octets, and one decuplet.

In the early, hot universe a state named the *Quark gluon plasma* (QGP) existed. It is supposed that the QCD transition from QGP to hadronic matter took place at $T = 150 - 200MeV$ at $t = 10^{-5} - 10^{-4}s$ after the Big Bang. The transition of free quarks and gluons in the QGP to confined particles in hadronic matter is called the *Deconfinement transition*. In the region of massless quarks QCD exhibits chiral symmetry, which is sponatneously broken. For hot temperatures this symmetry is expected to be restored. In the region of cold temperature and high baryon density there also exists a transition from hadronic matter to a color superconducting phase, see Figure 1.0.1. [29]

Using perturbative methods and simulations, some gaps in the QCD phase diagram could be filled. Though wide regions remain inaccessible. For nonzero chemical potential the reason is the sign problem, which makes standard Metropolis simulation not feasible. Several methods to solve this have been discovered, as phase quenched QCD, reweighting, purely imaginary chemical potential or simulating with the Compex Langevin algorithm, which is based on the *Complex Langevin Equation*. The latter will be the topic of this thesis, in particular the application to QCD on the lattice.

QCD on the lattice discretizes the theory onto a space-time lattice, where the discretization serves as a regulator. As full theory has many degrees of freedom, which make a simulation

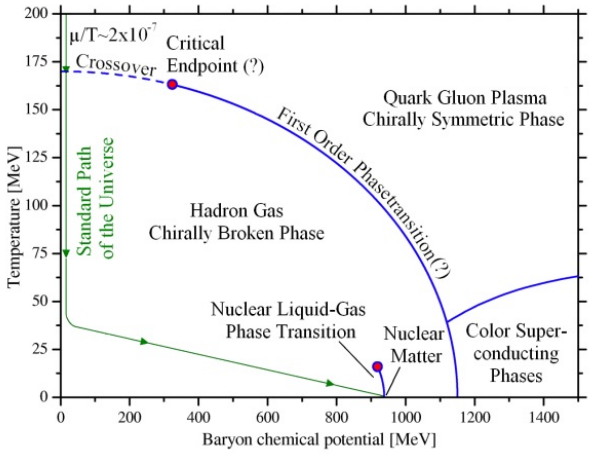

Figure 1.0.1: *QCD phase diagram, taken from [9].*

long and numerically costly, an effective theory will be introduced, which resembles QCD in a defined parameter region, having far less degrees of freedom than the original theory.

The goal of this thesis is twofold. The first part considers testing the Complex Langevin algorithm in the Deconfinement region for an effective lattice theory. As CL has been shown to work improperly in some cases, we will discuss some tools to control the simulation to obtain reasonable results. After an introduction to continuum QCD and lattice QCD, as well as an effective theory in chapter 2, we will continue in chapter 3 with introducing the aspects of the (Complex) Langevin equation (CLE). This will especially involve presenting the tools that can be used to control CL dynamics. It will also be shown how the CLE is applied to the effective theory. Numerical analysis of the deconfinement transition with and without fermionic contributions will be presented and discussed in section 5.2, as well as the application of the tools, which were introduced to control the dynamics of the CLE.

The second part contemplates the chiral condensate, which is the order parameter of the chiral transition. This will be purpose of chapter 4. The chiral condensate will be derived from the QCD action, followed by an analytical calculation of the chiral condensate in the effective theory. Though Wilson fermions, which will be used throughout the thesis, break chiral symmetry explicitly, it is of interest to see, if chiral restoration will take place nevertheless. This will be the subject of section 5.3.

Chapter 2

Quantum Chromodynamics

In this section we will recap some information about Quantum Chromodynamics (QCD) in the continuum as well as the discretization of QCD on the lattice (LQCD). The discretization serves as a regulator to the theory. [11] An effective Polyakov loop theory for strong coupling and heavy quarks in QCD had been derived, using Wilson fermions. [13][17] The main aspects of this effective theory will be displayed. Important symmetries of QCD and the effective theories will be discussed as well as the Columbia plot, giving an overview over phase transitions for zero chemical potential. Detailed information can be found in [11][15][28].

2.1 Continuum QCD

Quantum chromodynamics describes the theory of the strong interaction, acting on quarks and gluons. The fermions of the theory, the quarks, are described by Dirac 4-spinors,

$$\psi_{f,\alpha,c}(x), \quad \bar{\psi}_{f,\alpha,c}(x), \tag{2.1.1}$$

with indices in flavor space $f = 1, 2, ...N_f,\ N_f = 6$, in Dirac space $\alpha = 0, 1, 2, 3$ and in color space, $c = 1, 2, ..N_c^2 - 1,\ N_c = 3$. $x = (x_0, x_1, x_2, x_3)$ is a vector in Minkowski space-time. The bosons of the theory are the gluons,

$$A_{\mu,cd}(x). \tag{2.1.2}$$

$\mu = 0, 1, 2, 3$ is the Lorentz index and c, d are color indices. Gluons carry color charges as well and therefore are self-interacting with each other.
The continuum Lagrangian has a fermionic and a gluonic part. In Minkowski space-time it takes the form

$$\mathscr{L}_M = \mathscr{L}_f + \mathscr{L}_g = \sum_f \bar{\psi}_{f,\alpha,c}(i\gamma_\mu D^\mu - m)\psi_{f,\alpha,c} - \frac{1}{4}F^a_{\mu\nu}F^{a\mu\nu}. \tag{2.1.3}$$

$F^a_{\mu\nu}(x)$ is the field strength tensor of the gauge fields and defined in the following way:

$$F^a_{\mu\nu} = \partial_\mu A^a_\nu - \partial_\nu A^a_\mu + g f_{abc} A^b_\mu A^c_\nu, \tag{2.1.4}$$

with the gauge coupling g and the structure constant f_{abc}. We quantize the theory using Feynman's path integral formalism. Then we can describe the partition function of a quanized theory as an integral over the action,

$$\mathscr{Z}_M = \int d[\bar{\psi}, \psi, A] e^{i\mathscr{S}_M} = \int d[\bar{\psi}, \psi, A] e^{i\int d^4x \mathscr{L}_M}. \tag{2.1.5}$$

The integration measure over the entire field space was abbreviated as

$$d[\bar{\psi}, \psi, A] = \prod_x d\ \bar{\psi}(x) d\ \psi(x) dA(x). \tag{2.1.6}$$

The action is defined as the space-time integral over the Lagrangian:

$$\mathscr{S}_M = \int d^4x \mathscr{L}_M. \tag{2.1.7}$$

The formulation in Minkowski space-time, denoted by the index M, has a complex integrand $e^{i\mathscr{S}_M}$ for a real action $\mathscr{S}_M$, which will become oscillating. This would make numerical calculations not feasible. Therefore one can apply a Wick rotation changing from real to imaginary time:

$$t \to -i\tau,\ \mathscr{S}_M \to iS_E,\ \mathscr{L}_M \to -L_E. \tag{2.1.8}$$

This relates the Euclidean space-time and the Minkowski space-time. We furthermore compactify the Euclidean time τ to the interval $(0, \beta)$. β is the inverse temperature, $\beta = 1/T$. After Wick rotating the system we get the Lagrangian in Euclidean space-time

$$L_E = \bar{\psi}(\not{D}_\mu + m)\psi + \frac{1}{4} F^a_{\mu\nu} F^a_{\mu\nu}. \tag{2.1.9}$$

The sign of the mass term has now changed, compared to the term in Minkowski space-time. The partition function in Euclidean space-time then reads

$$Z_E = \int d[\bar{\psi}, \psi, A] e^{-S_E} = \int d[\bar{\psi}, \psi, A] e^{-\int_0^{1/T} d\tau \int d^3x L_E}. \tag{2.1.10}$$

To distinguish the Euclidean metric from the Minkowski metric, we will number the Euclidean Lorentz indices $\mu = 1, 2, 3, 4$, where $\mu = 4$ corresponds to the time component in Euclidean space-time. From now on we will stay with the Euclidean action without denoting it explicitly anymore, leaving out the superscript "E".

2.2 QCD on the lattice

To perform lattice simulations we need to discretize the theory of QCD onto a lattice. In this section we will see how the discretization to the lattice is done. We will introduce the gauge fields on the lattice, followed by adding fermions. The latter is a more challenging business. This overview follows [15]. We define the four dimensional lattice Λ as

$$\Lambda = \{n = (n_1, n_2, n_3, n_4) \mid n_1, n_2, n_3 = 0, 1, ...N_s - 1;\ n_4 = 0, 1, ..N_\tau - 1\}, \tag{2.2.1}$$

where $n \in \Lambda$ denotes points on the lattice with lattice spacing a. For simplicity $a_s = a_\tau = a$, but in general they can be chosen distinctly. N_τ is the temporal extent of the lattice and N_s is the spatial extent. We will sometimes refer to the spatial lattice $\Lambda_s \subset \Lambda$,

$$\Lambda_s = \{\boldsymbol{n} = (n_1, n_2, n_3) \mid n_1, n_2, n_3 = 0, 1, ...N_s - 1\}. \tag{2.2.2}$$

2.2.1 Gauge fields on the lattice

The gauge fields can be written as gauge links $U_\mu(n)$ on the lattice, connecting the lattice points n and $n + a\hat{\mu}$ in positive μ-direction. We can also define gauge links that are oriented in negative μ-direction as $U_{-\mu}(n) = U_\mu^\dagger(n - a\hat{\mu})$. The relation between the gauge links, which are elements of the $SU(3)$ group, and the continuum gauge fields, which are elements of a Lie algebra, is

$$U_\mu(n) = e^{igaA_\mu(n)}, U_\mu(n) \in SU(3). \tag{2.2.3}$$

A gauge invariant quantity is the shortest, non-trivial closed loop formed by four gauge links, the *plaquette*:

$$U_{\mu,\nu}(n) = U_\mu(n)U_\nu(n + \hat{\mu})U_\mu^\dagger(n + \hat{\nu})U_\nu^\dagger(n). \tag{2.2.4}$$

Now we can use the plaquette to define the gauge-invariant Wilson gauge action:

$$S_g = \frac{\beta}{2N_c} \sum_P (\mathrm{Tr}(U_P) + \mathrm{Tr}(U_P^\dagger)), \quad \beta = \frac{2N_c}{g^2}. \tag{2.2.5}$$

This action consists of a sum over permutations of the plaquettes and the inverse of the coupling constant g.
One can show that the trace over a closed loop is a gauge-invariant quantity. Two commonly used objects are the *Wilson loop* and the *Polyakov loop*.

Wilson loop

The Wilson loop describes a loop between spatial points m and n and temporal points 0 and n_t,

$$\mathcal{L} : (\boldsymbol{m}, n_t) \xrightarrow{S} (\boldsymbol{n}, n_t) \xrightarrow{T^\dagger} (\boldsymbol{n}, 0) \xrightarrow{S^\dagger} (\boldsymbol{m}, 0) \xrightarrow{T} (\boldsymbol{m}, n_t). \tag{2.2.6}$$

$S(\boldsymbol{m}, \boldsymbol{n}, n_t)$ is a *Wilson line*, connecting two spatial points $\boldsymbol{m}, \boldsymbol{n}$ at time n_t and $T(\boldsymbol{n}, n_t)$ is the temporal transporter connecting the times 0 and n_t at the same point $\boldsymbol{n}$. To make this loop invariant we have to take the trace, which defines the Wilson loop:

$$W[U] = \mathrm{Tr}\left[\prod_{(n,\mu)\in\mathcal{L}} U_\mu(n)\right]. \tag{2.2.7}$$

Polyakov loop

Next we consider a loop with temporal extent N_τ and we can gauge the spatial links to $\mathbb{1}$, leading to $S = \mathbb{1}$. This leaves us with two temporal propagators $T(\boldsymbol{m}, N_\tau), T(\boldsymbol{n}, , N_\tau)^\dagger$, which are oriented in opposite directions. Due to periodic boundary conditions in temporal direction those are closed loops winding around the temporal extent. This quantity is a temporal Wilson line,

$$W(\boldsymbol{m}) = \prod_{j=0}^{N_\tau - 1} U_4(\boldsymbol{m}, j). \tag{2.2.8}$$

We can make these loops gauge-invariant, by taking the trace,

$$L(\boldsymbol{m}) = \mathrm{Tr}W(\boldsymbol{m}) = \mathrm{Tr}\left[\prod_{j=0}^{N_\tau - 1} U_4(\boldsymbol{m}, j)\right]. \tag{2.2.9}$$

This quantity defines the Polyakov loop.
The Polyakov loop plays an important rule in the pure gauge deconfinement transition. We consider the correlator of a static quark - anti-quark pair,

$$\langle L(\boldsymbol{m})L(\boldsymbol{n})^\dagger\rangle = e^{-F_{q\bar{q}}(r)/T}. \tag{2.2.10}$$

$F_{q\bar{q}}$ is the free energy of the quark anti-quark pair with $r = a|\boldsymbol{m}-\boldsymbol{n}|$. The free energy is growing with the distance between the quark and the anti-quark r, and therefore

$$\lim_{r\to\infty}\langle L(\boldsymbol{m})L(\boldsymbol{n})^\dagger\rangle = \langle L(\boldsymbol{m})\rangle\langle L(\boldsymbol{n})^\dagger\rangle = |\langle L\rangle|^2 \to 0. \tag{2.2.11}$$

This makes the Polyakov loop serve as an order parameter for the deconfinement transition, where $\langle L\rangle$ vanishes in the confined phase and $\langle L\rangle$ is finite in the deconfined phase. For low temperatures the system stays in the confined phase, until at a critical temperature T_c the system undergoes a phase transition and will stay in the second phase for $T > T_c$.
The expectation value of a single Polyakov loop can be seen as the probability of observing a single static quark,

$$|\langle L\rangle| \propto e^{-F_q/T}. \tag{2.2.12}$$

In the confined phase $F_q \to \infty$, which means one would need an infinite amount of energy to remove a single quark from the system.

2.2.2 Fermions on the lattice

A more delicate business is to introduce fermions to the theory on the lattice. We will see that a naive introduction analogously to introducing the gauge fields will not be sufficient. We will introduce the Wilson action for fermions.

Naive discretization of the fermion action and fermion doubling

We use the discretized fermion spinors [15]

$$\psi(n),\ \bar{\psi}(n), n \in \Lambda. \tag{2.2.13}$$

One can discretize the partial derivative acting on the quark field using the central difference method,

$$\partial_\mu\psi(n) = \frac{1}{2a}(\psi(n+\hat{\mu}) - \psi(n-\hat{\mu})) + O(a^2). \tag{2.2.14}$$

It appears that the fermion action is not gauge-invariant when using this discretization of the derivative. To make the action invariant we need to add gauge links U_μ and we get a naive formulation of the fermion action: [20]

$$\begin{aligned} S_N &= a^4\frac{1}{2a}\sum_{n,\mu}\left[\bar{\psi}_n\gamma_\mu U_{\mu,n}\psi_{n+\hat{\mu}} - \bar{\psi}_n\gamma_\mu U^\dagger_{\mu,n}\psi_{n-\hat{\mu}}\right] + a^4 m\sum_n\bar{\psi}_n\psi_n \\ &= a^4\sum_n\bar{\psi}_n\left(\frac{1}{2a}\sum_\mu\gamma_\mu\left[U_{\mu,n}\delta_{n,m-\hat{\mu}} - U^\dagger_{\mu,n}\delta_{n,m+\hat{\mu}}\right] + m\delta_{nm}\right)\psi_m \\ &\equiv a^4\sum_n\bar{\psi}_n D(n,m)\psi_m. \end{aligned} \tag{2.2.15}$$

This action is indeed invariant under a gauge transformation.
$D(n,m)$ is the naive Dirac operator in coordinate-space. One can transform the Dirac operator to momentum-space and calculate the inverse of it,

$$D^{-1}(p) = \frac{m - \frac{i}{a}\sum_\mu \gamma_\mu \sin(p_\mu a)}{m^2 + \frac{1}{a^2}\sum_\mu \gamma_\mu \sin^2(p_\mu a)}. \tag{2.2.16}$$

The massless inverse propagator $D^{-1}(p)$ has poles for $p_\mu = 0, \pi/a$, which means for $p = (p_0, p_1, p_2, p_3)$ there are in total 16 different momenta p_μ leading to a pole of $D^{-1}(p)$. This corresponds to 16 fermions, where we would expect to get only one. These 15 unphysical fermions are called doublers and their existence arising from the naive formulation of the fermion action is called *fermion doubling* or *species doubling*. One possibility to remove the doublers is the introduction of an additional term to the action, the *Wilson term*.

Wilson fermions

To remove the doublers, as just mentioned, we can add the Wilson term. Adding Wilson fermions adds a mass term which highers the mass of the fermion doublers to values around the cutoff energy. Therefore the doublers decouple from the theory. The mass term looks as follows [28]:

$$\begin{aligned} m\sum_n \bar\psi_n\psi_n \;&\to\; m\sum_n \bar\psi_n\psi_n + \frac{ar}{2}\sum_{n\mu}\partial_\mu\bar\psi_n\partial_\mu\psi_n \\ &= m\sum_n \bar\psi_n\psi_n + \frac{ar}{2}\sum_{n\mu}\frac{1}{a}(\bar\psi_{n+a\hat\mu} - \bar\psi_n)\frac{1}{a}(\psi_{n+a\hat\mu} - \psi_n) \\ &= \left(m + \frac{4r}{a}\right)\sum_n \bar\psi_n\psi_n - \frac{r}{2a}\sum_{n\mu}(\bar\psi_{n+a\hat\mu}\psi_n + \bar\psi_n\psi_{n+a\hat\mu}). \end{aligned} \tag{2.2.17}$$

The parameter r is called the *Wilson parameter*. In most applications one will see it set to $r = 1$. However, we will continue the derivation with a general r until we will derive the chiral condensate. For the simulations $r = 1$ was used.
Adding the Wilson term to the naive fermion action we get the result for the fermionic action with Wilson fermions,

$$\begin{aligned} S_F &= a^4\left(\frac{1}{2a}\sum_{n,\mu}\left[\bar\psi_n\gamma_\mu U_{\mu,n}\psi_{n+\hat\mu} - \bar\psi_n\gamma_\mu U^\dagger_{\mu,n-\hat\mu}\psi_{n-\hat\mu}\right]\right. \\ &\quad \left. + \left(m + \frac{4r}{a}\right)\sum_n \bar\psi_n\psi_n - \frac{r}{2a}\sum_{n\mu}(\bar\psi_n U_{\mu,n}\psi_{n+a\hat\mu} + \bar\psi_n U^\dagger_{\mu,n-\hat\mu}\psi_{n-a\hat\mu})\right) \\ &= a^4\left(\left(m + \frac{4r}{a}\right)\sum_n \bar\psi_n\psi_n - \frac{1}{2a}\sum_{n,\mu}\left[\bar\psi_n(r-\gamma_\mu)U_{\mu,n}\psi_{n+\hat\mu} + \bar\psi_n(r+\gamma_\mu)U^\dagger_{\mu,n-\hat\mu}\psi_{n-\hat\mu}\right]\right) \\ &= a^3\left((am+4r)\sum_n \bar\psi_n\psi_n - \frac{1}{2}\sum_{n,\mu}\left[\bar\psi_n(r-\gamma_\mu)U_{\mu,n}\psi_{n+\hat\mu} + \bar\psi_n(r+\gamma_\mu)U^\dagger_{\mu,n-\hat\mu}\psi_{n-\hat\mu}\right]\right). \end{aligned} \tag{2.2.18}$$

It is commonly used to rescale the fermion fields by a factor $a^{-3/2}$ [19], and with

$$C = am + 4r \equiv 1/(2\kappa_f) \tag{2.2.19}$$

we obtain the rescaled fermion fields

$$\bar{\psi} \to \bar{\psi}_r = a^{-3/2} C^{-1/2} \bar{\psi}, \quad \psi \to \psi_r = a^{-3/2} C^{-1/2} \psi. \tag{2.2.20}$$

Alltogether the rescaled fermion action reads [20]

$$S^f_{F,r} = a^4 \left(\sum_n \bar{\psi}_n \psi_n - \kappa_f \sum_{n,\mu} \left[\bar{\psi}_n (r - \gamma_\mu) U_{\mu,n} \psi_{n+\hat{\mu}} + \bar{\psi}_n (r + \gamma_\mu) U^\dagger_{\mu,n-\hat{\mu}} \psi_{n-\hat{\mu}} \right] \right). \tag{2.2.21}$$

The index r denotes quantities formulated using the rescaled fields $\bar{\psi}_r, \psi_r$. As the rescaled action is commonly used as the Wilson fermion action, we will leave out the index r in upcoming calculations and come back to this specific notation, when it is needed to derive the expression for the chiral condensate.

2.3 An effective Polyakov loop theory for LQCD

Now that we know how the QCD action on the lattice looks like, we will derive an effective action, which reproduces QCD in some particular parameter region and is numerically less costly than the full theory. We will shortly review the most important steps of deriving the effective theory.

We start with LQCD in $(3+1)$ dimensions including the Wilson gauge action from Equation 2.2.5 and the action for Wilson fermions from Equation 2.2.21. Combining these results we can write the partition function

$$Z = \int d[U_\mu] \prod_{N_f} \det Q_f e^{-S_g}. \tag{2.3.1}$$

The integration measure was abbreviated as

$$\int d[U_\mu] = \prod_{n \in \Lambda} \prod_{\mu=1}^{4} \int dU_\mu(n). \tag{2.3.2}$$

To derive the effective action we have to perform two series expansions: For the gauge action we have to perform a strong coupling expansion in $\beta = \frac{2N_c}{g^2} \to 0$ and for the fermion determinant we do a hopping parameter expansion in $\kappa = 1/(2am+8) \to 0$. We will though see that the theory will be valid for higher values of the expansion parameters, the strong coupling expansion will be valid up to the region of the deconfinement transition, where $\beta \approx 6$. [17] We will derive an expression for the gauge contribution to the effective action and the fermion contribution, respectively. In the end the effective partition function will be of the form

$$Z_{eff} = \int d[U_4] e^{-S_{eff}}, \; -S_{eff} = \ln \int d[U_i] \prod_{N_f} \det Q_f e^{-S_g}. \tag{2.3.3}$$

2.3.1 Pure gauge action in the strong coupling limit

The derivation of the effective theory for the strong coupling expansion in $U(N_c)$, and in particular $N_c = 2, 3$, with Wilson gauge action has been done in detail in [17]. We will focus on $N_c = 3$ and start with the partition function

$$Z = \int d[U_\mu] \prod_P \exp \left[\frac{\beta}{2N_c} (\mathrm{Tr} U_P + \mathrm{Tr} U_P^\dagger) \right]. \tag{2.3.4}$$

Using periodic boundary conditions in temporal direction and integrating over spatial gauge links $U_i(\boldsymbol{n}, n_4)$ to get the effective action:

$$\begin{aligned} Z_{eff} &= \int d[U_4] e^{-S_{eff}} \\ -S_{eff} &= \ln \int d[U_i] e^{-S_g} \equiv \lambda_1 S_1 + \lambda_2 S_2 + \dots \end{aligned} \tag{2.3.5}$$

The effective action has been expanded around $\beta = 0$ applying a character expansion. Then it was sorted by orders of effective couplings $\lambda_n = \lambda_n(\beta, N_\tau)$. After integrating out the spatial gauge links the S_n will only depend on temporal gauge links $U_4(\boldsymbol{n}, n_4)$. The theory can then be reformulated in terms of Polyakov loops,

$$L_j \equiv L(\boldsymbol{n}_j) \equiv \mathrm{Tr} W(\boldsymbol{n}_j) \equiv \mathrm{Tr} \prod_{n_4=0}^{N_\tau - 1} U_4(\boldsymbol{n}_j, n_4). \tag{2.3.6}$$

I introduced the shortcut $L_j = L(\boldsymbol{n}_j)$ for readability. This effective theory is now three dimensional, as the time dependence is only implicit.

Performing a character expansion and finally doing a finite cluster expansion results in the action for nearest and next-to-nearest neighbor interactions for $SU(3)$:

$$\begin{aligned} S_1 &= \sum_{<ij>} \ln \left[1 + \lambda_1 (L_i L_j^* + L_i^* L_j)\right], \ \lambda_1 = u^{N_\tau} + O(u^{N_\tau + 4}) \\ S_2 &= \sum_{[kl]} \ln \left[1 + \lambda_2 (L_k L_l^* + L_k^* L_l)\right], \ \lambda_2 = u^{2N_\tau + 2} + O(u^{2N_\tau + 4}) \end{aligned} \tag{2.3.7}$$

$< ij >$ denotes the set of all nearest neighbor pairs on the lattice, separated by the lattice spacing a and $[kl]$ denotes the set of all next-to-nearest neighbor pairs with a distance $a\sqrt{2}$ apart. λ_1, λ_2 are the respective nearest and next-to-nearest neighbor couplings and can be expressed in terms of $u = \frac{\beta}{18} + O(\beta^2)$[1] and the exact structure depends on N_τ. Corrections to the leading order $\lambda_1(u, N_\tau) = u^{N_\tau}$ come from additional plaquettes and can be found in [17].

The contribution of higher order representations can be included as well, e.g. the one from the adjoint representation,[2]

$$S_a = \sum_{\langle ij \rangle} (1 + \lambda_a (\chi_a(W_i) \chi_a(W_j))), \ \lambda_a = \frac{9}{8} u^{2N_\tau} + O(2u^{N_\tau + 1}) \tag{2.3.8}$$

with the characters in the adjoint representation $\chi_a(W_i) = |L_i|^2 - 1$.

[1] Higher order corrections to u up to $O(\beta^{14})$ can be found in [19], eq. 3.357 and following.

[2] This is how the contribution to the gauge action of the adjoint representation was implemented in the Complex Langevin algorithm and the Metropolis algorithm presented in [25]. It has been ruled out and discussed recently, that this definition is not sufficient. The results, which will be presented in chapter 5, had already been generated and thus will suffer from this issue.

2.3.2 Heavy fermions in the hopping parameter expansion

Next we introduce fermions to the effective theory. This will be done via a hopping parameter expansion in $\kappa_f = 1/(2am_f + 8) = 0$ [20]. This is an expansion around static, infinitely heavy quarks, as $\kappa_f \propto \frac{1}{m_f} \to 0 \;\leftrightarrow m_f \to \infty$. f is the flavor index, the mass and hence the hopping parameter take different values for different quarks. We will start in the strong coupling region $\beta = 0$. Including dynamical quarks then gives corrections to the static limit. For the kinetic part we will derive the contributing action in different orders of κ_f, up to κ_f^4.

We start with rewriting and expanding the Wilson Dirac operator Q_f in terms of the hopping parameter, [20]

$$\det(Q_f) = \det[\mathbb{1} - \kappa_f M] = \exp(\mathrm{Tr}\log[\mathbb{1} - \kappa_f M]) = \exp\left(\sum_{l=1}^{\infty} \frac{\kappa_f}{l} \mathrm{Tr} M^l\right), \tag{2.3.9}$$

with the *hopping matrix* M. We can factorize the quark determinant into a contribution for static and kinetic quarks respectively,

$$\det(Q_f) = \det(Q_{f,stat}) \cdot \det(Q_{f,kin}) = \det[\mathbb{1} - T] \det[\mathbb{1} - \frac{S^+_{n,n+\hat{i}} + S^-_{n,n+\hat{i}}}{\mathbb{1} - T}]. \tag{2.3.10}$$

$Q_{f,stat}$ is the inverse static propagator, which describes hoppings in temporal direction, and $Q_{f,kin}$ is the inverse kinetic quark propagator, which describes hoppings in spatial and temporal direction.
In the following the static and the kinetic determinant will be discussed. In the end we will get an expression for the effective action.

Static quark determinant

For the static quark contribution we only consider temporal hoppings, as static quarks are assumed to be infinitely heavy and thus only propagate in time. Forming closed quark lines can only be achieved by windings around the temporal extent, which was defined as the temporal Wilson line. With this the contribution for static quarks takes the form

$$\det_{c,s,n}(Q_{f,stat}) = \prod_{\boldsymbol{n}} \det_c[\mathbb{1} + h_1(\kappa_f, N_\tau, \mu)W]^2 \det_c[\mathbb{1} + \bar{h}_1(\kappa_f, N_\tau, \mu)W^\dagger]^2. \tag{2.3.11}$$

We can make use of relations for the spin- and the color determinant and rewrite the static determinant in terms of traces over temporal Wilson lines, the Polyakov loops. Doing so we get the contributions of quarks and anti-quarks to the fermion action of the static determinant,

$$\det Q_{f,stat} = \prod_{\boldsymbol{n}} (1 + h_1 L_{\boldsymbol{n}} + h_1^2 L^\dagger_{\boldsymbol{n}} + h_1^3)^2 (1 + \bar{h}_1 L^\dagger_{\boldsymbol{n}} + \bar{h}_1^2 L_{\boldsymbol{n}} + \bar{h}_1^3)^2, \tag{2.3.12}$$

with the effective fermionic coupling constants $h_1 = e^{N_\tau(a\mu + \ln 2\kappa)}$, $\bar{h}_1 = e^{N_\tau(-a\mu + \ln 2\kappa)}$.
The static determinant for N_f distinct flavors looks like

$$\det(Q_{stat}) = \prod_{f=1}^{N_f} \det(Q_{f,stat}), \tag{2.3.13}$$

and for N_f degenerate flavors it looks like

$$\det(Q_{stat}) = \det(Q_{f,stat})^{N_f} = \prod_{\boldsymbol{n}} (1 + h_1 L_{\boldsymbol{n}} + h_1^2 L^\dagger_{\boldsymbol{n}} + h_1^3)^{2N_f} (1 + \bar{h}_1 L^\dagger_{\boldsymbol{n}} + \bar{h}_1^2 L_{\boldsymbol{n}} + \bar{h}_1^3)^{2N_f}. \tag{2.3.14}$$

Kinetic quark determinant up to order κ^4

Next we consider dynamical quarks. The kinetic quark determinant consists of the static quark propagator and two spatial hoppings, in positive (S^+) and negative (S^-) spatial direction. From (2.3.10) we get

$$\det Q_{kin} = \det\left[\mathbb{1} - \frac{S^+ + S^-}{\mathbb{1} - T}\right] = \det\left[\mathbb{1} - P - M\right] = \exp\left(\mathrm{Tr}\sum_{l=1}^{\infty}(-\frac{1}{l}(P+M)^l)\right) \quad (2.3.15)$$

We introduced the new quantities P (M), which contain the static quark propagator and a spatial hop in positive (negative) direction. It is necessary to derive an expression for the static propagator before one continues with calculating the expression for the kinetic quark determinant. The static propagator describes purely temporal hoppings and has been calculated in [20]. Knowing the expression for the static propagator one can perform the sum in (2.3.15). Each spatial hop P and M comes with a factor of κ. We will perform the sum up to $n = 4$, so that we arrive at the desired κ^4-contribution of the kinetic determinant. To form a closed loop, we need an equal amount of P's and M's, so terms with an unequal number of P's and M's will not contribute, e.g. P, M, $PPPM$, $PMMM$ and permutations of that.
After performing the sum and collecting terms with the same contribution we obtain

$$\begin{aligned} e^{-S_{kin}} = \det Q_{kin} &= \exp\left(-\mathrm{Tr}(PM) - \mathrm{Tr}(PPMM) - \frac{1}{2}\mathrm{Tr}(PMPM) + O(\kappa^6)\right) \\ &= 1 - \mathrm{Tr}(PM) - \mathrm{Tr}(PPMM) - \frac{1}{2}\mathrm{Tr}(PMPM) + \frac{1}{2}(\mathrm{Tr}(PM))^2 + O(\kappa^6). \end{aligned} \quad (2.3.16)$$

To be able to perform the integration over the spatial links U_i we expanded the exponential in the second step.

We furthermore only consider pairs of P's and M's that hop in the same spatial direction and therefore form closed loops. There arise different contributions of the aforementioned terms [18]:

$$\begin{aligned} \sum_{ij}\mathrm{Tr}(P_iM_j) &= \sum_i \mathrm{Tr}(P_iM_i) \\ \sum_{ijkl}\mathrm{Tr}(P_iP_jM_kM_l) &= \sum_i \mathrm{Tr}(P_iP_iM_iM_i) + \sum_{i\neq j}\mathrm{Tr}(P_iP_jM_jM_i) + \sum_{i\neq j}\mathrm{Tr}(P_iP_jM_iM_j) \\ \frac{1}{2}\sum_{ijkl}\mathrm{Tr}(P_iM_jP_kM_l) &= \frac{1}{2}\sum_i \mathrm{Tr}(P_iM_iP_iM_i) + \frac{1}{2}\sum_{i\neq j}\mathrm{Tr}(P_iM_jP_iM_j) + \frac{1}{2}\sum_{i\neq j}\mathrm{Tr}(P_iM_jP_jM_i) \\ \frac{1}{2}\sum_{ijkl}\mathrm{Tr}(P_iM_j)\mathrm{Tr}(P_kM_l) &= \frac{1}{2}\sum_i \mathrm{Tr}(P_iM_i)\sum_j \mathrm{Tr}(P_jM_j) \end{aligned} \quad (2.3.17)$$

The final results for the κ^4- corrections can be found in the appendix of [20].

Leading order κ^2 contribution

The leading order correction to static determinant is a nearest-neighbour interaction of order κ^2, which means we include two spatial hops. We already discussed, that only closed loops

give contributions and therefore to form a closed loop with two spatial hoppings the P and M have to describe spatial hoppings in the same spatial direction, P_i, M_i. The kinetic determinant of order κ^2 then takes the form

$$\det Q_{kin} = e^{-\sum_i \mathrm{Tr}(P_i M_i)}. \tag{2.3.18}$$

If we want to calculate the partition function of the leading order kinetic determinant, we have to perform the gauge integral over the determinant. This can not be done with the determinant in exponential form. Therefore we have to expand the exponential, [20]

$$\begin{aligned}\int d[U_i] \det Q_{kin} &= 1 - \int d[U_i] \sum_i \mathrm{Tr}(P_i M_i) + O(\kappa^4) \\ &= 1 - 2h_2 N_f \sum_{\boldsymbol{n},i} (W_{11}(\boldsymbol{n}) - W_{11}^\dagger(\boldsymbol{n})) \cdot (W_{11}(\boldsymbol{n}+\hat{i}) - W_{11}^\dagger(\boldsymbol{n}+\hat{i})) + O(\kappa^4).\end{aligned} \tag{2.3.19}$$

The leading order correction to the static determinant is an interaction between two neighboring lattice points. From the partition function we see that this interaction can take place between two fermions, two antifermions or one fermion and one antifermion. The strength of this interaction to leading order is described by the coupling

$$h_2 = \frac{\kappa^2 N_\tau}{N_c}. \tag{2.3.20}$$

The degrees of freedom are now the traces over Wilson lines, for which we introduced the following abbreviation,

$$W_{n+m,n} \equiv \mathrm{Tr}\frac{(h_1 W)^n}{(1+h_1 W)^{n+m}}, \quad W^\dagger_{n+m,n} \equiv \mathrm{Tr}\frac{(\bar{h}_1 W^\dagger)^n}{(1+\bar{h}_1 W^\dagger)^{n+m}}. \tag{2.3.21}$$

Those quantities don't have a temporal contribution anymore. It can be shown that the $W_{n+m,n}$ can be reformulated in terms of Polyakov loops. This will be shown and applied in chapter 3. To get the correct convergence behavior it is convenient to do a resummation [20] and write the action back into the exponential.[3]

2.3.3 Gauge corrections

We started the derivation for the fermionic part of the effecitve theory in the strong coupling limit, at $\beta = 0$. Introducing a nonzero β also introduces mixing terms between strong coupling and hopping parameter expansion terms. The contributions coming from the mixing terms can be absorbed into the coupling constants such that $\lambda_1(\beta) = \lambda_1(\beta, \kappa)$, $h_1(\kappa) = h_1(\kappa, \beta)$ and $h_2(\kappa) = h_2(\kappa, \beta)$ and for higher order couplings respectively. There will be corrections to the gauge action, coming from fermions and corrections to the fermion action coming from gauge links.

Fermion corrections to gauge action
The first correction comes from the possibility to replace each gaug plaquette by four spatial hoppings. This can be done allover the lattice and therefore this can be seen as a shift in β,

$$\beta \to \beta + 48 N_f \kappa^4. \tag{2.3.22}$$

[3] For the κ^2 contribution the resummation has been explicitly shown in [25].

It is also possible to only replace two neighboring plaquettes by six spatial hoppings,

$$\lambda_1(\beta,\kappa) = u^{N_\tau} + \frac{16 N_f N_\tau \kappa}{9u^2}. \tag{2.3.23}$$

Gauge corrections to fermion action
The gauge corrections to the nearest-neighbor interaction are

$$h_1(\kappa,u,N_\tau \geq 3) = \exp\left[N_\tau(\mu+\ln(2\kappa))\right] \exp\Big[6N_\tau\kappa^2 u \left(\frac{1-u^{N_\tau-1}}{1-u} + 4u^4 - 12\kappa^2 + 9\kappa^2 u + 4\kappa^2 u^2 - 4\kappa^4\right)\Big], \tag{2.3.24}$$

and analogously for $\bar{h}_1$. Corrections to higher order gauge couplings up to κ^4-corrections can be found in [20].

2.4 Symmetries of full QCD and the effective action

2.4.1 $Z(3)$ symmetry

QCD in the pure gauge sector and in the quenched limit, which is pure gauge combined with static, infinitely heavy quarks, $m_f \to \infty$, exhibits the $Z(Nc=3)$, or center symmetry. [20][24] For a center transformation,

$$U_4(\boldsymbol{x},t) \to z U_4(\boldsymbol{x},t), \tag{2.4.1}$$

one has to multiply all temporal gauge links U_4 at one particular time $x_4 = t$ with the same element z,

$$z = \{1, e^{i2/3\pi}, e^{-i2/3\pi}\} \ \in Z(3) \subset SU(3). \tag{2.4.2}$$

z is an element of the center group $Z(3)$ of $SU(2)$ and commutes with the gauge links. It can be shown, that the plaquette is invariant under a center transformation. [15] This is due to the fact that plaquette closes in such a way that there is one temporal gauge link oriented in one direction and another temporal gauge link oriented in opposite direction. By the property $zz^\dagger = \mathbb{1}$ this factor cancels out by a trivially closing loop. From this follows that a pure gauge theory, formed in terms of plaquettes is invariant under a center transformation. The pure gauge part of the effective theory is constructed in a way, such that it is invariant under a $Z(3)$ transformation.
A single Polyakov loop winds around the temporal extent and picks up a center element,

$$L(\boldsymbol{x}, x_4 + N_\tau) \to z L(\boldsymbol{x}, x_4). \tag{2.4.3}$$

Therefore a Polyakov loop is not invariant under a $Z(3)$ transformation.
If the $Z(3)$ symmetry is realized, the Polyakov loop will average out over those three phases,

$$\langle L \rangle = \langle 1L + e^{i2/3\pi}L + e^{-i2/3\pi}L \rangle = 0. \tag{2.4.4}$$

In case of a broken $Z(3)$ symmetry, one of the three sectors is favored to be populated and therefore $\langle L \rangle$ does not vanish anymore. This is another perspective to show that the Polykov loop serves as an order parameter for the $Z(3)$ transition, as it was also argued in section 2.2.1. The breaking of the center symmetry happens at a critical temperature T_c.

What happens, if we add dynamical fermions to the theory? When performing the sum in the exponent in Equation 2.3.15, one has to take into account all loops, which also includes terms like $\kappa^{N_\tau}(L+L^*)$. As Polyakov loops are not invariant under $Z(3)$ transformations, dynamical quarks break center symmetry explicitly. Therefore the Polyakov loop is strictly speaking not an order parameter anymore. One can view the dynamical quarks corresponding to a symmetry breaking term in the potential, [29]

$$V(L) \to V(L) - h_1 Re(L), \tag{2.4.5}$$

with $h_1 \propto (2\kappa)^{N_\tau}$ (for $\mu = 0$). The hopping parameter is proportional to the inverse mass. Therefore a small value of κ corresponds to a high mass. Furthermore a small value of $\kappa < 1$ leads to a small value of h_1. Hence the explicit symmetry breaking effect of big masses is small. It can be shown that there is a critical coupling h_c. For values $h < h_c$ the transition is of first order and for $h > h_c$ the transition becomes a crossover. This will be subject of section 5.2.

2.4.2 Chiral symmetry

QCD with N_f massless quarks exhibits chiral symmetry: [15]

$$U(N_f)_L \otimes U(N_f)_R = SU(N_f)_L \otimes SU(N_f)_R \otimes U(1)_V \otimes U(1)_A, \tag{2.4.6}$$

where the symmetry $SU(N_f)_L \otimes SU(N_f)_R$ is called chiral symmetry. Chiral symmetry leads to a decoupling of left- and right-handed massless fermions in the action,

$$L(\psi, \bar{\psi}, A) = \bar{\psi}_R \not{D} \psi_R + \bar{\psi}_R \not{D} \psi_R. \tag{2.4.7}$$

Where

$$\psi_{R,L} = P_{R,L}\psi, \ \bar{\psi}_{R,L} = \bar{\psi} P_{R,L}, \tag{2.4.8}$$

with the left- and right-handed projectors

$$P_{R,L} = \frac{1}{2}(1 \pm \gamma_5). \tag{2.4.9}$$

The mass-term of the action mixes the two components,

$$m\bar{\psi}\psi = m(\bar{\psi}_R \psi_L + \bar{\psi}_L \psi_R), \tag{2.4.10}$$

and therefore a massterm explicitly breaks the chiral symmtery.

We consider again the symmetry of the massless fermion Lagrangian. The axial $U(1)_A$-symmetry is explicitly broken by quantum effects, called *axial anomaly*. The axial Noether current corresponding to this symmetry, $j_{\mu,5} = \bar{\psi}\gamma_\mu\gamma_5\psi$, is not conserved, $\partial_\mu j_{\mu,5} \neq 0$. This is called *Adler-Bell-Jackiw anomaly*. [23]
The chiral symmetry is spontaneously broken by the vacuum expectation value of scalar quark densities, into

$$SU(2)_L \otimes SU(2)_R \to SU(2)_V. \tag{2.4.11}$$

In real-world QCD there is an approximate chiral symmetry for the two lightest quarks, the up- and down-quark. Compared to the other quarks they have rather light masses, $m_u = 2.16(49)MeV, \ m_d = 4.67(48)MeV$[7] and therefore are referred to as light quarks. If

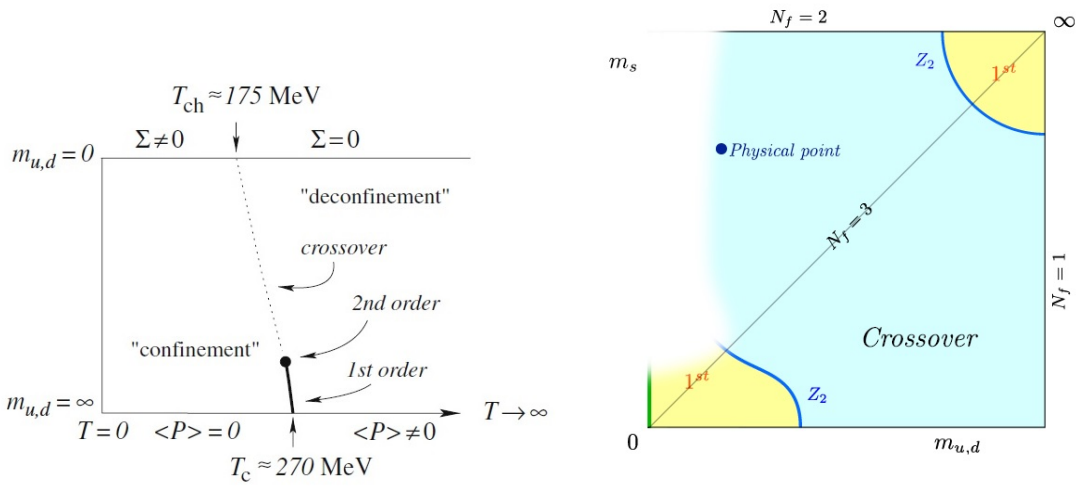

(a) Deconfinement transition taken from [15].

(b) Columbia plot taken from [27]

Figure 2.4.1: *Phase structure of QCD for* $\mu = 0$.

chiral symmetry was realized one would expect degenerate masses for the nucleons and their respective particles with opposite parity. But one observes that nucleons have the masses $m_N \approx 940MeV$, while $m_{N*} \approx 1535MeV$. [15]
The order parameter for chiral symmetry is the chiral condensate $\langle\bar{\psi}\psi\rangle$. The chiral condensate is not invariant under a chiral transformation, thus a non-vanishing chiral condensate corresponds to the spontaneously broken chiral symmetry. It is expected that for high temperatures chiral symmetry is restored.
The Goldstone theorem tells, that to a spontanously broken continous symmetry there exist massless Goldstone bosons for each generator of the broken symmetry. For massless QCD with $N_f = 2$ this would correspond to $N_f^2 - 1 = 3$ massless Goldstone bosons, the pions. As the two lightest quarks have nonzero masses, the pions gain their masses by explicit chiral symmetry breaking.

In the effective theory with Wilson fermions chiral symmetry is explicitly broken, even in the massless case. This is due to the introduction of the Wilson-term, that solves the problem of the doublers, but leads to an explicit breaking of chiral symmetry. The *No-go theorem* states, that one can not construct a chiral symmetric theory on the lattice and getting rid of the fermion doublers at the same time. [21]

2.4.3 LQCD transitions at $\mu = 0$

We saw that the deconfinement transition is related to a spontaneous breaking of the $Z(3)$ symmetry. The phase transition takes place at a critical temperature $T_c \approx 270MeV$, as can be seen in Figure 5.2.11(a). In the case of two degenerate quark masses, $m_u = m_d$, when decreasing the mass the first order transtion goes over into a second order transition and afterwards the transition becomes a crossover. Phase transitions of Lattice QCD at zero chemical potential can be described by the Columbia plot. The Columbia plot in Figure 5.2.11(b) shows the type of phase transition depending on the quark masses for degenerate up- and down-quarks and the strange-quark. The masses each range from 0 to ∞. The

upper right corner describes the pure gauge case, as infinitely heavy quarks decouple from the theory. The deconfinemnt transition is of first order and weakens with finite, decreasing quark masses. This is because dynamical quarks break the $Z(3)$ symmetry explicitly, the lower the mass, the more severe is the breaking. The case which was seen in Figure 5.2.11(a) is to be found on the upper horizontal axis. The upper left part of the plot is blurred out, because so far it is not confirmed what the exact pattern of the phase transition there is. The effective theory has been derived using a hopping parameter expansion $\kappa \to 0$, corresponding to heavy quarks. Therefore the deconfinement transition is located in the upper right corner of the Columbia plot.

The lower left corner describes a system with zero masses, exhibiting chiral symmetry. This symmetry is spontaneously broken. The phase transtion will be first order and will weaken for increasing, finite quark masses.

Chapter 3

The Complex Langevin Equation

If we are introducing a nonzero chemical potential, we have to deal with a complex action. This action can not be simulated with common Metropolis algorithm as this is based on selecting a probability corresponding to the action. This issue is known as the *sign problem* and makes use of other algorithms necessary. One candidate is letting a system evolve following a *Complex Langevin Equation*.
In this chapter the basics of the (Complex) Langevin equation ((C)LE) will be presented. First we will picture the approach by Parisi and Wu [10][22] considering the (real) Langevin equation (LE). We will then discuss the changes originating from complexifying the equation and hence the evolution. Connected to this we will recap the two main problems of CLE, namely the instability of the simulations and the convergence to the wrong limit and how to solve those. Instabilities of the simulation can be cured using an adaptive stepsize method with appropriate small stepsize [3]. This will be discussed in 3.2. The convergence to a wrong result can be controlled by applying the Langevin operator to an observable. This will be explained in 3.3. At the end of this chapter the CLE will be applied to the effective theory, that was presented in the previous chapter. This will also include the numerical setup for the simulations, which will be discussed and analysed later.

3.1 The approach by Parisi and Wu

The general assumption of *Stochastic quantization*, or equivalently the application of the Langevin equation, is that equilibrium is reached for $t \to \infty$ and that the correlation functions of a statistical system in equilibrium become equal to the corresponding Green functions,

$$\lim_{t\to\infty} \langle \phi(x_1,t)\cdots\phi(x_k,t)\rangle_\eta = \langle \phi(x_1)\cdots\phi(x_k)\rangle. \tag{3.1.1}$$

Therefore the average values of physical observables can be obtained as stochastic averages in equilibrium. [4]

First one introduces a new fictitious time t as an additional parameter of the fields ϕ, in which the system will evolve,

$$\phi(\boldsymbol{x}) \to \phi(x,t), \tag{3.1.2}$$

where x is a d-dimensional vector in Euclidean space-time. For our purpose a $d = 4$ dimensional Euclidean vector with the spatial vector $\boldsymbol{x}$ and Euclidean time x_4 is sufficient,

$$x = (x_1, x_2, x_3, x_4) = (\boldsymbol{x}, x_4). \tag{3.1.3}$$

The second step is to describe the fictitious time evolution of the fields as a stochastic process using the Langevin equation,

$$\frac{\partial\phi(x,t)}{\partial t} = \underbrace{-\frac{\partial S(\phi(x,t))}{\partial\phi(x,t)}}_{drifftterm\ K(x,t)} + \underbrace{\eta(x,t)}_{Gaussian\ noise} \quad . \tag{3.1.4}$$

One can consider the system being coupled to a thermal heat reservoir with temperature T, reaching a thermal equilibrium for large t. [22] The driftterm describes a driving force. The coupling to the heat reservoir can be described by the Gaussian noise field η, which corresponds to thermal fluctuations. The average of the Gaussian noise term has to vanish and it shouldn't have a correlation in time and space. This is described by the *fluctuation-dissipation* theorem or *Nyquist* theorem,

$$\langle\eta_i^n\rangle = 0,\ \langle\eta_i^n\eta_j^m\rangle = 2\delta_{ij}\delta_{nm}. \tag{3.1.5}$$

The goal of applying the LE to a physical system is to converge to the probability measure of the equilibrium, e^{-S}, where observables can be measured. One can prove that for a real action this is fulfilled. In the above case we only considered real variables and therefore the system will converge to its equilibrium distribution.

Complex action

As the QCD action, in particular the fermion determinant, will become complex if we include a nonzero chemical potential μ [12], we need the Complex Langevin equation (CLE) to describe the corresponding evolution. Now convergence to e^{-S} is not guaranteed anymore, as $S \in \mathbb{C}$ and therefore e^{-S} cannot be interpreted as a probability distribution. [6] The evolution equation still looks the same as in Equation 3.1.4, but now the process will drift into the complex plane. One can split up the CLE in a real and a complex part [2],

$$\begin{aligned}\frac{\partial\phi^R(x,t)}{\partial t} &= K^R(x,t) + \eta^R(x,t)\\ \frac{\partial\phi^I(x,t)}{\partial t} &= K^I(x,t) + \eta^I(x,t).\end{aligned} \tag{3.1.6}$$

The driftterms are then defined as

$$\begin{aligned}K^R(x,t) &= -Re\frac{\partial S(\phi(x,t))}{\partial\phi(x,t)}\\ K^I(x,t) &= -Im\frac{\partial S(\phi(x,t))}{\partial\phi(x,t)}.\end{aligned} \tag{3.1.7}$$

One issue of the CLE is convergence to a wrong limit. To avoid this it was shown in [3] that choosing $\eta^I = 0$ is useful and will be considered in the following.

As a last step we have to solve the CLE. This will be done numerically and therefore one can discretize the CLE corresponding to the new time t on the lattice,

$$\begin{aligned}\phi_n^R(\vartheta+1) &= \phi_n^R(\vartheta) + \epsilon K_n^R[\phi(\vartheta)] + \sqrt{\epsilon}\eta_n(\vartheta)\\ \phi_n^I(\vartheta+1) &= \phi_n^I(t) + \epsilon K_n^I[\phi(\vartheta)]\end{aligned} \tag{3.1.8}$$

The index n denotes the n^{th} lattice point and we consider the ϑ^{th} step in the new fictitious time $t = \epsilon\cdot\vartheta$. ϵ is the stepsize in t-direction and $\vartheta \in \mathbb{N}_0$. At each time step t the fields at each lattice point $\phi(n), n = 0,\dots N_s^3 - 1$ have to be updated, the driftterms have to be calculated and the Gaussian white noise η has to be chosen randomly.

3.2 Adaptive stepsize

One of the main problems of applying Complex Langevin dynamics is the instability of the simulations, also called *runaways*. It was shown in [1] that they appear when the driftterms show large fluctuations and drift into unstable directions in the complex field space. This can be solved using an adaptive stepsize which detects those fluctuations of the driftterms and choses appropiately small stepsizes in those regions. Nevertheless it is not proven that an adaptive stepsize method can cure the problem of instabilities in general.
In the analysis of the results two different methods of applying an adaptive stepsize will be compared: a method used by Neuman[1] and one method discussed by Aarts [1].
For each Langevin step ϑ we have one driftterm $K(\boldsymbol{x}, \vartheta)$ at one particular spatial point $\boldsymbol{x}$, whose value is higher than those for all other $\boldsymbol{x}_j$. This maximal dirftterm is denoted by $K_{max}(\vartheta)$ and is obtained by

$$K_{max}(\vartheta) = \max_n |K_n(\vartheta)| = \max_n \sqrt{K_n^{R2}(\vartheta) + K_n^{I2}(\vartheta)}. \tag{3.2.1}$$

This maximal driftterm will be used to control the stepsize. We should also mention that the discretization of the Langevin time becomes $t_j = \sum_{i=1}^{j} \epsilon_i$, as due to the adaptive procedure the stepsize is not equal anymore.

3.2.1 Aarts' adaptive stepsize method

In [1] were shown two methods for chosing an adaptive stepsize. The second method presented therein was used for the numerical solution of the CLE of this thesis and is referred to as *Aarts' adaptive stepsize method*. In this adaptive stepsize method ϵK_{max} is bounded in the following way:

$$\frac{1}{p}\mathcal{K} \leq \epsilon K_{max} \leq p\mathcal{K}. \tag{3.2.2}$$

$p, \mathcal{K}$ have to be chosen beforehand. It was shown that a choice of $p = 2, \mathcal{K} = 2 \times 10^{-4}$ was an appropriate choice. Changing them "by a factor two or more"[2], would only change the statistics but not the results.

3.2.2 Neuman's adaptive stepsize method

This method was used in the CL code by Mathias Neuman and serves for a comparison with the aforementioned method. It will be referred to as *Neuman adaptive stepsize method*. For the application we have to calculate the maximal driftterm, as it was defined in Equation 3.2.1. After we have found the maximal, finite driftterm we can calculate the stepsize via

$$\epsilon(\vartheta) = \min\left(\epsilon_{max}, \frac{0.1}{K_{max}(\vartheta)}\right). \tag{3.2.3}$$

ϵ_{max} has to be chosen by hand and serves as an upper bound for the stepsize.

[1] This method was implemented in the Complex Langevin code Mathias Neuman left in phil-shared
[2] [1], p. 158.

3.3 Langevin operator

The second main problem of CL dynamics is the convergence to a wrong limit. This can be caused by either "insufficient falloff of the probability distribution in the imaginary directions or too strong growth of the time-evolved observables in the imaginary directions".[3] Therefore it is necessary to have some tools to check if the results are reliable. One possibility would be to compare with data obtained with other algorithms, like Metropolis. But as in the regions of interest Metropolis and other resampling methods fail due to the *Sign Problem*, it is required to have other tools to check the convergence. A criterion of correctness was introduced in [5]. To check if a simulation converges to the correct result, one can apply the Langevin operator to an observable. If the average value of this quantity vanishes, this proofs that the result is correct,

$$\langle \tilde{L}O \rangle = 0. \tag{3.3.1}$$

The Langevin operator $\tilde{L}$ is defined by[4]

$$\tilde{L} \equiv [\nabla_z - (\nabla S_z)]\nabla_z. \tag{3.3.2}$$

It will be shown how to apply it to the Polyakov loop in the next section.

3.4 Implementation of CL on the lattice for the effective theory

We will now discuss in further detail how the CLE is implemented and in particular how it is applied to the effective Polyakov loop theory for QCD on the lattice. The discretization of the CLE was done according to Equation 3.1.8. To be able to apply this discretization scheme we need to formulate the effective theory in terms of complex fields ϕ. How this is done will be shown first, followed by an explicit example for the calculation of the driftterms.

3.4.1 Reformulation into a Polyakov loop theory

The effective theory is formulated in terms of traces over temporal Wilson lines as shown in section 2.3. The theory can be reformulated in terms of Polyakov loops. We start with parametrizing the Polyakov loops such that the temporal gauge links take a diagonal form,

$$U_4 = \mathrm{diag}(e^{i\phi_a}, e^{i\phi_b}, e^{-i(\phi_a+\phi_b)}), \tag{3.4.1}$$

with eigenvalues $e^{i\phi_l},\ l = a, b, c,\ \phi_c = \phi_a + \phi_b$. [16] The Polyakov loop can then be expressed in the following way

$$L(\phi_a, \phi_b) = e^{i\phi_a} + e^{i\phi_b} + e^{-i(\phi_a+\phi_b)},\ \phi_a, \phi_b \in [-\pi, \pi). \tag{3.4.2}$$

Changing the integration measure from temporal gauge links to Polyakov loops introduces a Jacobian e^V. Changing from an integration over Polyakov loops to an integration over the complex fields ϕ_a, ϕ_b introduces the same Jacobian a second time. After changing the integration measure we get the following expression for the partition function:

$$Z = \int d[U_4] e^{-S_{eff}} = \int d[L] e^{-S_{eff}} e^V = \int d[\phi_a] d[\phi_b] e^{-S_{eff}} e^{2V}. \tag{3.4.3}$$

[3] [5], p. 1-2.

[4] For details about the derivation of the Langevin operator see [3][5].

The $SU(3)$ potential, which was introduced by the Jacobian, takes the form [16]

$$V(\boldsymbol{n}) = -\ln\left[\sin^2\left(\frac{\phi_a(\boldsymbol{n})-\phi_b(\boldsymbol{n})}{2}\right)\sin^2\left(\frac{2\phi_a(\boldsymbol{n})+\phi_b(\boldsymbol{n})}{2}\right)\sin^2\left(\frac{\phi_a(\boldsymbol{n})+2\phi_b(\boldsymbol{n})}{2}\right)\right]. \tag{3.4.4}$$

It can be shown that the theory can be reformulated in terms of Polyakov loops, using the generating function, [20]

$$G[\alpha,\beta] = \ln\det\left[\alpha+\beta h_1 W\right] = \ln\left[\alpha^3+\alpha^2\beta h_1 L+\alpha\beta^2 h_1^2 L^\dagger+\beta^3 h_1^3\right]. \tag{3.4.5}$$

To get the relation between the $W_{n+m,n}$, which appear in the action of the effective theory, and the Polyakov loops, one has to take the derivative of the generating function w.rp.t. $\alpha,\ \beta$ and in the end set $\alpha=\beta=1$,

$$W_{n+m,n} \equiv \mathrm{Tr}\frac{(h_1 W)^n}{(1+h_1 W)^{n+m}} = \frac{(-1)^{m+n-1}}{(m+n-1)!}\left(\frac{\partial}{\partial\alpha}\right)^m\left(\frac{\partial}{\partial\beta}\right)^n G[\alpha,\beta]\Big|_{\alpha=\beta=1}. \tag{3.4.6}$$

As we already saw in section 2.3.2 the κ^2 contribution contains $W_{11},\ W_{11}^\dagger$, where we made use of the definition in Equation 3.4.6. Those quantities can be reformulated in terms of Polyakov loops. For $m=0, n=1$ one gets

$$W_{11}(\boldsymbol{n}) = \mathrm{Tr}\frac{h_1 W(\boldsymbol{n})}{1+h_1 W(\boldsymbol{n})} = \frac{h_1 L(\boldsymbol{n})+2h_1^2 L^*(\boldsymbol{n})+3h_1^3}{1+h_1 L(\boldsymbol{n})+h_1^2 L^*(\boldsymbol{n})+h_1^3}, \tag{3.4.7}$$

$$W_{11}^\dagger(\boldsymbol{n}) = \mathrm{Tr}\frac{\bar{h}_1 W^\dagger(\boldsymbol{n})}{1+\bar{h}_1 W^\dagger(\boldsymbol{n})} = \frac{\bar{h}_1 L^*(\boldsymbol{n})+2\bar{h}_1^2 L(\boldsymbol{n})+3\bar{h}_1^3}{1+\bar{h}_1 L^*(\boldsymbol{n})+\bar{h}_1^2 L(\boldsymbol{n})+\bar{h}_1^3}. \tag{3.4.8}$$

3.4.2 Numerical setup

Initializing the fields

Now we take a look at how to initialize the fields ϕ_a, ϕ_b that were used to parametrize the Polyakov loops. In Equation 3.4.2 we stated, that $\phi_a, \phi_b \in [-\pi, \pi)$. The choice of the initial configuration is not as important, if one has a long enough thermalization procedure, during which the equilibrium distribution is reached as the fields will evolve during the Complex Langevin evolution and also become complex. The fields were initialized in the following way,

$$\phi_{a/b,init} = 0.1 \cdot R, \tag{3.4.9}$$

where R is a random number, normally distributed with $\mu=0,\ \sigma=\sqrt{2}$. With this we have approximately $R \in [-4,4)$ and therefore $\phi_a, \phi_b \in [-0.4, 0.4)$.
Due to the Nyquist theorem Equation 3.1.5 the Gaussian white noise $\eta(n,t)$ is distributed in the same way as R and during the simulation one chooses $\eta = R$ randomly with $\mu=0, \sigma=\sqrt{2}$.

Adaptive stepsize method

In section 3.2 it was in general shown how to apply an adaptive stepsize method to a system with one complex field evolving in CL time. Now I will show how to implement the adaptive stepsize method using two complex fields $\phi_a,\ \phi_b$, which parametrize the Polyakov loop,

$$\phi_{a/b}(\boldsymbol{n}_i) = \phi_{a/b}^R(\boldsymbol{n}_i) + i\phi_{a/b}^I(\boldsymbol{n}_i). \tag{3.4.10}$$

Each of the two fields follows the above discretized Langevin equation. We now have to modify Equation 3.2.1, which was defined for only one complex field. We are using the combined absolute values of $|K_a|, |K_b|$ to define the maximal driftterm,

$$K_{max}(\vartheta) = \max_{\boldsymbol{n}} |K_{\boldsymbol{n}}(\vartheta)| = \max_{\boldsymbol{n}}(|K_{a,\boldsymbol{n}}(\vartheta)| + |K_{b,\boldsymbol{n}}(\vartheta)|). \tag{3.4.11}$$

For the *Aarts' adaptive stepsize method* the parameters $p = 2,\ \mathcal{K} = 2 \cdot 10^{-2}$ were chosen.

3.4.3 Calculating driftterms for the effective action

We will now calulate the driftterms for the Haar measure potential and the static action. The driftterm for the κ^2-correction is shown in Appendix A.

Driftterm of the Haar measure potential

To calculate the driftterm of the Haar measure potential, which we saw in Equation 3.4.4, we have to take the derivatives of the potential w.rp.t. the fields ϕ_a, ϕ_b and then take the negative of this result. The Haar measure potential is already in a form depending on the fields ϕ_a, ϕ_b explicitly. After some derivation we get the following expressions for the driftterms

$$\begin{aligned} K_{a,\boldsymbol{n}}(\vartheta) &= +\cot\left(\frac{\phi_{a,\boldsymbol{n}} - \phi_{b,\boldsymbol{n}}}{2}\right) + 2\cot\left(\phi_{a,\boldsymbol{n}} + \frac{\phi_{b,\boldsymbol{n}}}{2}\right) + \cot\left(\frac{\phi_{a,\boldsymbol{n}}}{2} + \phi_{b,\boldsymbol{n}}\right), \\ K_{b,\boldsymbol{n}}(\vartheta) &= -\cot\left(\frac{\phi_{a,\boldsymbol{n}} - \phi_{b,\boldsymbol{n}}}{2}\right) + \cot\left(\phi_{a,\boldsymbol{n}} + \frac{\phi_{b,\boldsymbol{n}}}{2}\right) + 2\cot\left(\frac{\phi_{a,\boldsymbol{n}}}{2} + \phi_{b,\boldsymbol{n}}\right). \end{aligned} \tag{3.4.12}$$

The CL time dependence of the fields, $\phi_{a/b}(\boldsymbol{n}, \vartheta)$, was neglected for better readability.

Driftterm of the static determinant

The static determinant depends on Polyakov loops $L(\phi_a, \phi_b)$ and so we have to apply the chain rule,

$$K_{i,stat}(\boldsymbol{n}) = -\left(\frac{\partial S_{stat}(\boldsymbol{n})}{\partial L(\boldsymbol{n})}\frac{\partial L(\boldsymbol{n})}{\partial \phi_i(\boldsymbol{n})} + \frac{\partial S_{stat}(\boldsymbol{n})}{\partial L^*(\boldsymbol{n})}\frac{\partial L^*(\boldsymbol{n})}{\partial \phi_i(\boldsymbol{n})}\right). \tag{3.4.13}$$

The chain rule applies to both fields in the same way, thus we abbreviated the expression using $i = a, b$. For $N_f = 1$ the local action of the static determinant including quarks and anti-quarks is

$$\begin{aligned} S_{stat}(\boldsymbol{n}) &= -\log\left[(1 + h1L_{\boldsymbol{n}} + h_1^2 L^*_{\boldsymbol{n}} + h_1^3)^2 (1 + \bar{h}_1 L^*_{\boldsymbol{n}} + \bar{h}_1^2 L_{\boldsymbol{n}} + \bar{h}_1^3)^2\right] \\ &= -2\log\left(1 + h1L_{\boldsymbol{n}} + h_1^2 L^*_{\boldsymbol{n}} + h_1^3\right) - 2\log\left(1 + \bar{h}_1 L^*_{\boldsymbol{n}} + \bar{h}_1^2 L_{\boldsymbol{n}} + \bar{h}_1^3\right). \end{aligned} \tag{3.4.14}$$

With this we can calculate the driftterm as

$$\begin{aligned} K_{i,stat}(\vec{x}) &= -\left(\frac{\partial S_{stat}(\boldsymbol{n})}{\partial L(\boldsymbol{n})}\frac{\partial L(\boldsymbol{n})}{\partial \phi_i(\vec{x})} + \frac{\partial S_{stat}(\boldsymbol{n})}{\partial L^*(\boldsymbol{n})}\frac{\partial L^*(\boldsymbol{n})}{\partial \phi_i(\vec{x})}\right) \\ &= -\frac{\partial}{\partial L(\boldsymbol{n})}\frac{\partial L(\boldsymbol{n})}{\partial \phi_i}\left(-2\log\underbrace{(1 + h_1 L_{\vec{x}} + h_1^2 L^\dagger_{\vec{x}} + h_1^3)}_{\equiv u(\phi_a,\phi_b)} - 2\log\underbrace{(1 + \bar{h}_1 L^*_{\vec{x}} + \bar{h}_1^2 L_{\vec{x}} + \bar{h}_1^3)}_{\equiv v(\phi_a,\phi_b)}\right) \\ &= +2\left(\frac{h_1 * \frac{\partial L}{\partial \phi_i} + h_1^2 \frac{\partial L^*}{\partial \phi_i}}{1 + h_1 L_{\vec{x}} + h_1^2 L^*_{\vec{x}} + h_1^3} + \frac{\bar{h}_1 * \frac{\partial L^*}{\partial \phi_i} + \bar{h}_1^2 \frac{\partial L}{\partial \phi_i}}{1 + \bar{h}_1 L^*_{\vec{x}} + \bar{h}_1^2 L_{\vec{x}} + \bar{h}_1^3}\right). \end{aligned} \tag{3.4.15}$$

In the second line we defined $u(\phi_a, \phi_b), v(\phi_a, \phi_b)$ as an abbreviation of the argument of the logarithm. The definition of the derivative of a function inside a logarithm was used in the third line,

$$\frac{d}{dx}\log f(x) = \frac{\frac{d}{dx}f(x)}{f(x)}. \tag{3.4.16}$$

The derivative of u, v w.rp.t. ϕ_i is

$$\frac{\partial u}{\partial \phi_i} = h_1 * \frac{\partial L}{\partial \phi_i} + h_1^2 \frac{\partial L^*}{\partial \phi_i}, \qquad \frac{\partial v}{\partial \phi_i} = \bar{h}_1 * \frac{\partial L^*}{\partial \phi_i} + \bar{h}_1^2 \frac{\partial L}{\partial \phi_i}. \tag{3.4.17}$$

And the derivatives of L, L^* w.rp.t. ϕ_i are:

$$\frac{\partial L}{\partial \phi_i} = ie^{i\phi_i} - ie^{-i(\phi_a+\phi_b)}, \qquad \frac{\partial L^*}{\partial \phi_i} = -ie^{-i\phi_i} + ie^{i(\phi_a+\phi_b)}. \tag{3.4.18}$$

The driftterms of higher order corrections to the action can be obtained in the same way, but especially for the κ^4-contribution this expression will become very long and therefore are not shown here. The driftterms are calculated analytically and were hardcoded in the Complex Langevin simulation.

3.4.4 Langevin operator

The Langevin operator was introduced as a tool to check the correctness of the Complex Langevin dynamics. This can be applied to the Polyakov loop as an observable. We used the parametrization of the Polyakov loop as was motivated in Equation 3.4.2. This means that in our case we can write the Langevin operator as follows:

$$\tilde{L} \equiv \sum_{i=a,b} [\nabla_i - (\nabla_i S(\phi_a, \phi_b))]\nabla_i = \sum_{i=a,b} [\nabla_i + K_i(\phi_a, \phi_b)]\nabla_i. \tag{3.4.19}$$

We used that $K_i = -\nabla_i S(\phi_a, \phi_b)$. Thus applying the Langevin operator on L gives:

$$\langle \tilde{L}L \rangle = (\ [\nabla_a + K_a(\phi_a, \phi_b)]\nabla_a + [\nabla_b + K_b(\phi_a, \phi_b)]\nabla_b\ )\, L(\phi_a, \phi_b) \tag{3.4.20}$$

With the second derivative of L w.rp.t. the fields,

$$\frac{\partial^2 L}{\partial \phi_i^2} = -e^{i\phi_i} - e^{-i(\phi_a+\phi_b)}, \tag{3.4.21}$$

we get

$$\langle \tilde{L}L \rangle = -e^{i\phi_a} - e^{i\phi_b} - 2e^{-i(\phi_a+\phi_b)} + i[K_a(e^{i\phi_a} - e^{-i(\phi_a+\phi_b)}) + K_b(e^{i\phi_b} - e^{-i(\phi_a+\phi_b)})]. \tag{3.4.22}$$

The driftterms are obtained during the simulation, where the quantity $\tilde{L}L$ is complex. Thus we will save the real and imaginary part separately. The numerical analysis of this criterion for correctness will be done in subsection 5.2.1.

Chapter 4

Chiral condensate on the lattice

Chiral symmetry was introduced in subsection 2.4.2. The order parameter of this symmetry is the chiral condensate. In the symmetric phase, below a critical temperature T_c, the expectation value of the chiral condensate vanishes. For $T > T_c$ chiral symmetry is spontaneously broken, $\langle\bar{\psi}\psi\rangle \neq 0$. For high temperatiures the chiral symmetry is expected to be restored. [24] A spontaneous symmetry breaking requires an infinitely large system, $|\Lambda| \to \infty$. Furthermore it is mandatory to send $m \to 0$ so that there is no explicit symmetry breaking due to the mass term.

The goal of this section is to calculate the chiral condensate for the effective action analytically. We will start with deriving the relation between the rescaled and the unrescaled action. Then the expression for the chiral condensate will be deduced from the continuum QCD partition function. We will end this chapter with calculating the analytical expression for the chiral condensate up to κ^2-corrections from the effective theory.

4.1 Relation between the fermion fields in the QCD action and in the effective action

The rescaling procedure follows [15]. We remember from subsection 2.2.2 that we could write the fermion action like

$$S_F = a^3 \left((am + 4r) \sum_x \bar{\psi}_x \psi_x - \frac{1}{2} \sum_{x,\mu} \left[\bar{\psi}_x (r - \gamma_\mu) U_{\mu,x} \psi_{x+\hat{\mu}} + \bar{\psi}_x (r + \gamma_\mu) U^\dagger_{\mu,x-\hat{\mu}} \psi_{x-\hat{\mu}} \right] \right). \tag{4.1.1}$$

Rescaling the fermion fields $\bar{\psi}, \psi$ each with a factor $a^{-3/2} C^{-1/2}$, where $C^{(f)} = am^{(f)} + 4r \equiv 1/(2\kappa^{(f)})$, we obtain the rescaled fermion action[1]

$$S^{(f)}_{F,r} = \sum_x \bar{\psi}_{x,r} \psi_{x,r} - \kappa^{(f)} \sum_{x,\mu} \left[\bar{\psi}_{x,r} (r - \gamma_\mu) U_{\mu,x} \psi_{x+\hat{\mu},r} + \bar{\psi}_{x,r} (r + \gamma_\mu) U^\dagger_{\mu,x-\hat{\mu}} \psi_{x-\hat{\mu},r} \right]. \tag{4.1.2}$$

The index r denotes quantities formulated using the rescaled fields $\bar{\psi}_r, \psi_r$, and the index F denotes that only the fermionic part of the action is considered. The superscript (f) means one particular flavor. I also want to emphasize that the scaling parameter $C^{(f)}$ depends on the flavor mass and is therefore flavor sensitive. For now I will stay with one flavor and leave

[1] [20], eq. (3.14).

out the superscript for readability. The case including several flavors will be shown at the end of this section. This leads to the relation between S_F and $S_{F,r}$:

$$S_F = C \cdot S_{F,r}. \tag{4.1.3}$$

In the following I want to deduce the relation between Z_F and $Z_{F,r}$ and furthermore the relation between $\ln(Z_F)$ and $\ln(Z_{F,r})$. From this we can then derive the relation between $\langle\bar{\psi}\psi\rangle$ and $\langle\bar{\psi}\psi\rangle_r$. In the effective action section 2.3 the fermionic fields are contained in the Wilson Dirac operator. Therefore we start with the relation between the original and the rescaled operator:

$$Q[U] = C \cdot (\mathbb{1} - \kappa M[U]) \equiv C \cdot Q_r[U]. \tag{4.1.4}$$

This leads to the relation for the fermion determinant

$$\det(Q[U]) = \det(C \cdot Q_r[U]) = C^{4 \cdot N_c \cdot 1} \cdot \det(Q_r[U]), \tag{4.1.5}$$

where C is a number and Q is a matrix in Dirac, color and flavor space. Inserting this in the expression for the partition function leads to:

$$\begin{aligned} Z &= \int d[U_4] \int d[U_i] \det(Q[U]) e^{-S_g} \\ &= C^{4 \cdot N_c} \cdot \int d[U_4] \int d[U_i] \det(Q_r[U]) e^{-S_g} \\ &= C^{4 \cdot N_c} \cdot Z_r. \end{aligned} \tag{4.1.6}$$

Finally we find the expression

$$\ln(Z) = \ln(C^{4 \cdot N_c} \cdot Z_r) = 4 \cdot N_c \ln(C) + \ln(Z_r) = 4 \cdot N_c \ln\left(\frac{1}{2\kappa(m)}\right) + \ln(Z_r). \tag{4.1.7}$$

We see that from taking the logarithm of the partition function we get an additional term depending on the fermion mass.

Several flavors

If we include several flavors we have to multiply the different fermion determinants to get the partition function

$$\begin{aligned} Z &= \int d[U_4] \int d[U_i] \det(Q^{(u)}[U]) \det(Q^{(d)}[U]) \ldots e^{-S_g} \\ &= \int d[U_4] \int d[U_i] C^{(u)4 \cdot N_c} \det(Q_r^{(u)}[U]) C^{(d)4 \cdot N_c} \det(Q_r^{(d)}[U]) \ldots e^{-S_g} \\ &= (C^{(u)} \cdot C^{(d)} \cdot \ldots)^{4 \cdot N_c} \cdot \int d[U_4] \int d[U_i] \det(Q_r^{(u)}[U]) \det(Q_r^{(d)}[U]) \ldots e^{-S_g} \\ &= (C^{(u)} \cdot C^{(d)} \cdot \ldots)^{4 \cdot N_c} \cdot Z_r. \end{aligned} \tag{4.1.8}$$

We get an additional factor $C^{(f)4 \cdot N_c}$ for each flavor as each flavor comes with a rescaling factor $C^{(f)4 \cdot N_c}$. The logarithm of the partition function for two different flavors then looks like

$$\ln(Z) = \ln((C^{(u)} \cdot C^{(d)})^{4 \cdot N_c} \cdot Z_r) = 4 \cdot N_c \, (\ln(C^{(u)}) + \ln(C^{(d)})) + \ln(Z_r). \tag{4.1.9}$$

N_f degenerate flavors

We can simplify the expressions if we use N_f degenerate quarks. If we include N_f **quarks of the same flavor** we can also write

$$Z = \int d[U_4] \int d[U_i] (\det Q[U])^{N_f} e^{-S_g}. \tag{4.1.10}$$

For the quark determinant we then get, making use of (4.1.4):

$$\begin{aligned} (\det Q[U])^{N_f} &= (\det(C \cdot Q_r[U]))^{N_f} = (C^{4\cdot N_c} \cdot (\det Q_r[U]))^{N_f} \\ &= (C^{4\cdot N_c})^{N_f} \cdot (\det Q_r[U])^{N_f} = C^{4\cdot N_c \cdot N_f} \cdot (\det Q_r[U])^{N_f}. \end{aligned} \tag{4.1.11}$$

Inserting this in the expression for the partition function gives

$$\begin{aligned} Z &= \int d[U_4] \int d[U_i] (\det Q[U])^{N_f} e^{-S_g} \\ &= C^{4\cdot N_c \cdot N_f} \cdot \int d[U_4] \int d[U_i] (\det Q_r[U])^{N_f} e^{-S_g} \\ &= C^{4\cdot N_c \cdot N_f} \cdot Z_r. \end{aligned} \tag{4.1.12}$$

Finally we find the expression

$$\ln(Z) = \ln(C^{4\cdot N_c \cdot N_f} \cdot Z_r) = 4 \cdot N_c \cdot N_f \cdot \ln(C) + \ln(Z_r). \tag{4.1.13}$$

4.2 Derivation of the chiral condensate

The expectation value of an observable O is defined in the following way,

$$\langle O \rangle = \frac{1}{Z} \int d[\bar{\psi}, \psi, U] \; O e^{-S}. \tag{4.2.1}$$

The normalization factor is the inverse partition function,

$$Z = \int d[\bar{\psi}, \psi, U] \; e^{-S}. \tag{4.2.2}$$

We will stay with one flavor, if not explicitly stated elsewise. Therefore the superscript (f) will be neglected. With the definition Equation 4.2.1 we can write down the expectation value of the chiral condensate,

$$\begin{aligned} \langle \bar{\psi}\psi \rangle &= \frac{1}{Z} \int d[\bar{\psi}, \psi, U] \; \bar{\psi}\psi e^{-\int_0^{1/T} dx_4 \int d^3x \; \bar{\psi}_i (\not{D}_{\mu,E} + a m_i + \gamma_4 \mu_i)\psi_i + \frac{1}{4} F^a_{\mu\nu} F^{a\mu\nu}} \\ &= \frac{1}{Z} \int d[\bar{\psi}, \psi, U] \; \bar{\psi}\psi e^{-\int_0^{1/T} dx_4 \int d^3x \; \bar{\psi}_i a m_i \psi_i - \int_0^{1/T} dx_4 \int d^3x \; \bar{\psi}_i (\not{D}_{\mu,E} + \gamma_4 \mu_i)\psi_i + \frac{1}{4} F^a_{\mu\nu} F^{a\mu\nu}} \\ &= \frac{1}{Z} \int d[\bar{\psi}, \psi, U] \; \left(-\frac{T}{V}\right) \frac{\partial}{\partial a m} \left(e^{-\int_0^{1/T} dx_4 \int d^3x \; \bar{\psi}_i a m_i \psi_i} \right) e^{-\int_0^{1/T} dx_4 \int d^3x \; \bar{\psi}_i (\not{D}_{\mu,E} + \gamma_4 \mu_i)\psi_i + \frac{1}{4} F^a_{\mu\nu} F^{a\mu\nu}} \\ &= -\frac{T}{V} \frac{\partial(\ln(Z))}{\partial a m}. \end{aligned} \tag{4.2.3}$$

From the second to the third step we rewrote the observable $\bar{\psi}\psi$ as the derivative of the term $e^{-\int dx_4 d^3x \; m\bar{\psi}\psi}$ w.rp.t. the mass m, as the derivative brings down the factor $\bar{\psi}\psi$ from the exponent. Furthermore we have to take care that the mass term comes with a minus

sign. From the integration over $\int_0^{1/T} dx_4 \int d^3x$ we get an additional factor V/T. To normalize the chiral condensate we have to divide by this factor. In the last step the factor $1/Z$ gets absorbed into the outer derivative of $\partial \ln(Z)/\partial m$.

Having defined the expression for the chiral condensate we are interested in the relation between the chiral condensate and the rescaled chiral condensate. The expression T/V on the lattice takes the form $\frac{1}{a^4 N_\tau N_s^3}$. Making use of (4.1.7) we get for the case of one flavor:

$$\begin{aligned}
\langle\bar{\psi}\psi\rangle &= -\frac{1}{a^4 N_\tau N_s^3}\frac{\partial(\ln(Z))}{\partial am} \\
&= -\frac{1}{a^4 N_\tau N_s^3}\frac{\partial}{\partial am}\left(4\cdot N_c \ln(C) + \ln(Z_r)\right) \\
&= -\frac{1}{a^4 N_\tau N_s^3}\left(4N_c\frac{\partial(\ln(C))}{\partial am} + \frac{\partial(\ln(Z_r))}{\partial am}\right) \\
&= -\frac{1}{a^4 N_\tau N_s^3}\left(4N_c\frac{1}{C}\cdot 1 + \frac{\partial(\ln(Z_r))}{\partial am}\right) \\
&= -\frac{1}{a^4 N_\tau N_s^3}\left(4N_c\frac{1}{am+4r} + \frac{\partial(\ln(Z_r))}{\partial am}\right) \\
&= -\frac{1}{a^4 N_\tau N_s^3}\left(4N_c\cdot 2\kappa + \frac{\partial(\ln(Z_r))}{\partial am}\right) \\
&= -\frac{4N_c\cdot 2\kappa}{a^4 N_\tau N_s^3} - \frac{1}{a^4 N_\tau N_s^3}\frac{\partial(\ln(Z_r))}{\partial am} \\
&= -\frac{8N_c\ \kappa}{a^4 N_\tau N_s^3} + \langle\bar{\psi}\psi\rangle_r.
\end{aligned} \tag{4.2.4}$$

We used the definition of the chiral condensate corresponding to the action with rescaled fields:

$$\langle\bar{\psi}\psi\rangle_r = -\frac{1}{a^4 N_\tau N_s^3}\frac{\partial(\ln(Z_r))}{\partial am}. \tag{4.2.5}$$

From the last line we see that if we are using the rescaled fields $\bar{\psi}_r, \psi_r$, we get a shift term $-\frac{8N_c\kappa}{a^4 N_\tau N_s^3}$ to obtain the chiral condensate of the original fields. From this we get the relation between the chiral condensate of the rescaled and the original fields as

$$\langle\bar{\psi}\psi\rangle = \langle\bar{\psi}\psi\rangle_r - \frac{8N_c\ \kappa}{a^4 N_\tau N_s^3}. \tag{4.2.6}$$

For N_f **degenerate quarks** this relation looks like

$$\langle\bar{\psi}\psi\rangle = \langle\bar{\psi}\psi\rangle_r - \frac{8N_c N_f\ \kappa}{a^4 N_\tau N_s^3}. \tag{4.2.7}$$

To conclude the results from this derivation we have to consider the shift term for the chiral condensate of the effective theory to obtain the chiral condensate for QCD.

4.3 Analytical evaluation of the chiral condensate in the Strong coupling limit for $\mu = 0$

In this chapter we will derive the analytical expression for the chiral condensate, starting with the contribution of static quarks. We will continue with the expression for the κ^2-correction. Throughout this chapter $N_f = 1, 2$ degenerate quarks will be assumed. In the case of $N_f = 2$ considering $m = m_u = m_d$. As done before the superscript (f) will be neglected. We will start in the strong coupling limit and set $\beta = 0$ and furthermore set the Wilson parameter $r = 1$ from now on.

Before we explicitly calculate the chiral condensate for the different fermionic contributions, we will derive a more general expression of which derivatives have to be considered. Due to the rescaling of the fields the action does not depend on the fermion masses m explicitly, but implicitly through the hopping parameter $\kappa = \kappa(m)$. Therefore it is practical to formulate the derivative of the partition function w.rp.t. m using the chain rule. In the first step we take the outer derivative of the logarithm,

$$\frac{\partial(\ln(Z_r))}{\partial am} = \frac{1}{Z_r}\frac{\partial Z_r}{\partial am}. \tag{4.3.1}$$

The mass dependence of the effective action is contained in the fermionic coupling constants, $h_1(\kappa(m)),\ \bar{h}_1(\kappa(m)), h_2(\kappa(m)), h_{31}(\kappa(m)), \ldots$. This means that we have to include partial derivatives w.rp.t. the coupling constants,

$$\frac{\partial Z_r}{\partial am} = \frac{\partial Z_r}{\partial h_1}\frac{\partial h_1}{\partial \kappa}\frac{\partial \kappa}{\partial am} + \frac{\partial Z_r}{\partial \bar{h}_1}\frac{\partial \bar{h}_1}{\partial \kappa}\frac{\partial \kappa}{\partial am} + \frac{\partial Z_r}{\partial h_2}\frac{\partial h_2}{\partial \kappa}\frac{\partial \kappa}{\partial am} + \ldots. \tag{4.3.2}$$

The chain rule applies in the same way to the rescaled and the unrescaled fields. With the index (r) we refer both to the original and to the rescaled fields,

$$\begin{aligned}\langle\bar{\psi}\psi\rangle_{(r)} &= -\frac{1}{a^4 N_\tau N_s^3}\frac{\partial(\ln(Z_{(r)}))}{\partial am} \\ &= -\frac{1}{a^4 N_\tau N_s^3}\frac{1}{Z_{(r)}}\left(\frac{\partial Z_{(r)}}{\partial h_1}\frac{\partial h_1}{\partial \kappa}\frac{\partial \kappa}{\partial am} + \frac{\partial Z_{(r)}}{\partial \bar{h}_1}\frac{\partial \bar{h}_1}{\partial \kappa}\frac{\partial \kappa}{\partial am} + \frac{\partial Z_{(r)}}{\partial h_2}\frac{\partial h_2}{\partial \kappa}\frac{\partial \kappa}{\partial am} + \ldots\right).\end{aligned} \tag{4.3.3}$$

The first step will be to calculate the partition function analytically and from this we can take the derivatives w.rp.t. the mass for $N_f = 1$ up to $O(\kappa^2)$ explicitly. The analytical calculation for $N_f = 2$ is much more cumbersome. Thus the case of $N_f = 2$ has been calculated using Mathematica and the plotted results will be shown at the end of this section.

4.3.1 Static determinant

We will start with the static contribution to the chiral condensate. The partition function was calculated in [20], resulting in

$$\begin{aligned}Z_{\text{stat}} &= \int \prod_k dW_k e^{-\int [dU_i] S_{\text{stat}}} = \int \prod_k dW_k \det Q_{\text{k,stat}}^{N_f} \\ &= \prod_k \int dW_k \det Q_{k,\text{stat}}^{N_f} = \prod_k z_0 = z_0^V.\end{aligned} \tag{4.3.4}$$

The integrals over k are independent of each other and therefore factorize. Those gauge integrals of type

$$I(m,n)(\boldsymbol{n}) = \int dW(\boldsymbol{n})(\mathrm{Tr}W(\boldsymbol{n}))^n(\mathrm{Tr}W^\dagger(\boldsymbol{n}))^m = \int dW(\boldsymbol{n})(L(\boldsymbol{n}))^n(L^*(\boldsymbol{n}))^m. \tag{4.3.5}$$

can be performed analogously to [20], Appendix B[2]. The partition function for $N_f = 1$ takes the form

$$\begin{aligned} Z(h_1,\bar{h}_1) &= \int \prod_k dW_k(1 + h_1L_k + h_1^2L_k^* + h_1^3)^2(1 + \bar{h}_1L_k^* + \bar{h}_1^2L_k + \bar{h}_1^3)^2 \equiv z_0^V \\ &= [(1 + 4h_1^3 + h_1^6) + (4h_1 + 6h_1^4)\bar{h}_1 + (10h_1^2 + 6h_1^5)\bar{h}_1^2 + (4 + 20h_1^3 + 4h_1^6)\bar{h}_1^3 \\ &\quad + (6h_1 + 10h_1^4)\bar{h}_1^4 + (6h_1^2 + 4h_1^5)\bar{h}_1^5 + (1 + 4h_1^3 + h_1^6)\bar{h}_1^6\ ]^V. \end{aligned} \tag{4.3.6}$$

This expression depends on $h_1, \bar{h}_1$ only. As seen in the previous calculation we can express Z in terms of z_0 and get a rather simple expression for the outer derivative of the logaritm,

$$\frac{\partial \ln(Z)}{\partial am} = \frac{\partial \ln(z_0^V)}{\partial am} = \frac{V\partial \ln(z_0)}{\partial am} = \frac{V}{z_0}\frac{\partial z_0}{\partial am}. \tag{4.3.7}$$

Applying the chain rule to the inner derivative we get:

$$\frac{\partial z_0}{\partial am} = \frac{\partial z_0}{\partial h_1}\frac{\partial h_1}{\partial \kappa}\frac{\partial \kappa}{\partial am} + \frac{\partial z_0}{\partial \bar{h}_1}\frac{\partial \bar{h}_1}{\partial \kappa}\frac{\partial \kappa}{\partial am} = \left(\frac{\partial z_0}{\partial h_1}\frac{\partial h_1}{\partial \kappa} + \frac{\partial z_0}{\partial \bar{h}_1}\frac{\partial \bar{h}_1}{\partial \kappa}\right)\frac{\partial \kappa}{\partial am}. \tag{4.3.8}$$

As h_1 and $\bar{h}_1$ have the same dependence on κ, their derivatives w.rp.t. κ have the same structure,

$$\begin{aligned} \frac{\partial h_1}{\partial \kappa} &= \frac{\partial}{\partial \kappa}\exp(N_\tau a\mu)\cdot(2\kappa)^{N_\tau} = \exp(N_\tau a\mu)\cdot 2\cdot N_\tau(2\kappa)^{N_\tau-1} \\ &= \frac{2N_\tau}{2\kappa}\exp(N_\tau a\mu)\cdot(2\kappa)^{N_\tau} = \frac{N_\tau}{\kappa}\cdot h_1, \\ \frac{\partial \bar{h}_1}{\partial \kappa} &= \ldots = \frac{N_\tau}{\kappa}\cdot \bar{h}_1. \end{aligned} \tag{4.3.9}$$

For the derivative of κ w.rp.t. m we use Equation 2.2.19:

$$\kappa = \frac{1}{2am+8} \;\Leftrightarrow\; \frac{\partial \kappa}{\partial am} = -2\frac{1}{(2am+8)^2} = -2\kappa^2. \tag{4.3.10}$$

Inserting this in Equation 4.3.8 and using $V = a^3N_s^3$ gives

$$\frac{\partial \ln(Z)}{\partial am} = a^3N_s^3\frac{1}{z_0}\left(\frac{\partial z_0}{\partial h_1}\frac{\partial h_1}{\partial \kappa} + \frac{\partial z_0}{\partial \bar{h}_1}\frac{\partial \bar{h}_1}{\partial \kappa}\right)\frac{\partial \kappa}{\partial am} = -2\kappa^2a^3N_s^3\frac{1}{z_0}\left(\frac{\partial z_0}{\partial h_1}\frac{\partial h_1}{\partial \kappa} + \frac{\partial z_0}{\partial \bar{h}_1}\frac{\partial \bar{h}_1}{\partial \kappa}\right). \tag{4.3.11}$$

For the chiral condensate we then get

$$\begin{aligned} \langle\bar{\psi}\psi\rangle_r &= -\frac{1}{a^4N_\tau N_s^3}\frac{\partial(\ln(Z))}{\partial am} \\ &= -\frac{1}{a^4N_\tau N_s^3}\cdot\left(-2\kappa^2a^3N_s^3\frac{1}{z_0}\left(\frac{\partial z_0}{\partial h_1}\frac{\partial h_1}{\partial \kappa} + \frac{\partial z_0}{\partial \bar{h}_1}\frac{\partial \bar{h}_1}{\partial \kappa}\right)\right) \\ &= \frac{2\kappa^2}{aN_\tau}\frac{1}{z_0}\left(\frac{\partial z_0}{\partial h_1}\frac{\partial h_1}{\partial \kappa} + \frac{\partial z_0}{\partial \bar{h}_1}\frac{\partial \bar{h}_1}{\partial \kappa}\right). \end{aligned} \tag{4.3.12}$$

[2]A Mathematica script to evaluate gauge integrals over Polyakov loops has been provided by Amine Chabane, based on [14].

We can simplify this expression using the derivatives of $h_1, \bar{h}_1$ w.rp.t. κ from Equation 4.3.9,

$$\begin{aligned}\langle\bar{\psi}\psi\rangle_r &= \frac{2\kappa^2}{aN_\tau}\frac{1}{z_0}\left(\frac{\partial z_0}{\partial h_1}\frac{aN_\tau}{\kappa}\cdot h_1 + \frac{\partial z_0}{\partial \bar{h}_1}\frac{aN_\tau}{\kappa}\cdot \bar{h}_1\right) \\ &= \frac{2\kappa}{z_0}\left(\frac{\partial z_0}{\partial h_1}\cdot h_1 + \frac{\partial z_0}{\partial \bar{h}_1}\cdot \bar{h}_1\right).\end{aligned} \tag{4.3.13}$$

After some calculation the analytical expression for the chiral condensate of static quarks and anti-quarks with $N_f = 1$ looks like

$$\begin{aligned}\langle\bar{\psi}\psi\rangle_r = \frac{2\kappa}{z_0}\Big(&(12h_1^3 + 6h_1^6) + (8h_1 + 30h_1^4)\bar{h}_1 + (40h_1^2 + 42h_1^5)\bar{h}_1^2 \\ &+(12 + 120h_1^3 + 36h_1^6)\bar{h}_1^3 + (30h_1 + 80h_1^4)\bar{h}_1^4 \\ &+(42h_1^2 + 40h_1^5)\bar{h}_1^5 + (6 + 36h_1^3 + 12h_1^6)\bar{h}_1^6\Big).\end{aligned} \tag{4.3.14}$$

The equations containing the different derivatives from above look the same also for the case of $N_f > 1$ degenerate quarks. But the expression of z_0 will look different as this is calculated based on $\det(Q_{stat})^{N_f}$.

The analytical results of the partition function and the chiral condensate for static quarks and anti-quarks for $N_f = 2$ can be found in section B.1.

4.3.2 κ^2- correction to the chiral condensate

The analytical expression has already been calculated for fermions in the cold dense limit. [20] We will include anti-quarks in the derivation of the partition function including the static determinant and the κ^2-correction. Afterwards the chiral condensate will be calculated.

We start with evaluating the partition function,

$$\begin{aligned}Z &= \int\prod_k dW_k \det Q_{k,\text{stat}}^{N_f} \exp\left(-2h_2 N_f \sum_{<i,j>}(W_{11,i} - W_{11,i}^\dagger)(W_{11,j} - W_{11,j}^\dagger)\right) \\ &= \int\prod_k dW_k \det Q_{k,\text{stat}}^{N_f}(1 - 2h_2 N_f \sum_{<i,j>}(W_{11,i} - W_{11,i}^\dagger)(W_{11,j} - W_{11,j}^\dagger)) + O(\kappa^4) \\ &\equiv Z_{stat} + Z_{\kappa^2} + O(\kappa^4).\end{aligned} \tag{4.3.15}$$

The notation Z_{stat}, Z_{κ^2} is used to structure the calculations for readability. From the first to the second line we expanded the exponent. To be able to perform the gauge integral it's furthermore necessary to rewrite the Wilson loops in terms of Polyakov loops as shown in

Equation 3.4.6. With this we can write for the contribution of κ^2:

$$\begin{aligned}
Z_{\kappa^2} &= -\int \prod_k dW_k \det Q_{k,\text{stat}}^{N_f} 2h_2 N_f \sum_{i,j} (W_{11,i} - W_{11,i}^\dagger)(W_{11,j} - W_{11,j}^\dagger) \\
&= -\int \prod_k dW_k \det Q_{k,\text{stat}}^{N_f} 2h_2 N_f \sum_{i,j} \left(\frac{h_1 L_i + 2h_1^2 L_i^* + 3h_1^3}{1 + h_1 L_i + h_1^2 L_i^* + h_1^3} - \frac{\bar{h}_1 L_i^* + 2\bar{h}_1^2 L_i + 3\bar{h}_1^3}{1 + \bar{h}_1 L_i^* + \bar{h}_1^2 L_i + \bar{h}_1^3} \right) \cdot \\
&\qquad \times \left(\frac{h_1 L_j + 2h_1^2 L_l^* + 3h_1^3}{1 + h_1 L_j + h_1^2 L_j^* + h_1^3} - \frac{\bar{h}_1 L_j^* + 2\bar{h}_1^2 L_j + 3\bar{h}_1^3}{1 + \bar{h}_1 L_j^* + \bar{h}_1^2 L_j + \bar{h}_1^3} \right) \\
&= -2h_2 N_f \sum_{i,j} \int \prod_{\substack{k \neq i \\ k \neq j}} dW_k \det Q_{k,\text{stat}}^{N_f} \; dW_i \; dW_j \\
&\times \Big[(1 + h_1 L_i + h_1^2 L_i^* + h_1^3)^{2N_f - 1} (1 + \bar{h}_1 L_i^* + \bar{h}_1^2 L_i + \bar{h}_1^3)^{2N_f} (h_1 L_i + 2h_1^2 L_i^* + 3h_1^3) \\
&\quad - (1 + h_1 L_i + h_1^2 L_i^* + h_1^3)^{2N_f} (1 + \bar{h}_1 L_i^* + \bar{h}_1^2 L_i + \bar{h}_1^3)^{2N_f - 1} (\bar{h}_1 L_i^* + 2\bar{h}_1^2 L_i + 3\bar{h}_1^3) \Big] \\
&\times \Big[(1 + h_1 L_j + h_1^2 L_j^* + h_1^3)^{2N_f - 1} (1 + \bar{h}_1 L_j^* + \bar{h}_1^2 L_j + \bar{h}_1^3)^{2N_f} (h_1 L_j + 2h_1^2 L_j^* + 3h_1^3) \\
&\quad - (1 + h_1 L_j + h_1^2 L_j^* + h_1^3)^{2N_f} (1 + \bar{h}_1 L_j^* + \bar{h}_1^2 L_j + \bar{h}_1^3)^{2N_f - 1} (\bar{h}_1 L_j^* + 2\bar{h}_1^2 L_j + 3\bar{h}_1^3) \Big] .
\end{aligned} \tag{4.3.16}$$

We used that for $\boldsymbol{n}_i, \boldsymbol{n}_j$ the denominator of $(W_{11}^\dagger)$ W_{11} cancels with the (anti-)fermion part of static determinant. The temporal gauge integral over the product over spatial points $\boldsymbol{n}_k, k \neq i, k \neq j$ is the integral over the static determinant only, which we already saw in Equation 4.3.4. In the present case this integral appears $V - 2$ times, which results in z_0^{V-2}. The two terms at points $\boldsymbol{n}_i$ and $\boldsymbol{n}_j$ are treated separately and therefore are excluded from this integral. Let's consider the integral at spatial point $\boldsymbol{n}$. We can call the difference of these terms z_1,

$$\begin{aligned}
&\int dW_i \Big[(1 + h_1 L_i + h_1^2 L_i^* + h_1^3)^{2N_f - 1} (1 + \bar{h}_1 L_i^* + \bar{h}_1^2 L_i + \bar{h}_1^3)^{2N_f} (h_1 L_i + 2h_1^2 L_i^* + 3h_1^3) \\
&\quad - (1 + h_1 L_i + h_1^2 L_i^* + h_1^3)^{2N_f} (1 + \bar{h}_1 L_i^* + \bar{h}_1^2 L_i + \bar{h}_1^3)^{2N_f - 1} (\bar{h}_1 L_i^* + 2\bar{h}_1^2 L_i + 3\bar{h}_1^3) \Big] \\
&\quad \equiv z_1 .
\end{aligned} \tag{4.3.17}$$

The contribution to Z at space point $\boldsymbol{n}_j$ looks the same as the one at $\boldsymbol{n}_i$. As this contribution appears twice, at space points $\boldsymbol{n}_i$ and $\boldsymbol{n}_j$, this term contributes as z_1^2. Alltogether we can write in a compact way:

$$Z_{\kappa^2} = -3V \cdot 2h_2 N_f z_0^{V-2} z_1^2 . \tag{4.3.18}$$

The prefactor $3V$ comes from the sum over $\langle i, j \rangle$, where we have $d * V$ nearest neighbor pairs with $d = 3$. This leads to the expression for Z:

$$Z = Z_{\text{stat}} + Z_{\kappa^2} = z_0^V - 6V h_2 N_f z_0^{V-2} z_1^2 = z_0^V (1 - 6V h_2 N_f \frac{z_1^2}{z_0^2}). \tag{4.3.19}$$

As stated in the end of subsection 4.3.1 this expression is also valid for $N_f > 1$. What will be different for various N_f is the exact expression for z_0, z_1. Therefore also the upcoming calculation of the chiral condensate will be valid for different N_f.
We can do a resummation to ensure convergence, [20]

$$Z = z_0^V (1 - 6V h_2 N_f \frac{z_1^2}{z_0^2}) = z_0^V \exp(-6V h_2 N_f \frac{z_1^2}{z_0^2} + O(\kappa^4)). \tag{4.3.20}$$

Now we have derived the expression for the partition function. Taking the logarithm of it we get to the starting point of calculating the chiral condensate:

$$\begin{aligned}\ln(Z) &= \ln(z_0^V \exp(-6Vh_2N_f\frac{z_1^2}{z_0^2})) = \underbrace{V\ln(z_0)}_{\ln(Z_{\text{stat}})}\underbrace{-6Vh_2N_f\frac{z_1^2}{z_0^2}}_{\ln(Z_{\kappa^2})} \\ &= \ln(Z_{\text{stat}}) + \ln(Z_{\kappa^2}).\end{aligned} \tag{4.3.21}$$

Due to taking the logarithm of Z we can write this as a sum of the different contributions coming from the static determinant and the κ^2-correction:

$$\langle\bar{\psi}\psi\rangle \propto \frac{\partial\ln(Z)}{\partial am} = \frac{\partial(\ln(Z_{\text{stat}})+\ln(Z_{\kappa^2}))}{\partial am} = \frac{\partial\ln(Z_{\text{stat}})}{\partial am} + \frac{\partial\ln(Z_{\kappa^2})}{\partial am}, \tag{4.3.22}$$

which means that the chiral condensate is a sum of its so far two contributions

$$\langle\bar{\psi}\psi\rangle = \langle\bar{\psi}\psi\rangle_{\text{stat}} + \langle\bar{\psi}\psi\rangle_{\kappa^2}. \tag{4.3.23}$$

We already know the contribution of the static determinant, therefore we continue with the second term. Now we also have to consider the derivative of h_2 w.rp.t. κ:

$$\frac{\partial\ln(Z_{\kappa^2})}{\partial am} = \frac{\partial\ln(Z_{\kappa^2})}{\partial h_1}\frac{\partial h_1}{\partial\kappa}\frac{\partial\kappa}{\partial am} + \frac{\partial\ln(Z_{\kappa^2})}{\partial\bar{h}_1}\frac{\partial\bar{h}_1}{\partial\kappa}\frac{\partial\kappa}{\partial am} + \frac{\partial\ln(Z_{\kappa^2})}{\partial h_2}\frac{\partial h_2}{\partial\kappa}\frac{\partial\kappa}{\partial am}. \tag{4.3.24}$$

The derivative of h_2 w.rp.t. κ looks like

$$\frac{\partial h_2}{\partial\kappa} = \frac{2\kappa N_\tau}{N_c}. \tag{4.3.25}$$

We start the derivation with the explicit expression the derivative of $\ln(Z_{\kappa^2})$,

$$\begin{aligned}\frac{\partial\ln(Z_{\kappa^2})}{\partial am} &= \frac{\partial}{\partial am}(-6Vh_2N_f\frac{z_1^2}{z_0^2}) = -6VN_f\frac{\partial}{\partial am}(h_2\frac{z_1^2}{z_0^2}) \\ &= -6VN_f\left(\frac{\partial}{\partial h_1}\frac{\partial h_1}{\partial\kappa}\frac{\partial\kappa}{\partial am} + \frac{\partial}{\partial\bar{h}_1}\frac{\partial\bar{h}_1}{\partial\kappa}\frac{\partial\kappa}{\partial am} + \frac{\partial}{\partial h_2}\frac{\partial h_2}{\partial\kappa}\frac{\partial\kappa}{\partial am}\right)(h_2\frac{z_1^2}{z_0^2}).\end{aligned} \tag{4.3.26}$$

After some calculation we get the expression for the κ^2-contribution to the chiral condensate,

$$\begin{aligned}\langle\bar{\psi}\psi\rangle_{\kappa^2} &= -\frac{T}{V}\frac{\partial\ln(Z_{\kappa^2})}{\partial am} \\ &= -\frac{T}{V}12\kappa^2VN_f\frac{z_1}{z_0^2}\left(2h_2\left[\left(\frac{\partial z_1}{\partial h_1}\frac{\partial h_1}{\partial\kappa}+\frac{\partial z_1}{\partial\bar{h}_1}\frac{\partial\bar{h}_1}{\partial\kappa}\right)-\frac{z_1}{z_0}\left(\frac{\partial z_0}{\partial h_1}\frac{\partial h_1}{\partial\kappa}+\frac{\partial z_0}{\partial\bar{h}_1}\frac{\partial\bar{h}_1}{\partial\kappa}\right)\right]+z_1\frac{\partial h_2}{\partial\kappa}\right) \\ &= -12\kappa^2\frac{N_f}{aN_\tau}\frac{z_1}{z_0^2}\left(2h_2\left[\left(\frac{\partial z_1}{\partial h_1}\frac{\partial h_1}{\partial\kappa}+\frac{\partial z_1}{\partial\bar{h}_1}\frac{\partial\bar{h}_1}{\partial\kappa}\right)-\frac{z_1}{z_0}\left(\frac{\partial z_0}{\partial h_1}\frac{\partial h_1}{\partial\kappa}+\frac{\partial z_0}{\partial\bar{h}_1}\frac{\partial\bar{h}_1}{\partial\kappa}\right)\right]+z_1\frac{\partial h_2}{\partial\kappa}\right).\end{aligned} \tag{4.3.27}$$

We can again insert the expression of the derivatives of $h_1, \bar{h}_1, h_2$ from Equation 4.3.9 and

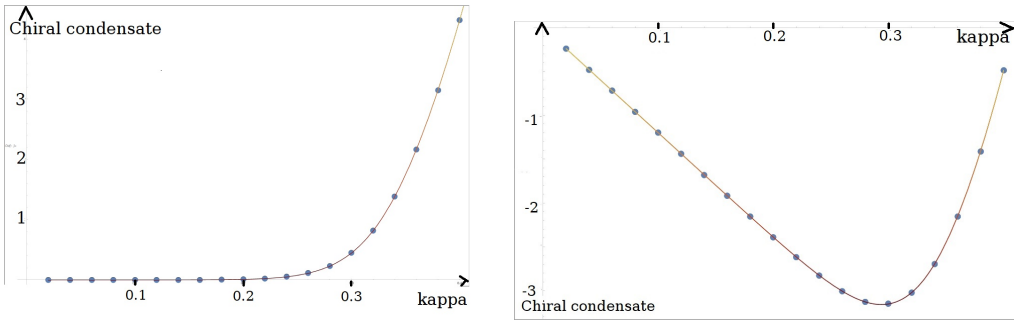

(a) Static determinant and κ^2 contribution. (b) Static determinant, κ^2 contributions and shift.

Figure 4.3.1: *Chiral condensate as a function of κ for fermionic contributions up to κ^2 only, with (right) and without (left) the shift. Comparison between analytical (line) and numerical (dots) results for $\beta = 0, N_\tau = N_s = 4, N_f = 2$.*

Equation 4.3.25 and get an expression for the κ^2-correction to the chiral condensate:

$$\begin{aligned}
\langle\bar{\psi}\psi\rangle_{\kappa^2} &= -\frac{T}{V}\frac{\partial \ln(Z_{\kappa^2})}{\partial am} \\
&= -12\kappa^2 \frac{N_f}{aN_\tau}\frac{z_1}{z_0^2}\left(2h_2\left[\left(\frac{\partial z_1}{\partial h_1}\frac{\partial h_1}{\partial \kappa}+\frac{\partial z_1}{\partial \bar{h}_1}\frac{\partial \bar{h}_1}{\partial \kappa}\right)-\frac{z_1}{z_0}\left(\frac{\partial z_0}{\partial h_1}\frac{\partial h_1}{\partial \kappa}+\frac{\partial z_0}{\partial \bar{h}_1}\frac{\partial \bar{h}_1}{\partial \kappa}\right)\right]+z_1\frac{\partial h_2}{\partial \kappa}\right) \\
&= -12\kappa^2 \frac{N_f}{aN_\tau}\frac{z_1}{z_0^2}\left(2h_2\left[\left(\frac{\partial z_1}{\partial h_1}h_1\frac{N_\tau}{\kappa}+\frac{\partial z_1}{\partial \bar{h}_1}\bar{h}_1\frac{N_\tau}{\kappa}\right)-\frac{z_1}{z_0}\left(\frac{\partial z_0}{\partial h_1}h_1\frac{N_\tau}{\kappa}+\frac{\partial z_0}{\partial \bar{h}_1}\bar{h}_1\frac{N_\tau}{\kappa}\right)\right]+z_1\frac{2h_2}{\kappa}\right) \\
&= -24\kappa^2 h_2 \frac{N_f}{aN_\tau}\frac{N_\tau}{\kappa}\frac{z_1}{z_0^2}\left(\left[\left(\frac{\partial z_1}{\partial h_1}h_1+\frac{\partial z_1}{\partial \bar{h}_1}\bar{h}_1\right)-\frac{z_1}{z_0}\left(\frac{\partial z_0}{\partial h_1}h_1+\frac{\partial z_0}{\partial \bar{h}_1}\bar{h}_1\right)\right]+z_1\frac{1}{N_\tau}\right) \\
&= -\frac{24}{a}\kappa h_2 N_f \frac{z_1}{z_0^2}\left(\left[\left(\frac{\partial z_1}{\partial h_1}h_1+\frac{\partial z_1}{\partial \bar{h}_1}\bar{h}_1\right)-\frac{z_1}{z_0}\left(\frac{\partial z_0}{\partial h_1}h_1+\frac{\partial z_0}{\partial \bar{h}_1}\bar{h}_1\right)\right]+z_1\frac{1}{N_\tau}\right) \\
&= -\frac{T}{V}24\frac{V}{T}N_f h_2 \kappa\left[\frac{z_1}{z_0^2}\left(\frac{\partial z_1}{\partial h_1}h_1+\frac{\partial z_1}{\partial \bar{h}_1}\bar{h}_1\right)-\frac{z_1^2}{z_0^3}\left(\frac{\partial z_0}{\partial h_1}h_1+\frac{\partial z_0}{\partial \bar{h}_1}\bar{h}_1\right)+\frac{1}{N_\tau}\frac{z_1^2}{z_0^2}\right] \\
&= -24 N_f h_2 \kappa\left[\frac{z_1}{z_0^2}\left(\frac{\partial z_1}{\partial h_1}h_1+\frac{\partial z_1}{\partial \bar{h}_1}\bar{h}_1\right)-\frac{z_1^2}{z_0^3}\left(\frac{\partial z_0}{\partial h_1}h_1+\frac{\partial z_0}{\partial \bar{h}_1}\bar{h}_1\right)+\frac{1}{N_\tau}\frac{z_1^2}{z_0^2}\right].
\end{aligned} \tag{4.3.28}$$

4.3.3 Comparison with numerical results for $N_f = 2$

To complete this chapter we compare analytical and numerical methods for the chiral condensate as a function of κ for $N_f = 2$. The simulation has been done using the Metropolis algorithm from [25]. The left image in Figure 4.3.1 shows the comparison of analytical and numerical results for the action using the static determinant and κ^2-corrections. In the right figure we also added the contribution of the shift that was introduced by rescaling the fermion fields. The numerical data for the chiral condensate for the pure fermion action agrees well with the analytical data.

Chapter 5

Results

In this chapter we will discuss the numerical results. We will start with some data analysis in section 5.1 and show how the localization and characterization of a phase transition can be obtained. Subsequently the numerical results for the Deconfinement transition are shown in section 5.2, starting with the pure gauge case. This is numerically less costly than simulating the full theory and therefore a good starting point to investigate several properties of the Complex Langevin dynamics applied to the effective theory. The next step is then to include fermions and higher gauge corrections and do the simulation based on the findings in the pure gauge simulation.
In section 5.3 the results for the chiral condensate will be shown.

5.1 Data analysis

In this section we recap useful information about the observables obtained from the simulations. We define how expectation values are obtained during a simulation and introduce some observables that were measured in the simulation, such as the Polyakov loop. Another important step of the data analysis is the estimation of errors. In this context we will discuss the binning procedure and *Bootstrap resampling*. Putting some physics in the data analysis, of particular interest are the localization and characterization of phase transitions. The necessary tools will be provided in the end of this subsection.

5.1.1 Observables

Expectation values in Euclidean field theory are obtained as

$$\langle O \rangle = \frac{1}{Z} \int d[U] e^{-S[U]} O[U], \tag{5.1.1}$$

with the partition function

$$Z = \frac{1}{Z} \int d[U] e^{-S[U]}. \tag{5.1.2}$$

This integral can in general not be evaluated analytically and therefore one uses computer simulations. The idea of a Monte Carlo (MC) simulation is to calculate those expectation values numerically. One assumes that at each MC step one measures an observable $O[U_n]$, where U_n is distributed with a probability $\propto e^{-S[U_n]}$, and from this one gets the expectation

value as

$$\langle O \rangle \approx \frac{1}{N} \sum_{U_n} O[U_n]. \tag{5.1.3}$$

N is the number of total measurements. In the simulation the observable $O[U_n]$ for each configuration U_n can also be seen as an observable at a particular Monte Carlo time t during the process, $O[U_n] \leftrightarrow O(t)$. To get the observables $O(t)$, we have to measure observables at each spatial lattice point $\boldsymbol{n}$ and average over the spatial volume,

$$O(t) = \frac{1}{N_s^3} \sum_{\boldsymbol{n} \in \Lambda_s} O(\boldsymbol{n}, t). \tag{5.1.4}$$

The order parameter of the Deconfinement transition is the Polyakov loop. To locate the phase transition we will observe the Polyakov loop as a function of the gauge coupling λ_1. At the phase transition the Polyakov loop expectation value $\langle L \rangle$ will change from 0 in the confined phase to a finite value in the deconfined phase. We will measure the absolute value of the Polyakov loop, which can be achieved by either taking the absolute value after or before averaging over the volume at a particular time t,

$$Q_1(t) = \frac{1}{N_s^3} |\sum_{\boldsymbol{n}} L_{\boldsymbol{n}}(t)|, \; Q_2(t) = \frac{1}{N_s^3} \sum_{\boldsymbol{n}} |L_{\boldsymbol{n}}(t)|. \tag{5.1.5}$$

The Polyakov loop is measured at each step in Monte Carlo time t, which in the Langevin simulation corresponds to the Langevin time, for each point $\boldsymbol{n} = 0, \ldots, Ns^3 - 1$ on the lattice. We hence get the Langevin time expectation value for the two Polyakov loop observables,

$$\langle Q_{1/2} \rangle = \frac{1}{N} \sum_t Q_{1/2}(t). \tag{5.1.6}$$

5.1.2 Error analysis

An important step in the analysis is to control the autocorrelation between data and the estimation of errors in the simulation. To reduce the correlation one can apply binning to the data. [8] The error estimation can be achieved with different methods, like Jackknife or bootstrap resampling. For the error estimation in this thesis the bootstrap resampling method was used. As an adaptive stepsize method was used during the simulation, we need to weight the sample data with the stepsize when applying the binning and the bootstrap resampling. This will be discussed after the introduction of the original methods.

Autocorrelation

An important question is over which period of simulation time the data are correlated. This is only a brief recap, as it is merely used to estimate how many sweeps are needed between each measurement. For more detailed information consult [8]. Numerical data obtained from a Monte Carlo algorithm are correlated. For an accurate estimation of the correlation between data the evaluation of the integrated autocorrelation time τ_{int} is necessary. If one picks an observable $O(t)$ at time t, the integrated autocorrelation time estimates after how many Monte Carlo steps the observable is independent of the inital one. Hence $O(t)$ and $O(t + \tau_{int})$ are supposed to be independent of each other. If a sample consits of N data, one would effectively have

$$N_{indep} = \frac{N}{\tau_{int}} \tag{5.1.7}$$

independent data. As a conclusion one can discard τ_{int} data in between two measurements.

Binning

To reduce the autocorrelation between the data it is useful to bin the data. From the original dataset of R data we build R_{bs} bins consisting of R_b data, $R_b \cdot R_{bs} = R$. The bins are formed in order, the first R_b data $x_1, \ldots, x_{R_b}$ go in the first bin, the data $x_{R_b+1}, \ldots, x_{2R_b}$ go in the second bin and so on. In general R does not have to be divisible by R_{bs} without remainder. Thus the last bin will contain less data that the other bins. Afterwards one calculates the average value for each bin,

$$\overline{x_j^b} = \frac{1}{R_b} \sum_{i=1+(j-1)R_b}^{j \cdot R_b} x_i, \ b = 1, \ldots, R_{bs}. \tag{5.1.8}$$

Those R_{bs} bin averages are in the next step used to calculate the errors. Hence the errors are not calculated from the original data set but from the binned data sets.

Weighted binning

When an adaptive stepsize is used one has to take the different stepsizes into consideration to calculate the Langevin time average. This is done by weighting the observables at each time step with the corresponding stepsize ϵ. Then the average values of the bins are obtained as

$$\overline{x^b_{j\,weighted}} = \frac{1}{R_b} \frac{\sum_{i=1+(j-1)R_b}^{j \cdot R_b} \epsilon_i x_i}{\sum_i \epsilon_i}, \ j = 1, \ldots, R_{bs}. \tag{5.1.9}$$

These averages will be used to calculate the errors in the next step, using the weighted bootstrap resampling method.

Bootstrap resampling

We will now discuss how to obtain the expectation values and the errors of the original or the binned data from the simulation. We assume a data set consisting of R data. From this set we randomly choose N data points, from which we form a bootstrap sample. It is possible to have the same x_i appearing repeatedly in one set. In this way we form M bootstrap samples,

$$\{x_1^1, x_2^1, \cdots x_N^1\}, \ \{x_1^2, x_2^2, \cdots x_N^2\}, \ \cdots \ \{x_1^M, x_2^M, \cdots x_N^M\}. \tag{5.1.10}$$

For each of the M bootstrap samples we have to calculate the average x_α^B,

$$x_\alpha^B = \frac{1}{N} \sum_{i=1}^{N} x_i^\alpha, \ i = 1, \ldots N, \ \alpha = 1, \ldots M. \tag{5.1.11}$$

We obtain the expectation value of the observable by taking the average over all bootstrap sets,

$$\overline{x^B} = \frac{1}{M} \sum_{\alpha=1}^{M} x_\alpha^B. \tag{5.1.12}$$

The error can be computed with the standard deviation of the bootstrap sample,

$$\sigma^2_{\overline{x^B}} = \frac{1}{M-1} \sum_{k=1}^{M} (\overline{x_B} - x_k^B)^2. \tag{5.1.13}$$

Weighted Bootstrap resampling

As we are using an adaptive stepsize method the same argument as for the weighted binning holds and we have to apply a weighted bootstrap sampling. For the weighted Bootstrap resampling we follow the steps shown before. Now we do an additional resampling for the weight factors, which is the adaptive stepsize ϵ,

$$\{\epsilon_1^1, \epsilon_2^1, \cdots \epsilon_N^1\},\ \{\epsilon_1^2, \epsilon_2^2, \cdots \epsilon_N^2\},\ \cdots\ \{\epsilon_1^M, \epsilon_2^M, \cdots \epsilon_N^M\}. \tag{5.1.14}$$

We then get the weighted average for one bootstrap sample as

$$x^B_{\alpha,weighted} = \frac{\sum_i \epsilon_i^\alpha \cdot x_i^\alpha}{\sum_i \epsilon_i^\alpha},\ i = 1, \dots N,\ \alpha = 1, \dots M. \tag{5.1.15}$$

And in the end we obtain the average over all bootstrap sets

$$\overline{x^B}_{weighted} = \frac{1}{M} \sum_{\alpha=1}^{M} x^B_{\alpha,weighted}. \tag{5.1.16}$$

5.1.3 Moments

A central point in statistics are moments, [8][27]

$$\lambda_n = \langle O^n \rangle. \tag{5.1.17}$$

In particular *reduced moments*, which are moments about the mean, will be useful in the course of the analysis of numerical results,

$$\mu_n = \langle (O - \langle O \rangle)^n \rangle. \tag{5.1.18}$$

The reduced second moment is the variance, and if we multiply this quantity by the spatial volume of the lattice we get the *susceptibility*,

$$\chi(O) = N_s^3\ \mu_2 = N_s^3 (\langle O^2 \rangle - \langle O \rangle^2). \tag{5.1.19}$$

The relation to the variance makes the susceptibility an indicator for how much the results are deviating from the mean. Away from a phase transition the system stays in one phase and the fluctuations around the mean are small. Around a phase transition there are two phases, in which the system can stay. The system fluctuates between those phases which results in large fluctuations. It follows that at the phase transition the susceptibilty shows a maximum and is therefore a quantity for locating a phase transition.
The location of the phase transition can also be determined by the vanishing third central moment μ_3,

$$\mu_3 = \langle (O - \langle O \rangle)^3 \rangle = \langle O^3 \rangle - 3\langle O^2 \rangle \langle O \rangle + 2\langle O \rangle^2. \tag{5.1.20}$$

One can furthermore define standardised reduced moments,

$$B_n = \frac{\mu_n}{\mu_2^{n/2}}. \tag{5.1.21}$$

B_3 is the skewness and can be used for analysis in the same way as the third reduced moment. B_4 is the kurtosis,

$$B_4 = \frac{\langle (O - \langle O \rangle)^4 \rangle}{\langle (O - \langle O \rangle)^2 \rangle^2} = \frac{\langle O^4 \rangle - 4\langle O^3 \rangle \langle O \rangle + 6\langle O^2 \rangle \langle O \rangle^2 - 3\langle O \rangle^4}{\langle O^2 \rangle^2 - 2\langle O^2 \rangle \langle O \rangle^2 + \langle O \rangle^4}. \tag{5.1.22}$$

	1st order	3D Ising	Crossover
$B_4(\beta_c)$	1	1.604	3

Table 5.1.1: *Order of the phase transition indicated by the value of the kurtosis at the phase transition, $B_4(\beta_c)$.*

Its minimum signals the phase transition and it can also used to determine the order of the phase transition, which is displayed in Table 5.1.1. It has to be stressed that the order of the phase transition can only be deduced from the value of B_4 at the critical temperature. Away from the phase boundary the order parameter fluctuates around the mean following a normal distribution. In this case the kurtosis is always 3, but does not necessarily denote a crossover. [27] Therefore to determine the order of the phase transition it is necessary to first locate the phase transition, e.g. analysing the susceptibility or the skewness and afterwards calculate the kurtosis in an appropriate region around the phase transition. The analysis of the order of the transition from the kurtosis is an elaborate business. For the purpose of this thesis it is sufficient to state that the susceptibility scales with the volume. At a first order phase transition the peak of the susceptibility increases with increasing spatial volume. For a crossover the peak of the susceptibility saturates with increasing volume.

5.2 Deconfinement transition in $SU(3)$ for $\mu = 0$

The deconfinement transition is related to the spontaneous breaking of the $Z(3)$ symmetry in pure gauge theory, signalling by a transition from vanishing Polyakov expectation value to a finite value. As dynamical quarks break $Z(3)$ symmetry explicitly, the Polyakov loop is strictly speaking not an order parameter anymore. Thus this explicit breaking becomes small for large quark mass, which applies to the effective theory which was derived for heavy quarks because of $\kappa \to 0$. So we can investigate the theory looking at the Polyakov loop as an approximate order parameter still.

The numerical results concerning the deconfinement transition will be shown in the next sections. We will start in the pure gauge case with only nearest neighbor interactions. In this regime we will investigate the Complex Langevin dynamics and check if the tools for correctness introduced in chapter 3 work properly. Afterwards we will simulate for the full effective theory including fermions applying the findings from the basic investigation in pure gauge.

5.2.1 Pure gauge theory for $N_\tau = 6$

The simulation of the pure gauge sector has been done for nearest neighbor interaction only, meaning that we include only the λ_1 part of the gauge action. It is though not necessary to use the Complex Langevin algorithm in the pure gauge case, as without fermions there is no sign problem, which arises from the complex fermion determinant. But this case is a rather simple way to check the properties of the CL evolution.
To prevent the simulation from *runaways*, the simulation has been done for different methods of the adaptive stepsize. As the Complex Langevin algorithm is known to give wrong results [3][5], we need different tools to check if the results are going in the correct direction. Therefore we will compare with data produced using the Metropolis algorithm from [25] and we will apply the Langevin operator proposed in [3][5]. The critical value $\lambda_{1,c}$ can be

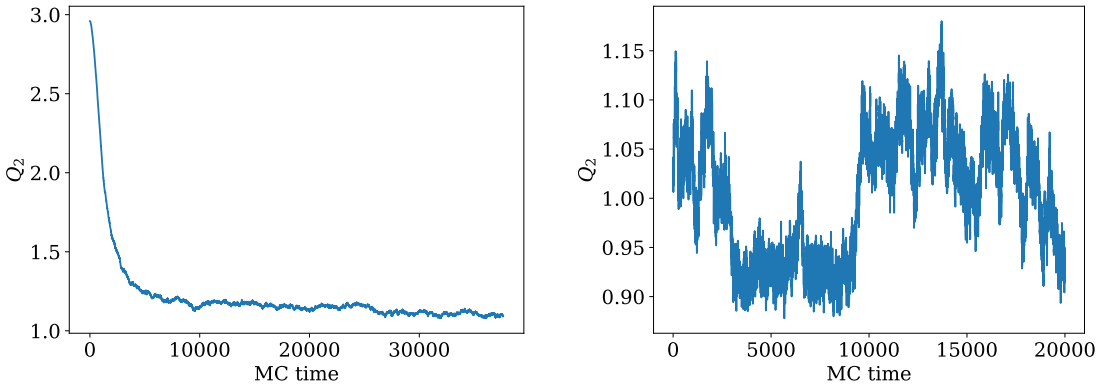

(a) Complex Langevin simulation.

(b) Metropolis simulation.

Figure 5.2.1: *Time evolution during the thermalization period of the Polyakov loop observable Q_2 for $N_\tau = 6, N_s = 12, \lambda_1 = 0.1878$.*

determined by looking at the susceptibility of the order parameter, which for the deconfinement transition is the Polyakov loop L. We will use the Polyakov loop observables Q_1, Q_2. The histograms and the evolution in Langevintime are as well useful tools to observe the developement of CL simulation.

Simulation parameters

A starting point for a successful simulation is to estimate how long the thermalization to equilibrium takes, how to achieve independent data and how many data are needed to give sufficiently accurate results.

We start with estimating which time the thermalization process requires. Therefore we look at the time evolution for Metropolis and CL. The trajectory through the thermalization process for Q_2 is shown in Figure 5.2.1. From this it can be deduced that around the phase transition for the CL simulation $30,000$ thermalization steps are sufficient. In the Metropolis simulation the system is already in the beginning fluctuating in the vicinity of the two phases. Hence for the Metropolis simulation one needs significantly less steps to reach equilibrium. Thus $2,000$ thermalization steps were chosen.

The next step is to estimate how many data have to be discarded in between two measurements to obtain approximately independent data. In Equation 5.1.7 it was shown that an amount of τ_{int} data has to be neglected to achieve this. For the Metropolis algorithm, which was used in this thesis to generate data for comparison with CL, the integrated autocorrelation time was computed in [25][1] to be $\tau_{int} \approx 120$ away from a phase transition and $\tau_{int} \approx 1600$ close to a phase transition. It was shown that 150 sweeps were sufficient. During the CL and Metropolis simulations 200 data were discarded in between each measurement.

[1]In [25] the definition of the autocorrelation from [15], $\tau_{int}^{Gattringer}$ was used. In this thesis the definition from [8] was used, τ_{int}^{Berg}, with the relation $\tau_{int}^{Berg} = 2\tau_{int}^{Gattringer}$. This is why I am using the estimate of τ_{int}, while in [25] $2\tau_{int}$ is used to estimate the autocorrelation between data.

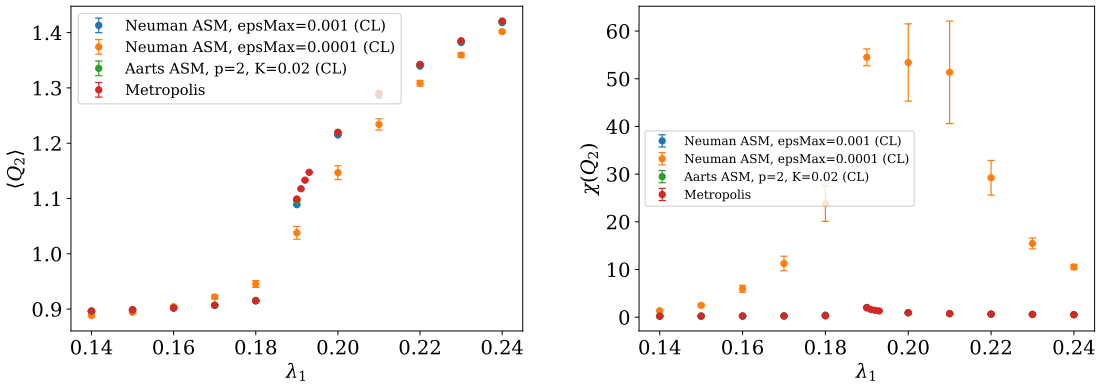

(a) $\langle Q_2 \rangle$. (b) $\chi(Q_2)$.

Figure 5.2.2: *$\langle Q_2 \rangle$ and susceptibility $\chi(Q_2)$ as a function of λ_1 for $N_\tau = 6, N_s = 16$ for different adaptive stepsize methods for the Complex Langevin simulation in comparison with the the Metropolis simulation.*

The Complex Langevin simulation in this section was done with 40,000 measurements, for the Metropolis simulation 10,000 data were generated.

Checking correctness of the Complex Langevin simulation

We start with comparing different methods of choosing an adaptive stepsize for CL with data generated using the aforementioned Metropolis algorithm. Figure 5.2.2 shows the average value of the the Polyakov loop observable Q_2 for different adaptive stepsize methods (ASM) for CL and comparing it with data obtained from the Metropolis simulation. The *Aarts ASM* with $p = 2, K = 0.02$ was used, as well as the *Neuman ASM*, once with $\epsilon_{max} = 10^{-3}$ and once with $\epsilon_{max} = 10^{-4}$. Comparing the *Neuman ASM* for different ϵ_{max}, but the same amount of data, we see that an $\epsilon_{max} = 10^{-4}$ is not sufficient to describe the correct behavior. For this limited simulation time the stepsize is to small to explore the configuration space properly. If the stepsize is too small we need higher statistics to achieve correct results, which makes the simulation computationally more expensive. Thus using $\epsilon_{max} = 10^{-3}$ is an appropriate choice as it agrees well with the Metropolis data, as well as the data using the *Aarts ASM* with the given parameters.

The next tool to check correctness is the application of the Langevin operator to the Polyakov loop. The expression of the Langevin operator acting on the Polyakov loop was derived in section 3.4. During the simulation the quantity $\tilde{L}L$ is complex. Thus we save the real and imaginary part separately, $\mathrm{Re}(\tilde{L}L)$, $\mathrm{Im}(\tilde{L}L)$. This quantities as a function of λ_1 are shown in Figure 5.2.3. In agreement with the results we got from comparing the CL with Metropolis, we also find here that the simulation using *Aarts ASM* and the *Neuman ASM* using $\epsilon_{max} = 10^{-3}$ show $Re(\tilde{L}L) \approx 0$ and $Im(\tilde{L}L) \approx 0$. The results from *Neuman's ASM* using $\epsilon_{max} = 10^{-4}$ for $\lambda_1 < \lambda_{1,c}$ show a noticeably higher deviation from zero than the results for the other two methods. Especially for $\lambda_1 > \lambda_{1,c}$ the deviation from zero is quite big, tough this is already away from the region of interest.

From this we can conclude that *Aarts ASM* with $p = 2$, $K = 0.02$ and *Neuman's ASM* with

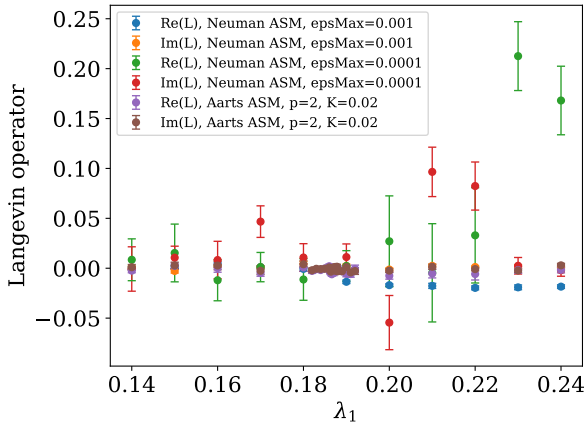

Figure 5.2.3: *Real part and imaginary part of the Langevin operator acting on L, respectively for $N_s = 16$. Comparison for different adaptive stepsize methods for the Complex Langevin simulation.*

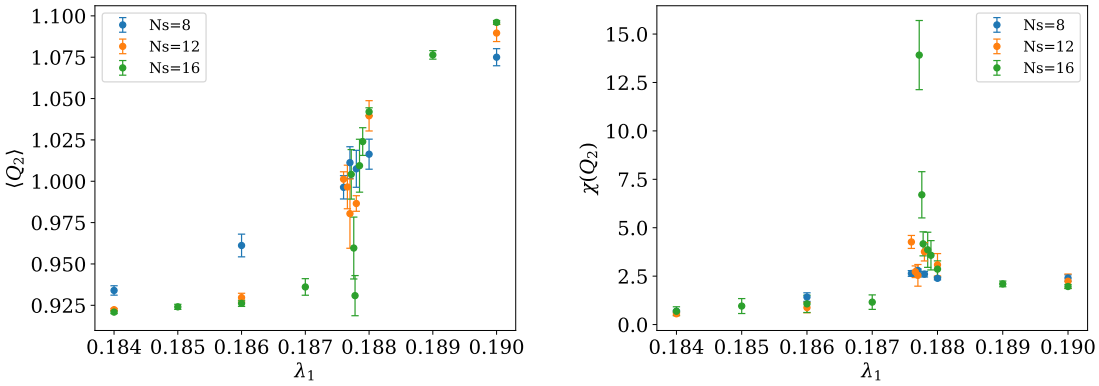

(a) $\langle Q_2 \rangle$.

(b) $\chi(Q_2)$.

Figure 5.2.4: *Locating the phase transition: $\langle Q_2 \rangle$ and susceptibility $\chi(Q_2)$ as a function of λ_1 for $N_\tau = 6$ for different spatial volumes. The simulation was done using the Complex Langevin algorithm with Aarts ASM for $p = 2, K = 0.02$.*

$\epsilon_{max} = 10^{-3}$ give sufficiently accurate results. This has been proven by comparison with Metropolis generated data and by applying the Langevin operator to the order parameter L. Hence we used the *Aarts ASM* with $p = 2, K = 0.02$ in the investigation for finding the critical value $\lambda_{1,c}$, at which the deconfinement transition takes place.

Locating the phase transition

We already discussed different moments and related quantities, that can be used to locate a phase transition. Additionally we look at the histograms around that region and at the trajectory in Langevin time space. We will also comment on issues of the CL simulation during this analysis.

We start with investigating the maximum of the susceptibility of the absolute value of the

	Q_1		Q_2	
N_s	$\lambda_{1,c}$	β_c	$\lambda_{1,c}$	β_c
8	0.1876(3)	6.3259(2)	0.1876(2)	6.3259(2)
12	0.1876(3)	6.3259(2)	0.18774(2)	6.32605(5)
16	0.18770(2)	6.325600(2)	0.18772(2)	6.3260(10)

Table 5.2.1: *Critical couplings $\lambda_{1,c}, \beta_c$ obtained from the peak of the susceptibility of Q_1, Q_2 for different spatial extents and $N_\tau = 6$. Results obtained from CL simulation.*

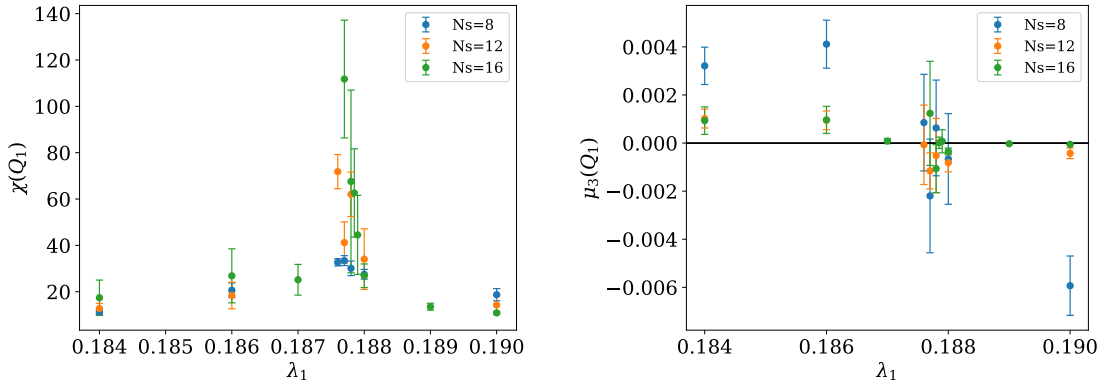

(a) $\chi(Q_1)$. (b) $\mu_3(Q_1)$.

Figure 5.2.5: *Locating the phase transition: susceptibility $\chi(Q_1)$ and third reduced moment $\mu_3(Q_1)$ as a function of λ_1 for $N_\tau = 6$ for different spatial volume. Simulation using CL. More data around the phase transition have been included compared to Figure 5.2.4.*

Polyakov loop, which is described by either Q_1 or Q_2. It is expected that Q_1 and Q_2 indicate the phase transition respectively at $\lambda_{1,c}^{Q_1} \approx \lambda_{1,c}^{Q_2}$. The first observable will be Q_2. The behavior of $\langle Q_2 \rangle$ and the respective susceptibility as a function of λ_1 are shown in Figure 5.2.4. As suspected, the change of $\langle Q_2 \rangle$ becomes steeper with increasing volume. With considering the susceptibility in Figure 5.2.4(b) we find $\lambda_{1,c} = 0.18772(2)$ for $N_s = 16$. The results for different volumes are found in Table 5.2.1. To achieve results with higher accuracy one would need more data around the phase transition, which would require high enough statistics and rather more sweeps in between the measurements, as the integrated autocorrelation time becomes larger around the phase transition.

Next we continue with studying the behavior of $\langle Q_1 \rangle$ around the phase transition. Figure 5.2.5 shows the susceptibility and the third reduced moment of Q_1. The susceptibility peaks at $\lambda_1 = 0.18770(2)$ for $N_s = 16$. Locating the value at which μ_3 crosses zero is more tricky, as μ_3 is fluctuating and changing between positive and negative values frequently close to the transition. Therefore the error is bigger, $\lambda_1 = 0.1878(1)$.

Including all these results we can say that $0.1877 < \lambda_{1,c} < 0.1879$ and thus $\lambda_{1,c} = 0.1878(1)$ when studying the peak of the susceptibility and the location at which the third reduced moment vanishes.

The next step is to look at the histograms and the Monte Carlo history to get some further knowledge about the dynamics of the Complex Langevin simulation. We will furthermore

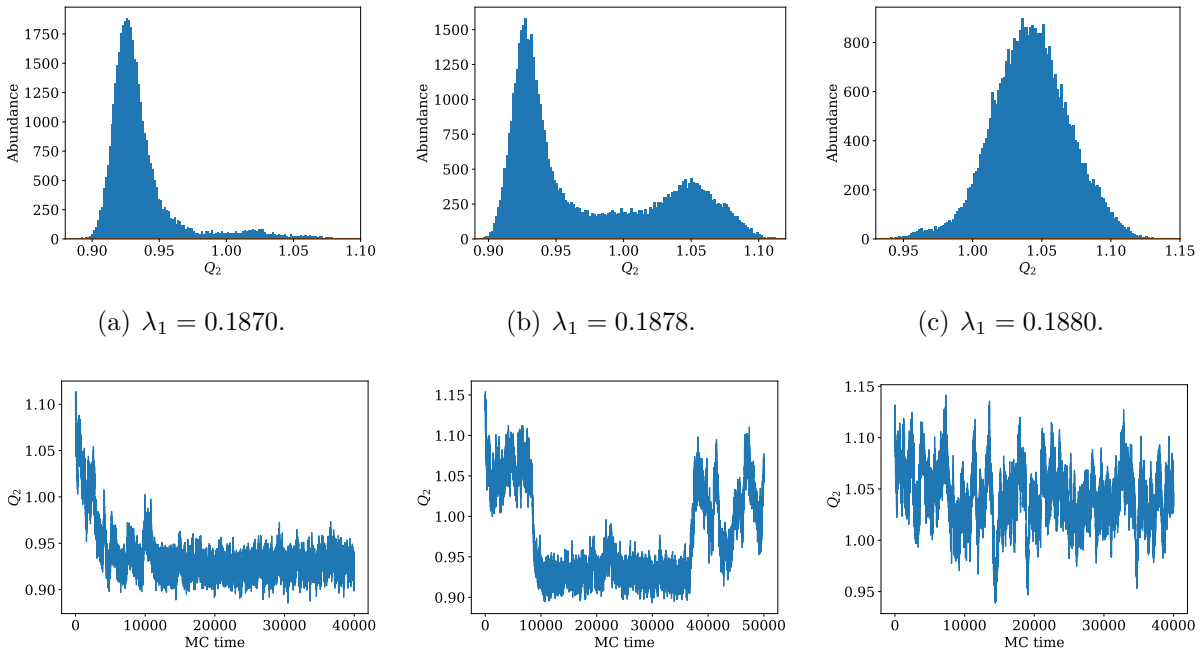

(a) $\lambda_1 = 0.1870$. (b) $\lambda_1 = 0.1878$. (c) $\lambda_1 = 0.1880$.

(d) $\lambda_1 = 0.1870$. (e) $\lambda_1 = 0.1878$. (f) $\lambda_1 = 0.1880$.

Figure 5.2.6: *Histograms and trajectories of the simulation for the observable Q_2 for $N_\tau = 6, N_s = 16$ slightly below, at and slightly above $\lambda_{1,c}$. The simulation was done using the Complex Langevin algorithm with Aarts ASM for $p = 2, K = 0.02$.*

compare it with the dynamics of the Metropolis simulation. The histograms show how much the two phases are visited during the simulation. Before the phase transition takes place the system is supposed to be in the first phase. When the system comes closer to the phase transition, tunneling to the second phase appears. We expect to see one peak at the value of the first phase and a smaller peak at the value of the second phase. At the phase transition both peaks become equally high. Going away from the phase transition to $\lambda_1 > \lambda_{1,c}$ the second phase is majorly visited and the peak corresponding to the first phase decreases until it vanishes as the system stays in the second phase.

Figure 5.2.6 shows the histograms and the Monte Carlo trajectories of the CL simulation for $N_s = 16$ slightly below, at and slightly above the critical coupling. We use the Polyakov observable Q_2 in the following description. We can see a transition between the two phases, around $Q_2^1 \approx 0.93$ in the first phase and $Q_2^2 \approx 1.05$ in the second phase. Before the transition takes place, shown at $\lambda_1 = 0.1870$, the system mainly stays in the first phase. Though looking at the corresponding trajectory it is not entirely clear, if the system is already tunneling or if it is not thermalized enough. For tunneling speaks that the peak value of $Q_{2,max} \approx 1.1$, which is around the mean of the second phase. For not enough thermalization speaks that in Figure 5.2.1 for CL we pass values of Q_2 which are higher than the mean of the phase before the system equilibrates and fluctuates around the mean. One could clarify this issue by investigating a higher amount of data and the corresponding history of the trajectory. We can compare this case already with the Metropolis data from Figure 5.2.7(a). For the same $\lambda_1 = 0.187$ the system stays in the first phase, except for a few fluctuations, and a thermalization of $2,000$ steps was already enough.

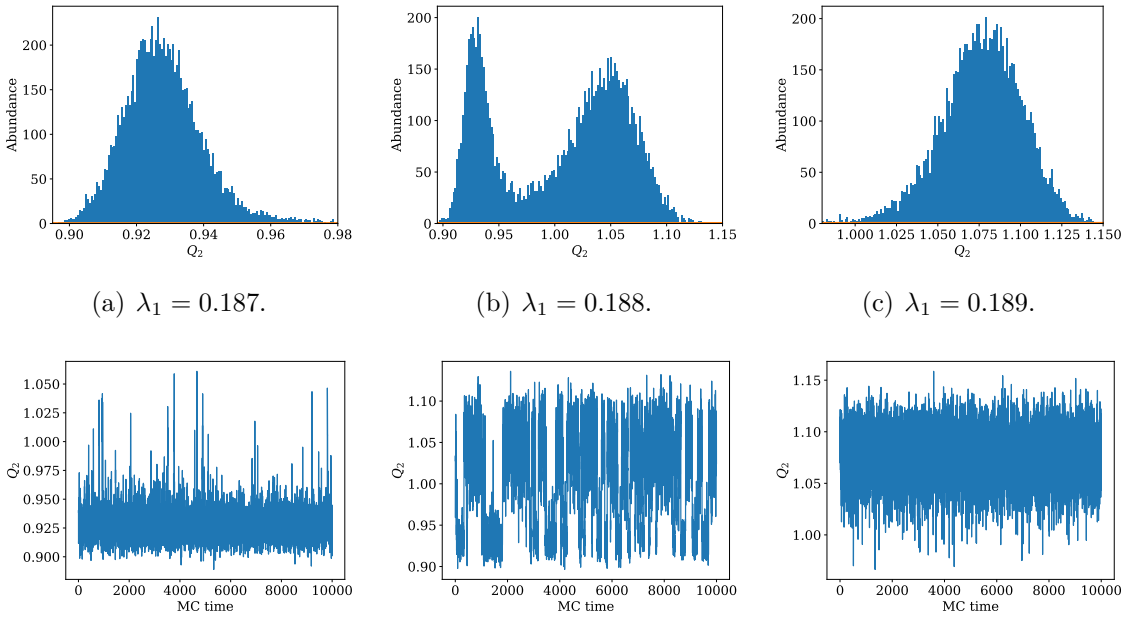

(a) $\lambda_1 = 0.187$. (b) $\lambda_1 = 0.188$. (c) $\lambda_1 = 0.189$.

(d) $\lambda_1 = 0.187$. (e) $\lambda_1 = 0.188$. (f) $\lambda_1 = 0.189$.

Figure 5.2.7: *Histograms and trajectories of the simulation for the observable Q_2 for $N_\tau = 6, N_s = 16$ slightly below, at and slightly above $\lambda_{1,c}$. The simulation was done using the Metorpolis algorithm.*

Another difference between Metropolis and CL dynamics occurs when we take a look at the vicinity of the phase transition around $\lambda_{1,c}$. There is a slight discrepancy between the results from the Complex Langevin simulation and the Metropolis simulation. We get $\lambda_{1,c}^{(CL)} = 0.1878(2)$ and $\lambda_{1,c}^{(M)} = 0.1880(5)$. Quantitatively both results are reliable, but it should be emphasized that the dynamics of the system differs depending on the algorithm used. The height of the two phases in the histogram for Metropolis, $\lambda_{1,c}^{(M)} = 0.188$ are almost equal, whereas for CL at $\lambda_1 = 0.1878$ the peak belonging to the first phase is noticeably higher. The reason for this is that in the Metropolis simulation the tunneling between the two phases happens much more often, cf. Figure 5.2.7(e), than in the simulation using CL, cf. Figure 5.2.6(e). And for CL already at $\lambda_1 = 0.188$ there is no significant tunneling happening anymore, although we have four times more data $(40,000)$ compared to the Metropolis simulation $(10,000$ data). What is noticeable as well is that the value of the critical coupling obtained by analyzing the susceptibility, $\lambda_{1,c} = 0.18772(2)$, differs from the observation done from the histograms, where $\lambda_{1,c} = 0.1878(2)$ is slightly below the phase transition.

We already saw that CL dynamics have a tunneling issue. It turns out that the severeness will depend on the spatial extent of the lattice. To see this we look at Figure 5.2.8. At $\lambda_1 = 0.1876 \Leftrightarrow \beta = 6.3259$, for $N_s = 12$ both phases are almost equally high, whereas for $N_s = 16$ the system stays more in the first phase, indicating that this is still $\beta < \beta_c$. This observation comes from too few tunneling especially for $N_s = 16$. Thus to obtain sufficient tunneling we need more data with increasing spatial volume. For $\lambda_1 = 0.1878 \Leftrightarrow \beta = 6.3261$, the abundance of states in the second phase grows for $N_s = 16$, meaning that we get closer to the phase transition.

In Figure 5.2.9 we see the histograms close around $\lambda_{1,c}$ for $N_s = 12$. This yields to $\lambda_{1,c} =$

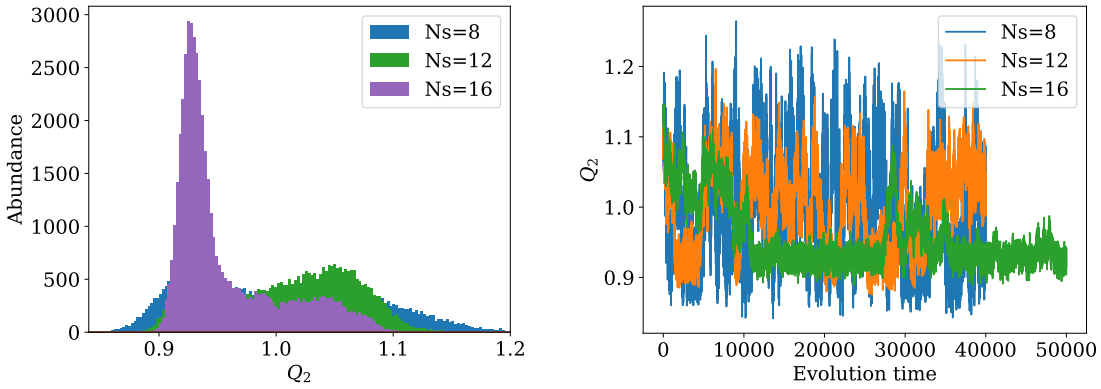

(a) Histograms for $\lambda_1 = 0.1876$.

(b) Time evolution for $\lambda_1 = 0.1876$.

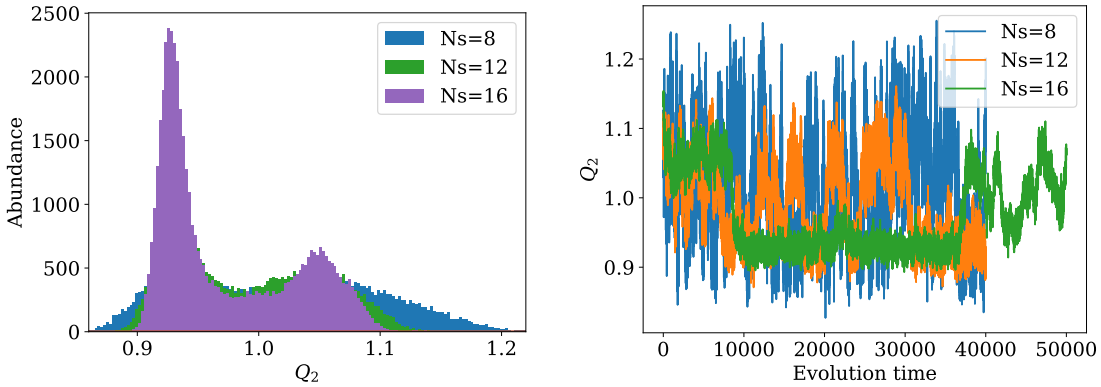

(c) Histograms for $\lambda_1 = 0.1878$.

(d) Time evolution for $\lambda_1 = 0.1878$.

Figure 5.2.8: *Histogram and time evolution of the simulation for the observable Q_2 for $N_\tau = 6$ for different volumes $N_s = 8, 12, 16$. The simulation was done using Complex Langevin algorithm with Aarts ASM for $p = 2, K = 0.02$.*

0.1772(2) for $N_s = 12$. In the error range this agrees with the result which was found when studying the peak of the susceptibility.

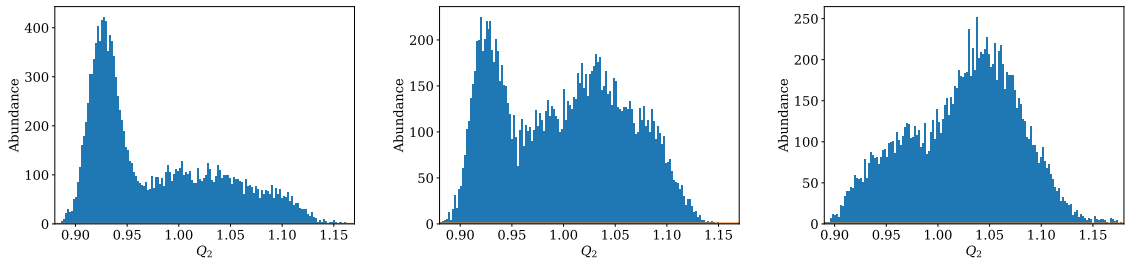

(a) $\lambda_1 = 0.18770$.

(b) $\lambda_1 = 0.18772$.

(c) $\lambda_1 = 0.18774$.

Figure 5.2.9: *Histogram of Q_2 for $N_\tau = 6, N_s = 12$ around the phase transition. The simulation was done using Complex Langevin algorithm with Aarts ASM for $p = 2, K = 0.02$.*

To conclude the results obtained from the Complex Langevin simulation, we find that $0.187 < \lambda_{1,c} < 0.188$. We can roughly approximate this result to $\lambda_{1,c}^{CL} = 0.1875(5)$. The

value $\lambda_{1,c} = 0.18788(30)$ from [17] lies in this range as well. Thus the accuracy of our CL simulation is rather broad in this region. A higher accuracy of the results could be achieved with higher statistics around the phase transition.

Compared to the Metropolis simulation the CL simulation is computationally excessively more expensive. The difference in the numerical performance comes from the the fact that calculating the driftterms at each Langevin time step takes longer than a Metropolis update. Aside from that the CL simulation requires a longer thermalization procedure and in general needs more data, depending on the volume, to show appropriate tunneling behavior. It is furthermore important to control the dynamics with the tools that were shown to ensure correct results.

Characterizing the phase transition

The order of the phase transition is of particular interest. It was discussed that analyzing the fourth standardized moment B_4 is quite a delicate business. Therefore we will look at the scaling of the susceptibility with spatial volume instead. We saw in Figure 5.2.4 and Figure 5.2.5 that the peak of the susceptibility grows with increasing spatial volume. This indicates the phase transition to be of first order.

The goal of investigating the pure gauge deconfinement transition was to get some information about the dynamics of the CL simulation and getting used to the tools which are advantageous to check the correctness of the results. To conclude the findings, an adaptive stepsize method has to be chosen, where the *Aarts AS* with $p = 2, K = 0.02$ gave satisfying results. Due to insufficient tunneling for higher spatial volume a choice of $N_s = 12$ with $N = 40,000$ data is appropriate. Higher spatial volumes require a higher amount of statistics. We need to stress that simulations with those parameters work well in the pure gauge case. For simulations including fermions it is still necessary to check the correctness of the results, especially comparing with results from a Metropolis simulation, applying the Langevin operator and using an adaptive stepsize method.

5.2.2 Adding quarks up to $O(\kappa^4)$ for $N_\tau = 4$

With the results from the investigation of the CL dynamics in the pure gauge effective theory we proceed with studying the deconfinement phase transition including quarks.

As argued in subsection 2.4.1 including dynamical quarks leads to an explicit breaking of the $Z(3)$ symmetry, which is though small for large fermion masses. It was shown that there exists a critical $h_{1,c}$, where at $h_1 < h_{1,c}$ there is expected to be a first order phase transition going into a crossover for $h_1 > h_{1,c}$ in the effective theory. At $(h_{1,c}, \lambda_{1,c})$ there is a second order tricritical point. This behavior is shown in Figure 5.2.10.

For $N_\tau = 4, N_f = 1$ for the full effective theory and $\langle Q_2 \rangle$ as order parameter the location of the critical endpoint was found to be at $(\lambda_c, h_c) = (0.16497(27), 0.00194(17))$[2]. [25]

[2] λ, h are equal to λ_1, h_1, which is used throughout this thesis. To not confuse the critical couplings at the critical point from [25], λ_c, h_c, with the critical couplings, at which the first order phase transition takes place, we will stay with the notation $\lambda_{1,c}, h_{1,c}$.

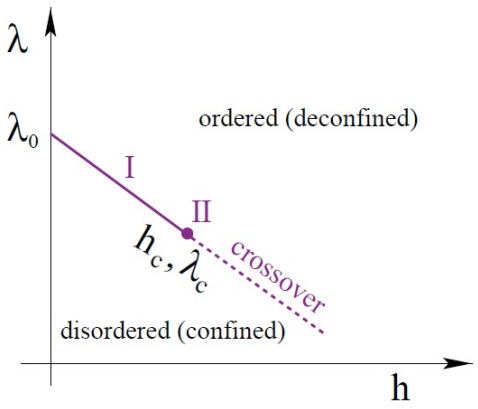

Figure 5.2.10: *Phase boundary of the deconfinement phase transition as expected for the effective theory, taken from [13].*

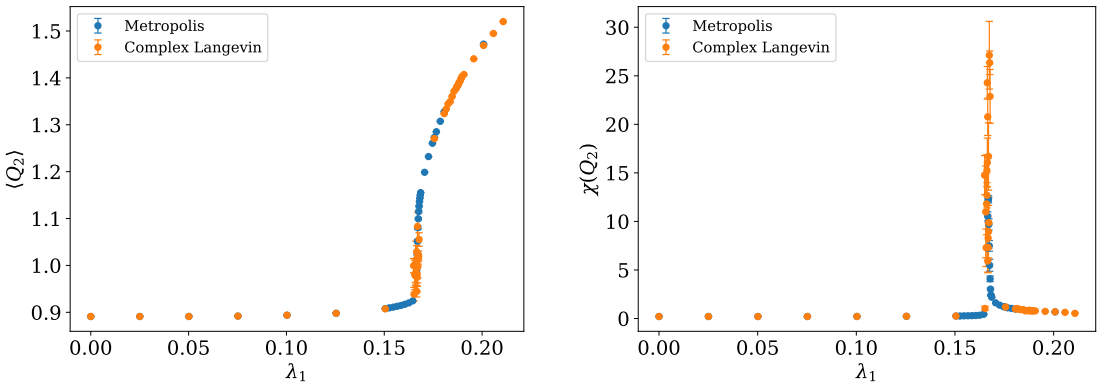

(a) $\langle Q_2 \rangle$. (b) $\chi(Q_2)$.

Figure 5.2.11: *Q_2 and corresponding susceptibility for $N_\tau = 4, N_s = 12, N_f = 1, h_1 = 0.0006$. Comparison between Metropolis and Complex Langevin simulation.*

We investigated one particular parameter set in the first order region, simulating at $h_1 = 0.0006 < h_c = 0.00194$. It follows that we are expecting to see a first order phase transition to take place at $\lambda_{1,c} > \lambda_c = 0.16497(27)$. We included the following contributions to the effective action in the simulation: The quark contributions were considered up to $O(\kappa^4)$ in the hopping parameter expansion. The gauge contributions include nearest neighbor coupling λ_1, next-to-nearest neighbor coupling λ_2, as well as the contribution from the adjoint representation λ_a[3] from the strong coupling expansion.

To see the big picture we first look at how the Polyakov loop observable Q_2 as a function of λ_1 changes in Figure 5.2.11, where the CL and Metropolis simulations are compared. Both simulations agree well.

Before we start with locating and characterizing the phase transition, we check if the criterion for correctness is fulfilled. Figure 5.2.12 shows the real and imaginary part of the Langevin operator acting on L to vanish for $\lambda_1 < \lambda_{1,c}$. This is an indicator for the simu-

[3]Short reminder: the contribution from the adjoint representation was implemented improperly, see comment in section 2.3.

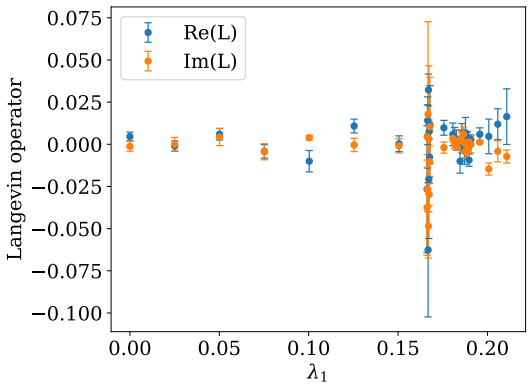

Figure 5.2.12: *Real and imaginary part of the Langevin operator acting on L for $N_\tau = 4, N_s = 12, h_1 = 0.0006$.*

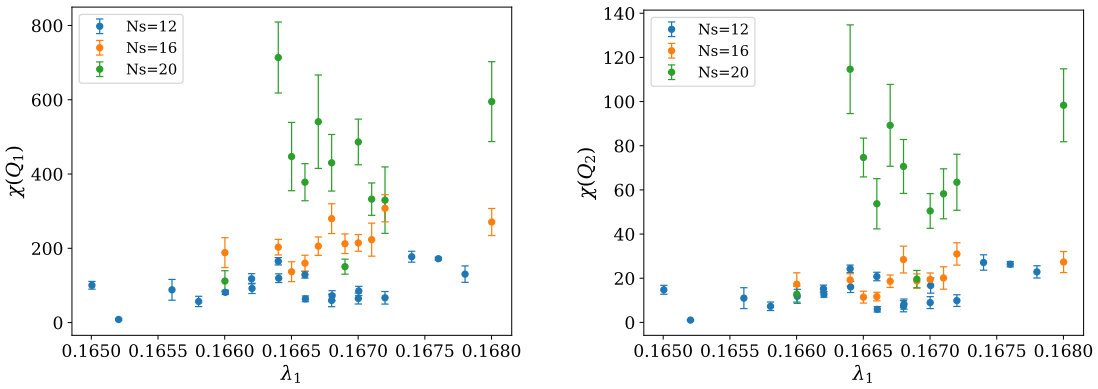

(a) $\chi(Q_1)$. (b) $\chi(Q_2)$.

Figure 5.2.13: *Susceptibility of the absolute Polyakov loop variables Q_1 and Q_2 for $N_\tau = 4, N_s = 12, N_f = 1, h_1 = 0.0006$.*

lation converging to the correct result. Around the phase transition the Langevin operator acting on L increases, though the deviation from zero is small enough to ensure reliable results. This is in agreement with what we found when we compared with the Metropolis simulation data. This means that the *Aarts AS* with $p = 2, K = 0.02$ and 200 sweeps in between the measurements is a good choice also for the effective theory including fermions.

To quantitatively locate the phase transition we already discussed three possible quantities, we focus on the maximum of the susceptibility. The location of the peak of the susceptibility for the quantities Q_1, Q_2 is contrasted in Figure 5.2.13 and the quantitative results obtained from the Complex Langevin simulation are shown in Table 5.2.2. We got the same results for the critical couplings of Q_1 and Q_2. For the Metropolis data we get $\lambda_{1,c}^{M} = 0.1666(2)$ for $N_s = 12$ for Q_1, Q_2 respectively. Including Metropolis and CL simulation for different volumes, the critical coupling has to be in the range $\lambda_{1,c}^{CL,N_s=12} = 0.1664(2) < \lambda_{1,c} < \lambda_{1,c}^{CL,N_s=16} = 0.1668(1)$. A rough estimate could be taken to be $\lambda_{1,c} = 0.1666(3)$ for the critical coupling at the first order transition for $h_1 = 0.0006$. This is indeed bigger than the critical coupling at the critical point $\lambda_c = 0.16497(27)$ and smaller than $\lambda_0 = 0.167310(32)$.

N_s	$\lambda_{1,c}$	$\beta_{1,c}$
12	0.1664(2)	6.0446(5)
16	0.1668(1)	6.0457(3)
20	0.1664(1)	6.0446(2)

Table 5.2.2: *Critical couplings $\lambda_{1,c}, \beta_c$ obtained from the peak of the the susceptibility of Q_1, Q_2 for different spatial extents N_s and $N_\tau = 4, N_f = 1, h_1 = 0.0006$. The critical coupling is found to be the same for Q_1 and Q_2 and therefore displayed only once. Results obtained from CL simulation.*

We are as well interested in the order of the phase transition. Therefore we look at how the peak of the susceptibility behaves with increasing volume. This can be seen in Figure 5.2.13. We see that the peak is growing with increasing spatial volume. This signals a first order phase transition as expected.

With these results we can say that, as in the pure gauge case, the Complex Langevin algorithm serves very well to describe the first order deconfinement transition of the full effective theory. We have tools by hand to control the CL dynamics and the next step would be to include a nonzero chemical potential, the purpose of why we started implementing the Complex Langevin equation. CL doesn't see the sign problem, which arises when including a chemical potential. A sufficient amount of statistics should be ensured to obtain accurate results.

5.3 Chiral condensate

As mentioned in subsection 2.4.3 there is a restoration of the chiral symmetry expected to take place in the small mass region for high temperature. We now want to see if this can be confirmed for Wilson fermions in the effective theory. The simulations in this section have been exclusively done using the Metropolis algorithm.

5.3.1 Numerical results

It is expected that QCD exhibits restoration of the chiral symmetry at high temperatures. Though chiral symmetry is explicitly broken by Wilson fermions, we want to check if there is a partial restoration happening. Large temperatures are realized at a small temporal lattice extent N_τ.
We look at the chiral condensate as a function of the gauge coupling β. For the simulation the definition of the chiral condensate as it was derived in Equation 4.2.3 was used. Commonly in literature the absolute value of the chiral condensate is taken. This is why the results herein have a global minussign compared to most results in literature. This is also valid for comparison with [20], fig 5.15, where the chiral condensate decreases with increasing β, where according to the above definition the chiral condensate increases for increasing β.

We recap the behavior of the different contributions of the effective action to the chiral condensate for $\kappa = 0.04$. The corresponding plots are shown in Figure 5.3.1. The contribution of the static determinant is small compared the other contributions and therefore negligible. The κ^2-correction doesn't change this behavior and therefore is not shown here explicitly.

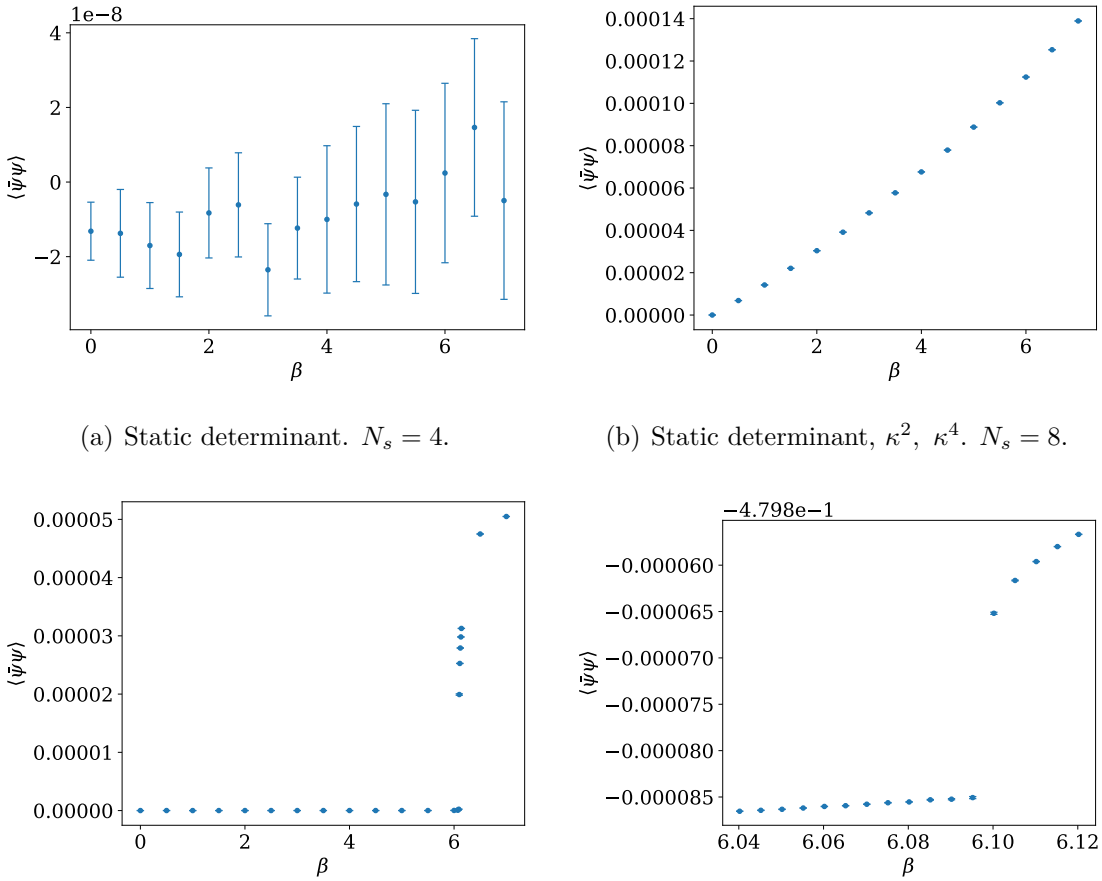

(a) Static determinant. $N_s = 4$.

(b) Static determinant, κ^2, κ^4. $N_s = 8$.

(c) Static determinant, λ_1. $N_s = 16$.

(d) Static determinant, κ^2, κ^4, λ_1, shift. $N_s = 16$.

Figure 5.3.1: *Chiral condensate as a function of β for $N_\tau = 4, N_f = 2, \kappa = 0.04$ shown for different contributions to the action and for different volumes.*

The κ^4-correction leads to an increase of the chiral condensate with β and is caused by vacuum graphs of order $\kappa^4 u$ and $\kappa^6 u^2$. [20] Including the λ_1 contribution leads to a rapid change of the order parameter, the chiral condensate, at the critical coupling $\beta = \beta_c$. The global shift, which is now also included in Figure 5.3.1(d), comes from the rescaled fields and therefore

$$\langle \bar{\psi}\psi \rangle(\beta = 0) = -\frac{8 N_f \; N_c \; \kappa}{N_\tau}. \tag{5.3.1}$$

For the parameters used in Figure 5.3.1, $\kappa = 0.04, N_\tau = 4, Nf = 2, N_c = 3$ the shift is $\langle \bar{\psi}\psi \rangle(\beta = 0) = -0.48$, which is successfully reproduced in the simulation.

The next interesting topic is to locate the phase transition and discuss the order of the transition. A small value of κ corresponds to heavy quarks. Thus we are close to the upper right corner in the Columbia plot. Decreasing the mass, we move along the upper horizontal line towards the upper left corner. As discussed earlier, the system is expected to undergo a first order transition in the heavy mass region for low κ, until a second order tricritical point is crossed, going over into a broad crossover region. For high κ, or equivalently small masses, we get close to the chiral limit. This is the region in the Columbia plot, which is still under

investigation. It is possible that chiral symmetry is restored, showing a first order transition.[4]

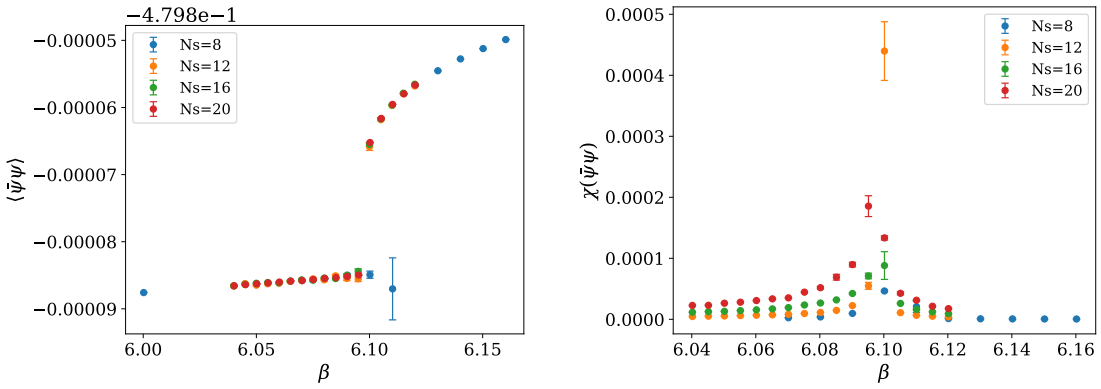

(a) $\langle\bar{\psi}\psi\rangle$. (b) $\chi(\bar{\psi}\psi)$.

Figure 5.3.2: *Chiral condensate and corresponding susceptibility as a function of β for $N_\tau = 4, \kappa = 0.04$ shown for different volumes.*

We first take a look at the case of heavy fermions, $\kappa = 0.04$. The simulation was done using the effective action including the static determinant, κ^2- and κ^4- corrections as well as the λ_1-correction. Figure 5.3.2 shows the chiral condensate as a function of β and the respective susceptibility. Looking at the chiral condensate we see that for $N_s = 8$ there is an outlier around the transition, which is not the case anymore if we decrease the volume. We infer that we need at least a spatial volume of $V = 12^3$ to obtain a good estimate for the chiral condensate. The location of the transition is determined by the maximum of the susceptibilty to be at $\beta_c = 6.100(5)$. Now we have to analyse the order of the phase transition. We see that the peak of the susceptibility grows with increasing volume, except for an outlier at the phase transition for $N_s = 12$. This corresponds to a first order transition.

Now we want to investigate how the transition as a function of the coupling β changes if we vary κ. We are using an action including the static determinant, κ^2, κ^4, λ_1 and the shift. Gauge fields have no explicit contribution to the chiral condensate but they change the evolution of the simulation. Figure 5.3.3 shows the chiral condensate and the respective susceptibility as a function of β around β_c for different values of κ. Increasing κ, the transition smoothes out, becoming a broad crossover. For small $\kappa = 0.04$ the chiral condensate at the phase transition changes quite rapidly and the susceptibility is rather narrow around the transition. The transition is of first order. This is in agreement with $\kappa_c = 0.0691(9)$, which was found in [13]. For $\kappa = 0.04 < \kappa_c$ we expected and saw a first order transition, for $\kappa > \kappa_c$ one expects the transition to be a crossover. This is indeed the case: the more we increase κ, the broader the chiral condensate and its susceptibility become around the phase transition. It was already argued that for small quark masses the $Z(3)$ symmetry is only slightly broken, we are still able to see the first order transition. With decreasing mass the breaking becomes more severe, the transition weakens and becoming a crossover. Hence up to $\kappa = 0.3$ we could not confirm a first order transition to take place, signalling the partial

[4] An overview over different scenarios of the Columbia plot in the chiral region can be found in [27], p. 48-49.

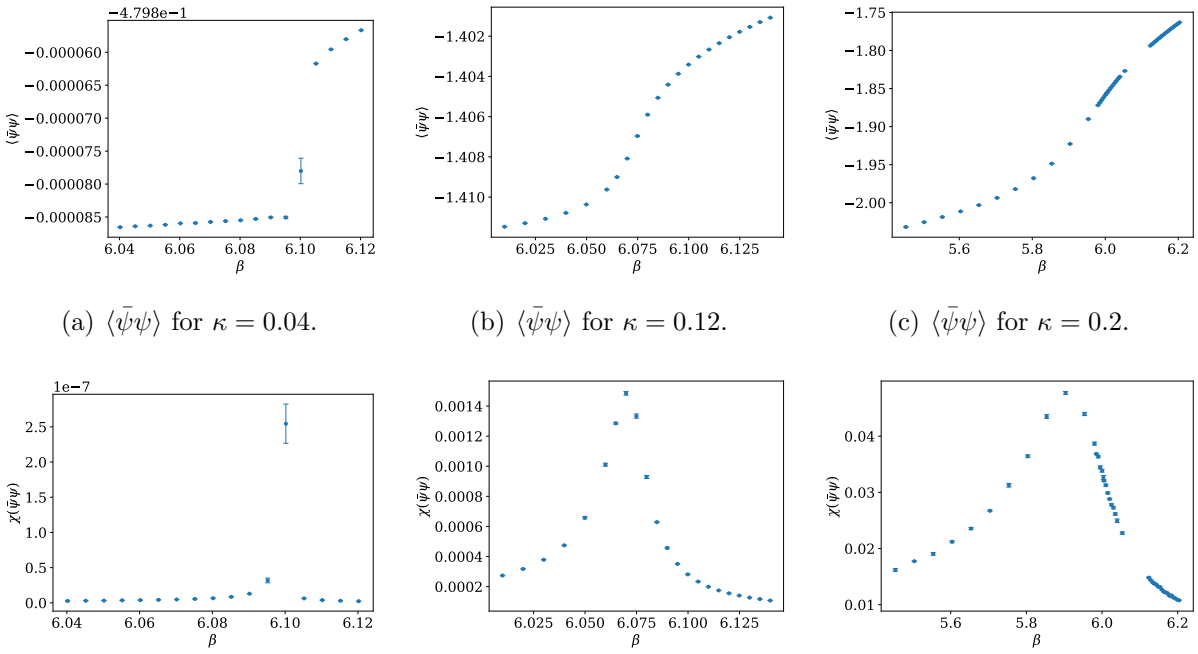

(a) $\langle\bar{\psi}\psi\rangle$ for $\kappa = 0.04$. (b) $\langle\bar{\psi}\psi\rangle$ for $\kappa = 0.12$. (c) $\langle\bar{\psi}\psi\rangle$ for $\kappa = 0.2$.

(d) $\chi(\bar{\psi}\psi)$ for $\kappa = 0.04$. (e) $\chi(\bar{\psi}\psi)$ for $\kappa = 0.12$. (f) $\chi(\bar{\psi}\psi)$ for $\kappa = 0.2$.

Figure 5.3.3: *Chiral condensate and respective susceptibility as a function of β for $N_\tau = 4, N_s = 12$ using the action including Static determinant, κ^2, κ^4, λ_1, shift for different values of κ.*

κ	β_c
0.04	6.100(5)
0.08	6.094(10)
0.12	6.070(5)
0.16	6.013(10)
0.20	5.90(5)

Table 5.3.1: *Critical coupling β_c for different values of κ for $N_\tau = 4, N_s = 12$.*

restoration of chiral symmetry.[5]

We analyzed the critical coupling β_c as a function of κ. The results are shown in Table 5.3.1 and visualized in Figure 5.3.4. The results agree quite with the results in [20]. Though the values presented in here are slightly smaller than the data to compare with.

Decreasing the mass even more, looking at $\kappa = 0.3$ in Figure 5.3.5, the transition becomes broader, as it was already argued. The susceptibility shows some odd behavior, as it is again increasing for $\beta > \beta_c$ away from the phase transition. This might be a convergence problem of being away from the phase transition. Thus this cannot be the maximum of susceptibility locating the phase transition, as from Table 5.3.1 we expect β_c to decrease with increasing κ. Nevertheless the peak of the susceptibility for $\kappa = 0.3$ saturates, telling that this is a crossover.

[5]Chiral symmetry is explicitly broken by Wilson fermions and thus cannot be restored in a strict sense, thus the term ”partial” restoration.

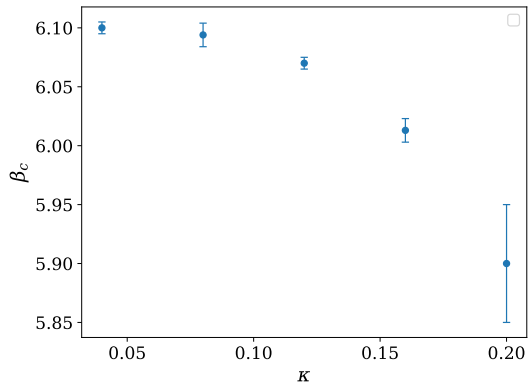

Figure 5.3.4: *Critical coupling β_c for different values of κ for $N_\tau = 4, N_s = 12$.*

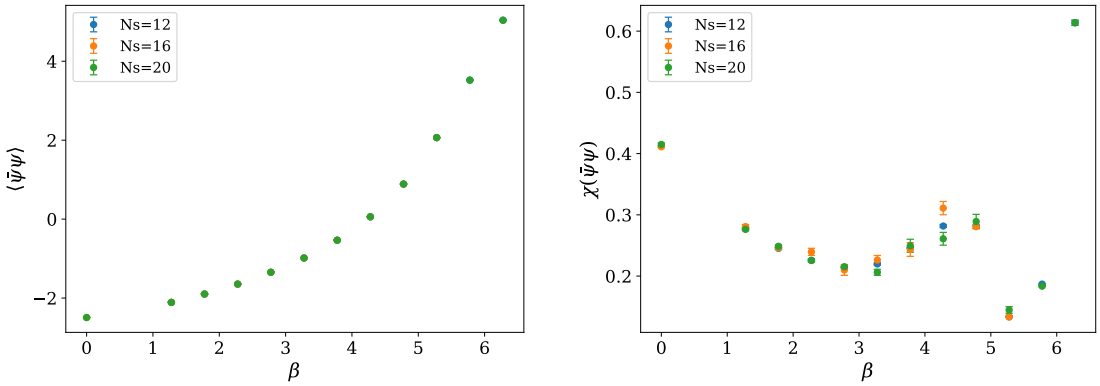

(a) $\langle\bar{\psi}\psi\rangle$. (b) $\chi(\bar{\psi}\psi)$.

Figure 5.3.5: *Chiral condensate and corresponding susceptibility as a function of the inverse coupling β for $N_\tau = 4, \kappa = 0.3$ for different spatial extents.*

We found found the critical coupling β_c as a function of κ being in good agreement with the results shown in [20]. It was shown that the chiral condensate and the Polyakov loop serve as appropriate indicators for a phase transition. We could confirm the deconfinement transition to be of first order in the case of $\kappa = 0.04$. With increasing κ the transition turns into a crossover, the crossover region spreads at least until $\kappa = 0.3$. Thus for Wilson fermions in the effective theory partial chiral restoration could not be emulated.

Chapter 6

Conclusion and outlook

In this thesis it was shown that the Complex Langevin equation can be used to describe the QCD deconfinement phase transition. The application of the Langevin operator as a criterion for correctness worked well and using an adaptive stepsize method led to well agreement between CL and Metropolis data, not only in the pure gauge case but also in the case with additional fermions.

The main issues of the CLE, which are convergence to the wrong limit and runaways, were shown to be controlled using the criterion for correctness and an adaptive stepsize method. Including nonzero chemical potential one has to carefully make use of these tools, to ensure correct results. This is the more important as one enters regions in which the sign problem becomes severe and therefore no data from e.g. Metropolis algorithm can be used to compare with. Nevertheless the simulation using the CLE has some disadvantages still, which are high numerical costs, as a long thermalization procedure is needed, and a large amount of data is required to ensure an appropriate tunneling behavior. For higher spatial volume more data are required.

So far in this thesis the region for zero chemical potential was investigated exclusively. As a next step one could add a chemical potential, which was the reason why we introduced the Complex Langevin method.

In the case of the chiral condensate an investigation of the different contributions to the action has been presented as well as the evolution of the critical coupling β_c depending on the inverse quark mass κ. For a (partial) restoration of chiral symmetry one would expect a first order phase transition for light quarks. In the case of the effective theory with Wilson quarks this could not be confirmed. However it was proven that at $\kappa = 0.04$ the chiral condensate and the Polyakov loop signal a first order phase transition, which becomes a crossover for increasing κ.

Appendix A

Driftterms

A.1 Chain rule for fermionic driftterms

The fermionic part of the effective action can be written as a sum over the action for different orders in κ, $S_{eff} = S_0 + S_2 + S_4$. We have to calculate the driftterms $K_i^j(\vec{x})$ locally, where $i = a, b$ denotes with respect to which field, ϕ_a or ϕ_b we take the derivative and $j = 0, 2, 4$ denotes the order in κ. The fermionic action depends on the $W_{m+n,n}(\boldsymbol{n})$. Thus we have to apply a more advanced chain rule than in the static case, namely

$$\begin{aligned} K_i^j(\boldsymbol{n}) &= -\frac{\partial S^j(\boldsymbol{n})}{\partial \phi_i(\boldsymbol{n})} \\ &= -\sum_W \frac{\partial S^j}{\partial W_{m+n,n}(\boldsymbol{n})} \left(\frac{\partial W_{m+n,n}(\boldsymbol{n})}{\partial L_{\boldsymbol{n}}(\phi_i)} \frac{\partial L_{\boldsymbol{n}}(\phi_i)}{\partial \phi_i(\boldsymbol{n})} + \frac{\partial W_{m+n,n}(\boldsymbol{n})}{\partial L^*_{\boldsymbol{n}}(\phi_i)} \frac{\partial L^*_{\boldsymbol{n}}(\phi_i)}{\partial \phi_i(\boldsymbol{n})} \right) \\ &\quad - \sum_{W^\dagger} \frac{\partial S^j}{\partial W^\dagger_{m+n,n}(\boldsymbol{n})} \left(\frac{\partial W^\dagger_{m+n,n}(\boldsymbol{n})}{\partial L_{\boldsymbol{n}}(\phi_i)} \frac{\partial L_{\boldsymbol{n}}(\phi_i)}{\partial \phi_i(\boldsymbol{n})} + \frac{\partial W^\dagger_{m+n,n}(\boldsymbol{n})}{\partial L^*_{\boldsymbol{n}}(\phi_i)} \frac{\partial L^*_{\boldsymbol{n}}(\phi_i)}{\partial \phi_i(\boldsymbol{n})} \right) \end{aligned} \tag{A.1.1}$$

We have to calculate the driftterms $K_i(\boldsymbol{n})$ locally, where $i = a, b$ denotes derivatives with respect to the fields ϕ_a and ϕ_b and $j = 2, 4$ corresponds to the order in κ. $j = 0$ denotes the static contribution. The fermionic driftterms then add up to

$$K_i(\boldsymbol{n}) = \sum_j K_i^j(\boldsymbol{n}). \tag{A.1.2}$$

A.1.1 Driftterm of the κ^2-correction

To apply the chainrule for the κ^2-correction from Equation A.1.1, we need to know the relation between $W_{11}, W_{11}^\dagger$ and the Polyakov loop. How to switch was shown in Equation 3.4.6, and we get the following results for $m = 0, n = 1$ [20]

$$W_{11}(\boldsymbol{n}) = \mathrm{Tr} \frac{h_1 W(\boldsymbol{n})}{1 + h_1 W(\boldsymbol{n})} = \frac{h_1 L(\boldsymbol{n}) + 2h_1^2 L^*(\boldsymbol{n}) + 3h_1^3}{1 + h_1 L(\boldsymbol{n}) + h_1^2 L^*(\boldsymbol{n}) + h_1^3}, \tag{A.1.3}$$

$$W_{11}^\dagger(\boldsymbol{n}) = \mathrm{Tr} \frac{\bar{h}_1 W^\dagger(\boldsymbol{n})}{1 + \bar{h}_1 W^\dagger(\boldsymbol{n})} = \frac{\bar{h}_1 L^*(\boldsymbol{n}) + 2\bar{h}_1^2 L(\boldsymbol{n}) + 3\bar{h}_1^3}{1 + \bar{h}_1 L^*(\boldsymbol{n}) + \bar{h}_1^2 L(\boldsymbol{n}) + \bar{h}_1^3}. \tag{A.1.4}$$

The next step is to take the derivatives of $W_{11}, W_{11}^\dagger$ w.rp.t. the Polyakov loop and its complex conjugate,

$$
\begin{aligned}
\frac{\partial W_{11}(\boldsymbol{n})}{\partial L_{\boldsymbol{n}}} &= \frac{h_1(1+h_1L_{\boldsymbol{n}}+h_1^2L^*_{\boldsymbol{n}}+h_1^3)-(h_1L_{\boldsymbol{n}}+2h_1^2L^*_{\boldsymbol{n}}+3h_1^2)\cdot h_1}{(1+h_1L_{\boldsymbol{n}}+h_1^2L^*_{\boldsymbol{n}}+h_1^3)^2} \\
&= \frac{h_1(1-h_1^2L^*_{\boldsymbol{n}}-2h_1^3)}{(1+h_1L_{\boldsymbol{n}}+h_1^2L^*_{\boldsymbol{n}}+h_1^3)^2} \\
\frac{\partial W_{11}(\boldsymbol{n})}{\partial L^*_{\boldsymbol{n}}} &= \frac{2h_1^2\cdot(1+h_1L_{\boldsymbol{n}}+h_1^2L^*_{\boldsymbol{n}}+h_1^3)-(h_1L_{\boldsymbol{n}}+2h_1^2L^*_{\boldsymbol{n}}+3h_1^3)\cdot h_1^2}{(1+h_1L_{\boldsymbol{n}}+h_1^2L^*_{\boldsymbol{n}}+h_1^3)^2} \\
&= \frac{h_1^2(2+h_1L_{\boldsymbol{n}}-h_1^3)}{(1+h_1L_{\boldsymbol{n}}+h_1^2L^*_{\boldsymbol{n}}+h_1^3)^2} \\
\frac{\partial W^\dagger_{11}(\boldsymbol{n})}{\partial L_{\boldsymbol{n}}} &= \frac{2\bar{h}_1^2\cdot(1+\bar{h}_1L^*_{\boldsymbol{n}}+\bar{h}_1^2L_{\boldsymbol{n}}+\bar{h}_1^3)-(\bar{h}_1L^*_{\boldsymbol{n}}+2\bar{h}_1^2L_{\boldsymbol{n}}+3\bar{h}_1^3)\cdot \bar{h}_1^2}{(1+\bar{h}_1L^*_{\boldsymbol{n}}+\bar{h}_1^2L_{\boldsymbol{n}}+\bar{h}_1^3)^2} \\
&= \frac{\bar{h}_1^2(2+\bar{h}_1L^*_{\boldsymbol{n}}-\bar{h}_1^3)}{(1+\bar{h}_1L^*_{\boldsymbol{n}}+\bar{h}_1^2L_{\boldsymbol{n}}+\bar{h}_1^3)^2} \\
\frac{\partial W^\dagger_{11}(\boldsymbol{n})}{\partial L^*_{\boldsymbol{n}}} &= \frac{\bar{h}_1(1+\bar{h}_1L^*_{\boldsymbol{n}}+\bar{h}_1^2L_{\boldsymbol{n}}+\bar{h}_1^3)-(\bar{h}_1L^*_{\boldsymbol{n}}+2\bar{h}_1^2L_{\boldsymbol{n}}+3\bar{h}_1^2)\cdot \bar{h}_1}{(1+\bar{h}_1L^*_{\boldsymbol{n}}+\bar{h}_1^2L_{\boldsymbol{n}}+\bar{h}_1^3)^2} \\
&= \frac{\bar{h}_1(1-\bar{h}_1^2L_{\boldsymbol{n}}-2\bar{h}_1^3)}{(1+\bar{h}_1L^*_{\boldsymbol{n}}+\bar{h}_1^2L_{\boldsymbol{n}}+\bar{h}_1^3)^2}.
\end{aligned}
\tag{A.1.5}
$$

Then we can plug these results into Equation A.1.1, where the derivatives only act on variables at spatial point $\boldsymbol{n}$, but not at $\boldsymbol{n}+\hat{i}$. The driftterm belonging to the κ^2-correction then reads

$$
\begin{aligned}
K_i^2(\boldsymbol{n}) &= -\frac{\partial S_2}{\partial W_{11,\boldsymbol{n}}}\frac{\partial W_{11,\boldsymbol{n}}}{\partial L_{\boldsymbol{n}}(\phi_i)}\frac{\partial L_{\boldsymbol{n}}(\phi_i)}{\phi_i(\boldsymbol{n})} - \frac{\partial S_2}{\partial W^\dagger_{11,\boldsymbol{n}}}\frac{\partial W^\dagger_{11,\boldsymbol{n}}}{\partial L_{\boldsymbol{n}}(\phi_i)}\frac{\partial L_{\boldsymbol{n}}(\phi_i)}{\phi_i(\boldsymbol{n})} \\
&= -\frac{\partial S_2}{\partial W_{11,\boldsymbol{n}}}\left(\frac{\partial W_{11,\boldsymbol{n}}}{\partial L_{\boldsymbol{n}}(\phi_i)}\frac{\partial L_{\boldsymbol{n}}(\phi_i)}{\phi_i(\boldsymbol{n})}+\frac{\partial W_{11,\boldsymbol{n}}}{\partial L^*_{\boldsymbol{n}}(\phi_i)}\frac{\partial L^*_{\boldsymbol{n}}(\phi_i)}{\phi_i(\boldsymbol{n})}\right) \\
&\quad -\frac{\partial S_2}{\partial W^\dagger_{11,\boldsymbol{n}}}\left(\frac{\partial W^\dagger_{11,\boldsymbol{n}}}{\partial L_{\boldsymbol{n}}(\phi_i)}\frac{\partial L_{\boldsymbol{n}}(\phi_i)}{\phi_i(\boldsymbol{n})}+\frac{\partial W^\dagger_{11,\boldsymbol{n}}}{\partial L^*_{\boldsymbol{n}}(\phi_i)}\frac{\partial L^*_{\boldsymbol{n}}(\phi_i)}{\phi_i(\boldsymbol{n})}\right) \\
&= -h_2N_f\sum_i\left(\frac{h_1(1-h_1^2L^*_{\boldsymbol{n}}-2h_1^3)\frac{\partial L_{\boldsymbol{n}}}{\phi_i(\boldsymbol{n})}+h_1^2(2+h_1L_{\boldsymbol{n}}-h_1^3)\frac{\partial L^*_{\boldsymbol{n}}}{\phi_i(\boldsymbol{n})}}{(1+h_1L_{\boldsymbol{n}}+h_1^2L^*_{\boldsymbol{n}}+h_1^3)^2}\cdots\right. \\
&\quad \left.\cdots-\frac{\bar{h}_1^2(2+\bar{h}_1L^*_{\boldsymbol{n}}-\bar{h}_1^3)\frac{\partial L_{\boldsymbol{n}}}{\phi_i(\boldsymbol{n})}+\bar{h}_1(1-\bar{h}_1^2L_{\boldsymbol{n}}-2\bar{h}_1^3)\frac{\partial L^*_{\boldsymbol{n}}}{\phi_i(\boldsymbol{n})}}{(1+\bar{h}_1L^*_{\boldsymbol{n}}+\bar{h}_1^2L_{\boldsymbol{n}}+\bar{h}_1^3)^2}\right)\cdot(W_{11}(\boldsymbol{n}+\hat{i})-W^\dagger_{11}(\boldsymbol{n}+\hat{i})).
\end{aligned}
\tag{A.1.6}
$$

A.1.2 Driftterms for κ^4-correction

The κ^4- corrections contain terms proportional to W_{11}, W_{21}, W_{22} and

$$
W_{00}(\boldsymbol{n}) \equiv \mathrm{Tr}\frac{1}{(1+h_1W(\boldsymbol{n}))(1+\bar{h}_1W^\dagger(\boldsymbol{n}))},
\tag{A.1.7}
$$

whose nomenclature is not strictly following the one that was introduced.[1] The κ^4- contribution is rather lengthy and thus the driftterms are not shown in full detail. Instead the

[1] A more accurate nomenclature can be found in [26], p. 15. The term W_{00} would then be named W_{1010}.

traced temporal Wilson lines and the derivatives w.rp.t. the Polyakov loop and its complex conjugate are shown, as those quantities are the key to construct the driftterms of the action shown in [20], *Appendix A*. The calculation of the driftterms is then straight forward, analogously to the case shown for the κ^2- contribution. For readability the spatial dependence is not shown explicitly anymore. We now give the explicit expressions for W_{21}, W_{22} and their conjugate, as well as the derivative of those quantities w.rp.t. the Polyakov loop and its complex conjugate.
For $m = n = 1$:

$$\begin{aligned} W_{21} &= \mathrm{Tr}\frac{h_1 W}{(1+h_1 W)^2} = \frac{h_1(L + 4h_1^3 L + 4h_1 L^* + h_1^4 L^* + h_1^2(9 + LL^*))}{(1 + h_1 L + h_1^2 L^* + h_1^3)^2} \\ W_{21}^\dagger &= \mathrm{Tr}\frac{\bar{h}_1 W^\dagger}{(1+\bar{h}_1 W^\dagger)^2} = \frac{\bar{h}_1(L^* + 4\bar{h}_1^3 L^* + 4\bar{h}_1 L + \bar{h}_1^4 L + \bar{h}_1^2(9 + LL^*))}{(1 + \bar{h}_1 L^* + \bar{h}_1^2 L + \bar{h}_1^3)^2}. \end{aligned} \tag{A.1.8}$$

For $m = 0, n = 2$:

$$\begin{aligned} W_{22} &= \mathrm{Tr}\left(\frac{h_1 W}{1+h_1 W}\right)^2 = \frac{h_1^2((4h_1^3 - 2)L^* + L^2 + 2h_1^2 L^{*2} + 3h_1^4 + 2h_1(-3 + LL^*))}{(1 + h_1 L + h_1^2 L^* + h_1^3)^2} \\ W_{22}^\dagger &= \mathrm{Tr}\left(\frac{\bar{h}_1 W^\dagger}{1+\bar{h}_1 W^\dagger}\right)^2 = \frac{\bar{h}_1^2((4\bar{h}_1^3 - 2)L + L^{*2} + 2\bar{h}_1^2 L^2 + 3\bar{h}_1^4 + 2\bar{h}_1(-3 + LL^*))}{(1 + \bar{h}_1 L^* + \bar{h}_1^2 L + \bar{h}_1^3)^2}. \end{aligned} \tag{A.1.9}$$

The derivative of the traced temporal Wilson lines w.rp.t. the Polyakov loop and its complex conjugate look like

$$\begin{aligned} \frac{\partial W_{21}}{\partial L} &= \frac{h_1^2(1 - 2L - 8h_1 L^* + h_1^2(L^* - 2(9 + LL^*)) + h_1^3(4 - 8L) - 2h_1^4 L^*)}{(1 + h_1 L + h_1^2 L^* + h_1^3)^3} \\ \frac{\partial W_{21}}{\partial L^*} &= \frac{h_1^2(4 - 2L + h_1(5L - 8L^*) + h_1^2(L^2 + 4L^* - 2(9 + LL^*))}{(1 + h_1 L + h_1^2 L^* + h_1^3)^3} \\ &\quad + \frac{h_1^2(h_1^3(5 + LL^* - 8L) + h_1^4(2L - 2L^*) + h_1^5 L^* + h_1^6)}{(1 + h_1 L + h_1^2 L^* + h_1^3)^3} \\ \frac{\partial W_{22}}{\partial L} &= \frac{2h_1^2(L + 3h_1 L^* + 6h_1^2 + h_1^3(L - L^{*2}) - 3h_1^4 L^* - 3h_1^5)}{(1 + h_1 L + h_1^2 L^* + h_1^3)^3} \\ \frac{\partial W_{22}}{\partial L^*} &= \frac{2h_1^2(-1 + 3h_1^2 L^* + h_1^3(7 + LL^*) + 3h_1^4 L - h_1^6))}{(1 + h_1 L + h_1^2 L^* + h_1^3)^3}. \end{aligned} \tag{A.1.10}$$

The derivatives of $W_{21}^\dagger, W_{22}^\dagger$ look similar, thus they are not displayed here.
The expression for W_{00} and the derivatives w.rp.t. the Polyakov loop can be obtained in the same way.

Appendix B

Chiral condensate

B.1 $N_f = 2$, contribution of the static determinant

B.1.1 Partition function

The analytic expression of the partition function for $N_f = 2$ reads

$$
\begin{aligned}
Z(h_1, \bar{h}_1) &= \int [dU_0] \prod_k (1 + h_1 L_k + h_1^2 L_k^* + h_1^3)^4 (1 + \bar{h}_1 L_k^* + \bar{h}_1^2 L_k + \bar{h}_1^3)^4 \\
&= z_0^V \\
&= [(1 + 20h_1^3 + 50h_1^6 + 20h_1^9 + h_1^{12}) \\
&+ (16h_1 + 180h_1^4 + 240h_1^7 + 40h_1^{10})\bar{h}_1 \\
&+ (136h_1^2 + 816h_1^5 + 570h_1^8 + 40h_1^{11})\bar{h}_1^2 \\
&+ (20 + 816h_1^3 + 2320h_1^6 + 800h_1^9 + 20h_1^{12})\bar{h}_1^3 \\
&+ (180h_1 + 2651h_1^4 + 3720h_1^7 + 570h_1^{10})\bar{h}_1^4 \\
&+ (816h_1^2 + 5312h_1^5 + 3720h_1^8 + 240h_1^{11})\bar{h}_1^5 \\
&+ (50 + 2320h_1^3 + 6832h_1^6 + 2320h_1^9 + 50h_1^{12})\bar{h}_1^6 \\
&+ (240h_1 + 3720h_1^4 + 5312h_1^7 + 816h_1^{10})\bar{h}_1^7 \\
&+ (570h_1^2 + 3720h_1^5 + 2651h_1^8 + 180h_1^{11})\bar{h}_1^8 \\
&+ (20 + 800h_1^3 + 2320h_1^6 + 816h_1^9 + 20h_1^{12})\bar{h}_1^9 \\
&+ (40h_1 + 570h_1^4 + 816h_1^7 + 136h_1^{10})\bar{h}_1^{10} \\
&+ (40h_1^2 + 240h_1^5 + 180h_1^8 + 16h_1^{11})\bar{h}_1^{11} \\
&+ (1 + 20h_1^3 + 50h_1^6 + 20h_1^9 + h_1^{12})\bar{h}_1^{12}\ ]^V .
\end{aligned}
\tag{B.1.1}
$$

B.1.2 Chiral condensate

For $N_f = 2$ and only considering the static determinant we get the chiral condensate as:

$$\begin{aligned}\langle\bar{\psi}\psi\rangle_r = \frac{2\kappa}{z_0}\Big(& (60h_1^3 + 300h_1^6 + 180h_1^9 + 12h_1^{12}) \\ & +(32h_1 + 900h_1^4 + 1920h_1^7 + 440h_1^{10})\bar{h}_1 \\ & +(544h_1^2 + 5712h_1^5 + 5700h_1^8 + 520h_1^{11})\bar{h}_1^2 \\ & +(60 + 4896h_1^3 + 20880h_1^6 + 9600h_1^9 + 300h_1^{12})\bar{h}_1^3 \\ & +(900h_1 + 21208h_1^4 + 40920h_1^7 + 7980h_1^{10})\bar{h}_1^4 \\ & +(5712h_1^2 + 53120h_1^5 + 48360h_1^8 + 3840h_1^{11})\bar{h}_1^5 \\ & +(300 + 20880h_1^3 + 81984h_1^6 + 34800h_1^9 + 900h_1^{12})\bar{h}_1^6 \\ & +(1920h_1 + 40920h_1^4 + 74368h_1^7 + 13872h_1^{10})\bar{h}_1^7 \\ & +(5700h_1^2 + 48360h_1^5 + 42416h_1^8 + 3420h_1^{11})\bar{h}_1^8 \\ & +(180 + 9600h_1^3 + 34800h_1^6 + 14688h_1^9 + 420h_1^{12})\bar{h}_1^9 \\ & +(440h_1 + 7980h_1^4 + 13872h_1^7 + 2720h_1^{10})\bar{h}_1^{10} \\ & +(520h_1^2 + 3840h_1^5 + 3420h_1^8 + 352h_1^{11})\bar{h}_1^{11} \\ & +(12 + 300h_1^3 + 900h_1^6 + 420h_1^9 + 24h_1^{12})\bar{h}_1^{12}\Big).\end{aligned} \tag{B.1.2}$$

B.2 $N_f = 2$, contribution of the κ^2- correction

The unresummed partition function looks like

$$Z = Z_{stat} + Z_{\kappa^2} = z_0^V(1 - 6Vh_2N_f\frac{z_1^2}{z_0^2}) + O(\kappa^4). \tag{B.2.1}$$

The contribution of the κ^2-correction to the partition function, z_1, for $N_f = 2$ looks like:

$$\begin{aligned}z_1 = & (15h_1^3 + 75h_1^6 + 45h_1^9 + 3h_1^{12}) + (135h_1^4 + 360h_1^7 + 90h_1^{10})\bar{h}_1 \\ & + (612h_1^5 + 855h_1^8 + 90h_1^{11})\bar{h}_1^2 \\ & + (15 + 1740h_1^6 + 1200h_1^9 + 45h_1^{12})\bar{h}_1^3 \\ & + (-135h_1 + 2790h_1^7 + 855h_1^{10})\bar{h}_1^4 \\ & + (-612h_1^2 + 2790h_1^8 + 360h_1^1 1)\bar{h}_1^5 \\ & + (-75 - 1740h_1^3 + 1740h1^9 + 75h1^{12})\bar{h}_1^6 \\ & + (360h_1 - 2790h_1^4 + 612h1^{10})\bar{h}_1^7 \\ & + (-855h_1^2 + 2790h_1^5 + 135h_1^{11})\bar{h}_1^8 \\ & + (-45 - 1200h_1^3 - 1740h_1^6 + 15h_1^{12})\bar{h}_1^9 \\ & + (-90h_1 - 855h_1^4 - 612h_1^7)\bar{h}_1^{10} \\ & + (90h_1^2 - 360h_1^5 - 135h_1^8)\bar{h}_1^{11} \\ & + (-3 - 45h_1^3 + 75h_1^6 - 15h_1^9)\bar{h}_1^{12}.\end{aligned} \tag{B.2.2}$$

Acknowledgements

I want to thank Owe Philipsen for the opportunity write my thesis in your working group and for the helpful discussions regarding this thesis. Thanks as well to the CRC-TR211 for being able to be part of this interesting cooperation.
I furthermore want to thank Dr. Jangho Kim for various discussions and supervision concerning the implementation of the Complex Langevin algorithm.
Thanks a lot to my collegues in the working group, especially Jonas Scheunert for your support regarding analytical derivations.
Thank you to Miguel Salg and Amine Chabane for providing your code to me and for always being open for a little talk.

References

[1] Aarts et al. "Adaptive stepsize and instabilities in complex Langevin dynamics". In: *Physics Letters B* 687.2-3 (2010), 154–159. DOI: 10.1016/j.physletb.2010.03.012.

[2] G. Aarts and F.A. James. "Complex Langevin dynamics in the SU(3) spin model at nonzero chemical potential revisited". In: *Journal of High Energy Physics* 2012.1 (2012). DOI: 10.1007/jhep01(2012)118.

[3] G. Aarts, E. Seiler and I.-O. Stamatescu. "Complex Langevin method: When can it be trusted?" In: *Physical Review D* 81.5 (2010). DOI: 10.1103/physrevd.81.054508.

[4] G. Aarts and I.-O. Stamatescu. "Stochastic quantization at finite chemical potential". In: *Journal of High Energy Physics* 2008.09 (2008), 018–018. DOI: 10.1088/1126-6708/2008/09/018.

[5] G. Aarts et al. "Complex Langevin: etiology and diagnostics of its main problem". In: *The European Physical Journal C* 71.10 (2011). DOI: 10.1140/epjc/s10052-011-1756-5.

[6] G. Aarts et al. "Controlling complex Langevin dynamics at finite density". In: *The European Physical Journal A* 49.7 (2013). DOI: 10.1140/epja/i2013-13089-4.

[7] M. Tanabashi et al. "Quark Summary Table". In: *Phys. Rev. D* 98 (3 2018), p. 40. DOI: 10.1103/PhysRevD.98.030001.

[8] B.A. Berg. "Introduction to Markov chain Monte Carlo simulations and their statistical analysis". In: *Lecture Notes Series, Institute for Mathematical Sciences, National University of Singapore* 7 (2004). arXiv: 0410490.

[9] Tillmann Boeckel and Jürgen Schaffner-Bielich. "Little inflation at the cosmological QCD phase transition". In: *Physical Review D* 85.10 (2012). DOI: 10.1103/physrevd.85.103506.

[10] P.H. Damgaard and H. Hueffel. "Stochastic quantization". In: *Physics Reports* 152.5 (1987), pp. 227 –398. DOI: https://doi.org/10.1016/0370-1573(87)90144-X.

[11] T. DeGrand and C. DeTar. *Lattice Methods for Quantum Chromodynamics*. World Scientific Publishing, 2006.

[12] Philippe de Forcrand. *Simulating QCD at finite density*. 2010. arXiv: 1005.0539 [hep-lat].

[13] M. Fromm et al. "The QCD deconfinement transition for heavy quarks and all baryon chemical potentials". In: *Journal of High Energy Physics* 2012 (2012). DOI: 10.1007/JHEP01(2012)042. arXiv: 1111.4953 [hep-lat].

[14] C. Gattringer. "Flux representation of an effective Polyakov loop model for QCD thermodynamics". In: *Nuclear Physics B* 850.2 (2011), 242–252. DOI: 10.1016/j.nuclphysb.2011.04.018.

[15] C. Gattringer and C.B. Lang. *Quantum chromodynamics on the lattice: An introductory presentation*. Vol. 788. Lecture notes in physics. 2010. URL: http://d-nb.info/995195447/04.

[16] F. Karsch and H.W. Wyld. "Complex Langevin Simulation of the SU(3) Spin Model with Nonzero Chemical Potential". In: *Phys. Rev. Lett.* 55 (21 1985), pp. 2242–2245. DOI: 10.1103/PhysRevLett.55.2242. URL: https://link.aps.org/doi/10.1103/PhysRevLett.55.2242.

[17] J. Langelage, S. Lottini and O. Philipsen. "Centre symmetric 3d effective actions for thermal SU(N) Yang-Mills from strong coupling series". In: *Journal of High Energy Physics* 2011, 57 (2011), p. 57. DOI: 10.1007/JHEP02(2011)057. arXiv: 1010.0951 [hep-lat].

[18] J. Langelage, M. Neuman and O. Philipsen. "Heavy dense QCD and nuclear matter from an effective lattice theory". In: *Journal of High Energy Physics* 2014.9 (2014). DOI: 10.1007/jhep09(2014)131. URL: http://dx.doi.org/10.1007/JHEP09(2014)131.

[19] I. Montvay and G.Münster. *Quantum Fields on a lattice*. Cambridge University Press, 1994.

[20] M. Neuman. "Effective Theory for Heavy Quark QCD at Finite Temperature and Density with Stochastic Quantization." PhD thesis. Johann-Wolfgang-Goethe Universität Frankfurt, 2015.

[21] H.B. Nielsen and M. Ninomiya. "Absence of neutrinos on a lattice: (I). Proof by homotopy theory". In: *Nuclear Physics B* 185.1 (1981), pp. 20–40. DOI: https://doi.org/10.1016/0550-3213(81)90361-8.

[22] G. Parisi and Y.-S. Wu. "Perturbation Theory Without Gauge Fixing". In: *Sci. Sin.* 24 (1981), p. 483.

[23] M.E. Peskin and D.V. Schroeder. *An introduction to quantum field theory*. 1995.

[24] O. Philipsen. *Lattice QCD at non-zero temperature and baryon density*. 2013. arXiv: 1009.4089 [hep-lat].

[25] M. Salg. "The deconfinement transition in an effective theory for heavy quark Lattice QCD to $\mathcal{O}(\kappa^4)$". MA thesis. Johann-Wolfgang-Goethe Universität Frankfurt, 2020.

[26] A. Schön. "Effective heavy quark theory of of strong coupling QCD in 1+1 dimensions." MA thesis. Johann-Wolfgang-Goethe Universität Frankfurt, 2018.

[27] A. Sciarra. "The QCD phase diagram at purely imaginary chemical potential from the lattice". PhD thesis. Johann-Wolfgang-Goethe Universität Frankfurt, 2016.

[28] J. Smit. *Introduction to Quantum Fields on the Lattice*. Cambridge University Press, 2002.

[29] K. Yagi, T. Hatsuda and Y. Miake. *Quark-gluon plasma : from big bang to little bang*. Cambridge [u.a.], 2005.

Selbständigkeitserklärung

Hiermit versichere ich, die vorliegende Arbeit gemäß §30(12) der Ordnung für den Bachelor- und den Masterstudiengang Physik der Johann Wolfgang Goethe-Universität Frankfurt am Main vom 24.04.2013 selbständig und ohne Benutzung anderer als der angegebenen Quellen und Hilfsmittel verfasst zu haben. Alle Stellen, Bilder und Zeichnungen, die wörtlich oder singemäß aus Veröffentlichungen oder aus anderen fremden Texten entnommen wurden, wurden als solche kenntlich gemacht. Diese Abschlussarbeit ist nicht, auch nicht auszugsweise, für eine andere Prüfung oder Studienleistung verwendet worden.

Datum Unterschrift